DISSERTATIONES
MEDICINAE
UNIVERSITATIS
TARTUENSIS
316

GEORGI DZAPARIDZE

Quantification and evaluation of the diagnostic significance of adenocarcinoma-associated microenvironmental changes in the prostate using modern digital pathology solutions

DISSERTATIONES MEDICINAE UNIVERSITATIS TARTUENSIS
316

DISSERTATIONES MEDICINAE UNIVERSITATIS TARTUENSIS
316

GEORGI DZAPARIDZE

Quantification and evaluation of the diagnostic significance of adenocarcinoma-associated microenvironmental changes in the prostate using modern digital pathology solutions

UNIVERSITY OF TARTU
Press

Department of Pathological Anatomy and Forensic Medicine, University of Tartu, Tartu, Estonia

Dissertation is accepted for the commencement of the degree of Doctor of Philosophy (medicine) on 15st of September, 2021, by the Council of the Faculty of Medicine, University of Tartu, Estonia.

Supervisors: associate professor Ave Minajeva (MD, PhD),
Institute of Biomedicine and Translational Medicine,
University of Tartu, Tartu, Estonia.

Reviewers: professor Margus Punab (MD, PhD),
Institute of Clinical Medicine, Faculty of Medicine,
University of Tartu, Tartu, Estonia.

tenured associate professor Peeter Ross (MD, PhD),
Department of Health Technologies, School of Information Technologies, Tallinn University of Technology.

Opponent: professor Ilze Štrumfa (MD, PhD),
Department of Pathology, Faculty of Medicine,
Riga Stradinš University, Riia, Latvia

Commencement: November 5th, 2021

Publication of this dissertation is granted by the University of Tartu.

This research was supported by the Institutional Research Funding from the Estonian Research Council and by the European Union through the European Regional Development Fund.

ISSN 1024-395X
ISBN 978-9949-03-717-9 (print)
ISBN 978-9949-03-718-6 (pdf)

Copyright: Georgi Dzaparidze, 2021

University of Tartu Press
www.tyk.ee

CONTENTS

LIST OF ORIGINAL PUBLICATIONS

1. Dzaparidze, Georgi; Anion, Evelin; Laan, Maris; Minajeva, Ave. (2020). The decline of FANCM immunohistochemical expression in prostate cancer stroma correlates with the grade group. Pathology International, 70 (8), 542−550. DOI: 10.1111/pin.12953.
2. Dzaparidze, Georgi; Kazachonok, Dmitri; Laht, Kristi; Taelma, Heleri; Minajeva, Ave (2020). Pathadin – The essential set of tools to start with whole slide analysis. Acta Histochemica, 122 (7), 151619. DOI: 10.1016/j.acthis.2020.151619.
3. Dzaparidze, Georgi; Kazachonok, Dmitri; Gvozdkov, Alexander; Taelma, Heleri; Laht, Kristi; Minajeva, Ave (2021). Diagnostic significance of stromal changes in biopsies of prostate adenocarcinoma. Pathology – Research and Practice, 153436. DOI: 10.1016/j.prp.2021.15343
4. Semjonov, E.; Minajeva, A.; Dzaparidze, G.; Gvozdkov, A.; Tamp, E. (2020). Patohistoloogilise diagnostika digilahendused Eestis. Eesti Arst, 99 (5), 320−321.

The source code, the full-sized digital slides and generated sets of images for training (dataset), as well as the trained model of Pathadin, are available at the GitLab repository:
https://gitlab.com/Digipathology/Pathadin
https://github.com/geodza/Pathadin

Contribution of Georgi Dzaparidze to original publications:

Paper I: Study design, data collection, interpretation of results, draft of the manuscript to which authors contributed, critical revision of the manuscript for intellectual content, and approval of the final manuscript.

Paper II: Conception and development of Pathadin, study design, data collection, interpretation of results, draft of the manuscript to which authors contributed, critical revision of the manuscript for intellectual content, and approval of the final manuscript.

Paper III: Study design, data collection, interpretation of results, draft of the manuscript to which authors contributed, critical revision of the manuscript for intellectual content, and approval of the final manuscript.

Paper IV: Draft of the manuscript to which authors contributed, critical revision of the manuscript for intellectual content, and approval of the final manuscript.

ABBREVIATIONS

AI	artificial intelligence
CG	control group, biopsy
CTRL	control, radical prostatectomy
DAB	diaminobenzidine
DP	digital pathology
EAU	European association of urology
EPE	extraprostatic extension
CAP	College of American Pathologists
G	ISUP grade group of prostate adenocarcinoma
GUI	graphical user interface
HR	homologous recombination
HSV	hue, saturation, value
IHC	immunohistochemistry
ISUP	International Society of Urological Pathology
ML	machine learning
mpMRI	multiparametric magnetic resonance Imaging
MT	Masson's trichrome stain
NCT	non-cancerous tissue
PCa	prostate adenocarcinoma
PNI	perineural invasion
PSA	prostate-specific antigen
ROI	a region of interest
RP	radical prostatectomy
SSI	stromal staining index
FANCM	Fanconi anemia complementation group M
TG	test group
TGC	test group with cancer
TGW	test group without cancer
TOST	two-one-sided t-tests
TRG	training material for the machine learning
WSI	whole slide imaging

1. INTRODUCTION

Prostate adenocarcinoma (PCa) is the second most frequently diagnosed cancer in males worldwide and the fifth leading cause of cancer death in men (Bray et al., 2018). In Estonia, according to 2017 data of the National Institute for Health Development, PCa was diagnosed in 1113 cases, making 25.2% of all diagnosed malignancies in men. It means that the analysis of histological samples in the form of biopsies, chips, or prostatectomy samples of the prostate makes a significant part of pathologists' practice. The gold standard for a definitive diagnosis prior to radical prostatectomy (RP) is a systematic biopsy sampling, usually taken in 12 cores (Bjurlin and Taneja, 2014). Some treatment modalities are only applicable if a patient is at low risk for biochemical recurrence of localized and locally advanced prostate cancer (D'Amico et al., 1998), as defined in 2021 European Association of Urology (EAU) guidelines. On the contrary, only palliative therapy is rational in some cases of high risk. Thus, it is essential to minimize the discrepancy between the histology report in a biopsy and the actual find in RP. However, despite the progress in biopsy sampling and advantages in radiology, there still is a risk of changing the grade of PCa in RP. A targeted biopsy is upgraded in 23.3% of cases, while systematic biopsy, still been primarily used, has an upgrade rate of 42.7% at RP, as shown in a recent meta-analysis (Goel et al., 2020).

A question arises whether there is a way to improve the process of diagnosis in biopsies. There are various ways to approach the problem using new biochemical, radiological, or histological methods (Alchin et al., 2015). One practical consideration, as also mentioned in the latest College of American Pathologists (CAP) templates, is to count stroma between cancerous foci in biopsy as a part of a tumor length as it better correlates with the finds in RP (Arias-Stella et al., 2015; Karram et al., 2011).

Analyzing components of the tumor microenvironment, a variety of clinical studies suggest that reactive stromal changes can indeed provide valuable information and show independent prognostic potential as, for example, in the breast (Conklin and Keely, 2012; Olumi et al., 2000), colon (Halvorsen and Seim, 1989; Sis et al., 2005), and other tissues. The significance of stromal changes in PCa has also been described (Ayala et al., 2003; Silva et al., 2015; Miles et al., 2019) and correlated with Gleason grade (Osorio et al., 2019). Along with progression towards higher Gleason grades, the stromal phenotype change is accompanied by a progressive decrease in smooth muscle content and an increase in the proportion of myofibroblasts and cancer-associated fibroblasts (Cunha et al., 2003; Kiaris et al., 2004).

In clinical practice, biopsies are taken systematically from specific sites of the prostate, with the location documented in the letter of the referral sent to a pathologist. Thus, knowing the location of the highest ISUP grade in the RP, biopsies from the area can be retrospectively reevaluated for possible additional information, such as stromogenic changes, which can be suspicious.

The stromogenic reaction may be challenging to quantify with only hematoxylin and eosin (H&E) staining. There are broadly available markers, including immunohistochemical (IHC), that can highlight reactive changes. In the current manuscript, two stainings were used to highlight the microenvironmental changes. The first one is broadly available Masson's trichrome (MT) that serves as a good highlighter both for the simultaneous analysis of smooth muscle and collagen change in PCa. The second one is Fanconi-anemia complementation group M (FANCM) immunohistochemistry marker – the DNA reparation complex protein expressed in the normal prostate (Kasak et al., 2018). It is relatively new, and there are only a few manuscripts that evaluate its significance in the stroma with no systematic evaluation in the prostate.

Still, even with additional staining, stromal changes are usually evaluated in a less precise qualitative way, combined into groups, which can lose some interconnections and thus is inappropriate for the description of new markers, such as FANCM. At the same time, digital slide easily allows accurate and fast analysis meaning that digital pathology (DP) can be of significant assistance.

DP is a digitalization process of histological slides using specialized scanning machines with a further computer-assisted analysis of the whole-slide images (WSI), while microscope cameras only provide small fields of view. Following the quantification of immunohistochemical and -fluorescence markers (cellular level), which can now be automatically evaluated by machine learning algorithms (Hamilton et al., 2014), the main focus for a couple of last years is on automatically completed tissue analysis and diagnosis. In combination with machine learning (ML) and modern hardware, the opportunity for a computer-assisted diagnosis to become a routine is very realistic. Nevertheless, despite the claims that ML can already outperform pathologists in definitive diagnoses, such as Gleason grading (Arvaniti et al., 2018; Bulten et al., 2020), there is a list of challenges to overcome before ML can be routinely applied (Madabhushi and Lee, 2016). Among these are the subjective opinion of pathologists during model training and extreme sensitivity to the slide quality, meaning if the trained model is used in different laboratory settings, results can be unsatisfactory.

While still new and somewhat unreliable for a pathologist, ML could already find its place in daily routine. An example of practical application is a creation of a simple model distinguishing the prostate's main histological components, such as fibromuscular stroma, nerves, glands, and fat. Such a model would allow the performance of further independent and automated quantification of component changes- MT and FANCM intensity. Also, it could be applied to a screen for features essential to report, yet sometimes tricky to find: for example, extraprostatic extension (EPE) and perineural invasion (PNI). These changes are not so diverse and primal for a diagnosis as cancer grading but still have a critical value. Moreover, it could help to separate the glandular component with further analysis of epithelial markers, such as Ki67.

Despite the fact that novel solutions for DP analysis, including the open-source ones, are constantly developed, by the time of the start of doctoral

studies, there were no programs for simple annotation, creation, and augmentation of the dataset, training, and visualization of the result, to experience ML from scratch.

The work aims to quantify and evaluate the diagnostic significance of microenvironmental changes around different Gleason grades by creating a computational imitation of pathologists' work. The machine should distinguish and highlight histological components and assess the amount of nuclear (Ki67) and cytoplasmic staining, thus covering almost all essential diagnostic features except cancer differentiation. The manuscript should also serve as a manual for everyone willing to start with DP and ML in pathology and to encourage staff working with histological samples to train their models in a simple way.

2. REVIEW OF LITERATURE

2.1 Histology of prostate

The histological structure of the prostate is usually described in three or four zones (McNeal, 1984), which are essential to distinguish in the context of the current manuscript:

1. The peripheral zone makes about 70% of prostatic volume, from apex posteriorly beneath the capsule to base, surrounding transition, and central zones. Fibromuscular stroma is relatively loose with widely spaced smooth muscle bundles, and glandular complexity is moderate. About 70–80% of prostatic cancers originate from this zone (Reissigl et al., 1997).
2. The transition zone is about 5% of the prostatic volume surrounding the proximal urethra. It contains moderately compact bundles of smooth muscle. It is the main site of nodular prostatic hyperplasia. Prostate cancer arises in the transition zone in approximately 10–25% of cases (Lee et al., 2015).
3. The central zone is nearly 25% of prostatic volume. It surrounds the transition zone to the angle of the urethra to the bladder base and the ejaculatory ducts. It is a site of 2.5–5% of prostate cancer (Cohen et al., 2008). The ducts are large and irregular; glands are complex, frequently with papillary infoldings. The stroma is dense.
4. Anterior fibromuscular zone: not always considered as a zone, sometimes viewed as a part of the peripheral zone, lacks the glandular components.

Most of the glandular tissue is found in the peripheral and central zones. Stroma is the densest in the central zone, the least dense in the peripheral zone. The study samples used during the research were from the peripheral zone.

2.2 Prostate adenocarcinoma

2.2.1 Epidemiology of PCa

Following lung cancer, prostate cancer is the second most frequent malignancy in men worldwide, counting 1,276,106 new cases and causing 358,989 deaths (3.8% of all deaths caused by cancer in men) in 2018 (Bray et al., 2018). Prostate cancer incidence rates are highly variable worldwide for reasons not fully understood. One possible explanation is dependence on PSA screening programs (Quinn et al., 2002, Patasius et al., 2019). Around 20–40% of the PCa diagnoses in Europe and the USA could be due to overdiagnosis through extensive PSA testing (Draisma et al., 2009).

The age-standardized rate in Europe is 62.1 per 100,000 people, according to GLOBOCAN 2018 (Rawla et al., 2019), and is the most frequently diagnosed cancer among men, accounting for 24% of all new cancers in 2018. Further-

more, the incidence rates in European countries continue to increase slightly (Mottet et al., 2017). Although prostate cancer incidence rates are high, most prostate cancer cases are detected when the cancer is confined to within the prostate.

The international mortality rates also vary considerably, being 10.1 per 100,000 people in Western Europe, and have been steadily declining for the past years in most western countries (Taitt et al., 2018). Although not fully clear, it may reflect early detection and improved treatment (Collin et al., 2008; Etzioni et al., 2008).

According to 2017 data of the Estonian National Institute for Health Development, PCa was diagnosed in 1113 cases, making 25.2% of all diagnosed malignancies among men. In the age group of 60–79, every eight will struggle with illness. Currently, Estonia has no official prostate cancer screening program, although, in clinical practice, physicians routinely offer the test to middle-aged and older men. According to the study covering patients from 1995–2014 (Innos et al., 2017), the overall 5-year relative survival ratio increased from 58% to 90% over the study period; survival increased considerably for all stages. This corresponds to general European trends.

After PCa is suspected (pathological PSA, digital rectal examination, imaging, etc.), the gold standard for diagnosis is biopsy with further histology reports.

2.2.2 Histological stains used in PCa diagnosis

2.2.2.1 Overview of the main stains

Central and usually the only stain used in PCa diagnosis is H&E. At the same time, there is a growing number of literature analyzing the role of additional staining for the confirmation of the diagnosis and prognosis. In addition to H&E, the most frequent stains include:

1. The “triple antibody cocktail” is the most widely used additional stain (Ross et al., 2020). It amplifies the atypical glandular component and shows the presence or lack of myoepithelial cells. It consists of:
   1.1 Alpha-methylacyl-CoA racemase
   1.2 p63
   1.3 High Molecular Weight Cytokeratin
2. PSA – sensitive and specific for prostatic tissue and adenocarcinoma of prostatic origin. Loss of PSA stain correlates to poor differentiation and poor prognosis (Bonk et al., 2019).
3. Chromogranin, synaptophysin, CD56. The markers are used for neuroendocrine cells, frequently looking similar to Gleason 5 patter (Fine, 2018).
4. Androgen for luminal cells and seminal vesicles.
5. 34 beta E12 for basal cells.

6. Paired-box gene 8 (PAX8). It helps to differentiate urothelial carcinoma variants and adenocarcinoma of the urinary bladder or prostate (PAX8 negative) (Tong et al., 2008).

Additionally, markers as Ki-67, p53, PTEN, MYC, and ERG are actively used despite the lack of validation (Carneiro et al., 2018).

As can be seen, the markers cover exclusively glandular components of PCa, although PCa is no longer viewed as a disease of abnormally proliferating epithelial cells but rather as affecting the complex interactions between the epithelial cell and the surrounding microenvironment (Chiarugi et al., 2014, Guo et al., 2021). Thus additional stains for microenvironmental changes are gaining more and more attention.

2.2.2.2 Ki67 in PCa

Ki67 is a nuclear protein associated with cell proliferation (Scholzen and Gerdes, 2000). The staining is not frequently used in PCa, although studies display a strong correlation with Gleason grade, association with stage, seminal vesicle invasion, and extracapsular extension (Tretiakova et al., 2016; Verma et al., 2015). It has a significant prognostic value, and the importance is as well shown in the prediction of recurrence in prostate biopsies (Fisher et al., 2013; Kammerer-Jacquet et al., 2019). It may also help to distinguish such challenging samples as, for example, high-grade prostatic intraepithelial neoplasia and intraductal carcinoma, both frequently displaying Alpha-methyacyl-CoA racemase, p63, and high molecular weight cytokeratin complex positivity.

Recent studies show that a combinatory PSA/Ki67 immunoreactivity score may help to subdivide prostate cancers into groups of different clinical outcomes (Hammarsten et al., 2019).

As the aim of the manuscript is not only to focus on the prostate but provide an applicatory solution to rationalize the time of practitioners compelled to counting positive cells, Ki67, being one of the most commonly used IHC stains in pathology, is a perfect marker for testing automated nuclei counting with open-source solutions.

2.2.3 Histological grading of prostate adenocarcinoma

In 1966, Dr. Donald Gleason introduced the method for predicting the outcome in prostate cancer by distinguishing five histological grades based on glandular architecture and microscopic appearance using a 4x – 10x objective magnification (Gleason, 1966).

With some essential changes, the general principle of the method is still used today. The Gleason grading system is used in all prostate adenocarcinomas, except those with treatment effects (for example, after androgen withdrawal or radiation therapy) (Humphrey et al., 2015).

It sums two patterns (grades), primary (most predominant in terms of the surface area of involvement) and secondary, into the Gleason score. If no secondary Gleason grade exists, the primary Gleason grade is doubled to arrive at a Gleason score. Gleason sum is slightly different in RP and biopsy.

In RP:

- The primary pattern is assigned to the dominant pattern of the tumor (>50% of the total pattern.
- The secondary pattern is assigned to the next most frequent pattern (50%<X>5%)
- The tertiary pattern- is frequently found in RP and is not incorporated into the final sum if < 5%. If Gleason pattern 5 is >5% and constitutes the third most common pattern, some pathologists include it as the secondary pattern

In biopsy:

- The most prevalent pattern is graded as primary
- Any amount of the worst pattern is graded as secondary

The grading rules were modified by the ISUP and WHO in 2005 (Epstein et al., 2005), 2014 and 2019 (van Leenders et al. 2019).

Since 2014, a simplified patient-centered grading system composed of 5 prognostic Grade Groups (G) is adopted and validated by biochemical recurrence hazards ratios on cases from 5 academic centers (Epstein et al., 2015). This grouping is similar to PI-RADS and denotes prognostically distinct stratification. Currently, the Grade Groups are as follows:

G1: Gleason score 3+3=6
G2: Gleason score 3+4=7
G3: Gleason score 4+3=7
G4: Gleason score 8 (4+4=8, 3+5=8, 5+3=8)
G5: Gleason score ≥ 9 (4+5=9, 5+4=9, 5+5=10)

Before choosing the treatment option, the standard for definitive diagnosis is a systematic biopsy sampling, usually taken in 12 cores (Bjurlin and Taneja, 2014). Considering prostate-specific antigen (PSA), radiology, and biopsy histology, the risk for biochemical recurrence of localized and locally advanced prostate cancer is stratified as follows: low, intermediate, or high risk, corresponding to International Society of Urological Pathology (ISUP) Grade 1 (G1), G2 and ≥G3. This makes the basis for a treatment plan: whether the patient is suitable for active surveillance or watchful waiting, can the nerve-sparing prostatectomy be performed, how to behave in the case of a negative biopsy sampling with a rising PSA, etc. Some treatment modalities are only applicable if a patient is of low risk, with active surveillance or watchful waiting as an example (Lu-Yao et al., 2009). Recognition of tumor features, such as multifocality, also provides critical prognostic information regarding tumor

behavior (Epstein et al., 2005). Thus, it is essential to minimize the discrepancy between the histology report in a biopsy and the RP's actual find. 90–95% of prostate cancer is of acinar type (Shah and Zhou, 2019), which is primarily handled in current research.

2.2.4 Biopsy and RP Concordance

Despite the rapid progress in biopsy sampling and advantages in radiology (as MRI- targeted procedure), there is still a risk of changing the grade of PCa in RP. A targeted biopsy is upgraded 23.3% of the time, while systematic biopsy, still been primarily used, has an upgrade rate of 42.7% at RP, as shown in a recent meta-analysis (Goel et al., 2020). Before the 2005 ISUP consensus, the rate was even lower (Arias-Stella et al., 2015). The downgrade, which is clinically not as essential but should be considered, can also happen in 6–36% (Fukagai et al., 2001; Ozok et al., 2010; Van Praet et al., 2014). Different factors, as PSA density (Sfoungaristos et al., 2013; Sfoungaristos and Perimenis, 2013; Vellekoop et al., 2014), age (Epstein et al., 2012; Seisen et al., 2015), prostate volume, and even obesity (Truong et al., 2013) were tested for possible predictive value; none is used clinically so far.

Additional information, which could be attained from biopsy samples, gains more and more attention. As the applied markers for cancerous epithelial cells may behave insufficiently in a clinical setting, an idea of evaluating the significance of microenvironmental changes as an always-available component has emerged (Planche et al., 2011; Boufaied et al., 2019).

2.3 Stromal changes in carcinomas and their diagnostic value

2.3.1 General aspects

Cancerous epithelial complexes are known to recruit and transform normal cells into reactive tumor stroma, which plays complex roles in promoting tumor progression. Along with the progression towards higher Gleason grades, the phenotype change into a reactive stroma is accompanied by a progressive decrease in smooth muscle content and an increase in the proportion of myofibroblasts and cancer-associated fibroblasts (Cunha et al., 2003; Kiaris et al., 2004; Olumi et al., 2000), accompanied by the corresponding decrease in α-smooth muscle actin expression (Ayala et al., 2003). Myofibroblasts in a transformed tumor stroma synthesize extracellular matrix proteoglycans and metalloproteinases, some of which are tested as potential histological stromal markers in PCa. For example, a gradual increase of asporin expression in PCa stroma is associated with the disease progression (Hurley et al., 2016; Rochette et al., 2017). Increased versican expression in PCa stroma has been correlated with a

patient's poor survival. The stromal staining intensity of decorin has been found to decrease in malignant areas, but no grade-dependent gradual changes or correlation with survival were reported (Henke et al., 2012; Suhovskih et al., 2013). Based on a meta-analysis of the literature, matrix metalloproteinase-2 expression is significantly associated with PCa (Xie et al., 2016).

Stromal changes are thought to have a crucial role in cancer invasion, metastasizing, and castrate- resistance (Eiro et al., 2017; Langley and Fidler, 2011; Yang et al., 2017). It is claimed that the stromogenic reaction found in biopsy is a predictor of further cancer recurrence (Kweldam et al., 2018). Stromal-epithelial crosstalk to prostate cancer initiation and progression provides the impetus for combinatorial microenvironment-targeting strategies (Karlou et al., 2010; Valkenburg et al., 2018).

Stromal changes are challenging to quantify in rational numbers using a microscope, as, for example, in H&E, both muscles and collagen may have similar staining and architectonics, distinguishable only for an experienced pathologist. In order to find a diagnostically significant pattern between stroma-gland cross-reaction, especially in terms of new markers, the evaluation of such should be precise.

To evaluate the stromogenic reaction in PCa and demonstrate the advantages of DP for this purpose, two stainings were used: broadly used Masson's trichrome (MT) and, relatively novel in the prostate, Fanconi Anemia Complementation Group M (FANCM) antibody.

2.3.2 Masson's trichrome

MT is three-color staining: most recipes produce red keratin and muscle fibers, blue or green collagen and bone, light red or pink cytoplasm, and dark brown to black cell nuclei. In the context of the prostate allowing simultaneous analysis of smooth muscle and collagen, an old and largely used marker, MT is a good highlighter of stromogenic reaction and a good alternative to vimentin or α-smooth muscle actin to quantify such change. Along with other carcinomas, MT is also suggested to be stained in PCa as an additional diagnostic marker (Krušlin et al., 2015; Tuxhorn et al., 2002). In the manuscript, the hypothesis of a gradual increase of collagen type I, proportional to the ISUP grade and its predictive value, is tested.

2.3.3 Fanconi Anemia Complementation Group M

FANCM displays DNA binding against fork structures and an ATPase activity associated with DNA branch migration (Coulthard et al., 2013). DNA reparation complex proteins perform a protective role by stabilizing DNA double-stranded breaks and repairing DNA interstrand crosslinks in the process of homologous recombination (HR) (Ceccaldi et al., 2016), and are an emerging target in cancer therapy (O'Rourke et al., 2019; Pan et al., 2017).

Bi-allelic pathogenic alterations, affecting HR-related genes, such as *BRCA1, BRCA2,* are associated with HR deficiency and are identified in epithelial compartments of various cancer types, including breast, ovaries, and prostate (Riaz et al., 2017), but no reports on their expression in tumor stroma have been published during a period when this manuscript was prepared. Among HR pathway DNA reparation genes, the *Fanconi anemia complementation group M (FANCM)* encodes a DNA-dependent ATPase critical in DNA repair, anti-crossover activity, and prevention of chromosomal breakage in mitosis and meiosis (Basbous and Constantinou, 2019; Tsui and Crismani, 2019; Xue et al., 2015; Yan et al., 2010). There are numerous reports of families with segregating *FANCM* mutations and clustering of various cancer types, such as breast and ovarian cancers (Bogliolo et al., 2018; Catucci et al., 2018; Nguyen-Dumont et al., 2018; Nikolaidi et al., 2019). The evidence has led to the hypothesis that an insufficient level of the FANCM expression may represent a novel candidate marker for histological evaluation of prostate cancer risk and progression.

It is shown that the stroma of the normal prostate displays intense staining of the FANCM protein (Kasak et al., 2018). The current study is the first report on the systemic analysis of the FANCM protein expression in the cancerous prostate.

3. DIGITAL PATHOLOGY

3.1 General aspects

To simplify the understanding of the current state of DP, two parts should be distinguished.

The first is an image acquisition subsystem (scanning device) and a workstation environment with a WSI viewer with basic tools: manual measurements, annotations, simple manipulations with the image, and telepathology. Gaining approval in the United States and European Union (García-Rojo et al., 2019) DP is evolving and growing steadily, vividly demonstrating all its advantages during COVID-19 pandemics (Browning et al., 2021; Cimadamore et al., 2020). The annual growth for DP in Europe and the US is expected to be 8.2% for the next five years, according to the recent Frost & Sullivan's analysis (https://frost.com).

In Estonia, the use of DP for routine diagnostics was first started at the East-Tallinn Central hospital pathology department in September 2019 when Pannoramic 250 flash III by 3DHistech was installed: a mid-range device with a 250 slide capacity and 20x or 40x optical magnification. The device successfully processes a daily load of approximately 500 slides and is actively used by eight pathologists of the department, based on the author's observation. Most of the digitalization for this manuscript is performed mainly on this station.

Despite the high diversity of manufacturers, the scanning devices evolve rapidly and generally synchronously, mainly varying on slide capacity, optical magnification, and a short list of additional features, such as z-stack, immunofluorescence, immersion (Cui and Zhang, 2021; Pantanowitz et al., 2018), thus are not reviewed in this work. The resulting image has a similar pyramid form with a small thumbnail on the top, and a high-resolution picture on the bottom layer, providing a high range of field of views, not accessible by the microscope. Digitalized images are a basis for the advanced analysis of DP.

3.2 Advanced analysis in DP

The manuscript focuses on the advanced possibilities linked with DP. The theme is one of the most prominent points of interest in modern pathology. As the slide is digitalized, computer assistance of varying complexity, starting from the fundamental image analysis such as color-thresholding and ending with automatic diagnosis via machine learning algorithms, can be applied. In terms of the shortage of pathologists, this could be a significant support to diagnostics. Following quantification of immunohistochemical and immunofluorescence markers (cellular level), which now can be reliably performed automatically (Hamilton et al., 2014), the main focus for a couple of last years is on an automated tissue analysis.

Despite the promising results in automatic diagnoses, such as Gleason grading that can reportedly outperform pathologists (Arvaniti et al., 2018;

Bulten et al., 2020), it is currently facing a list of challenges, making it difficult to apply routinely (Madabhushi and Lee, 2016). Among these challenges are the subjective opinion of pathologists during model training and extreme sensitivity to the quality of the slide, meaning that if the trained model is used in settings of a different lab, results can be unsatisfactory.

Nevertheless, obstacles seem to be temporary as labs become more standardized and the augmentation possibilities of the image dataset evolve. The new trend in pathology induced the rapid development of both commercial and open-source solutions for advanced analysis.

3.2.1 Open-source solutions for bioimage analysis

As within the frame of the current study, there was no way nor aim to objectively evaluate the quality of all the commercial solutions; all the provided tools are based on open-source algorithms and freeware.

The list of libraries for bioimage analysis is enormous and constantly expanding by adding utilities of particular functions, as can be seen, for example, in DigitalSlideArchive repository: https://github.com/DigitalSlideArchive

It means that a programmer can combine a tool satisfying even the most specific needs of a pathologist.

The list of main libraries, that make a core for WSI analysis:

1. OpenSlide (Goode et al., 2013) – a vendor-neutral library to work with the main WSI formats:
    1. Aperio (.svs, .tif)
    2. Hamamatsu (.vms, .vmu, .ndpi)
    3. Leica (.scn)
    4. MIRAX (.mrxs)
    5. Philips (.tiff)
    6. Sakura (.svslide)
    7. Ventana (.bif, .tif)
    8. Generic tiled TIFF (.tif)
2. Bio-Formats (Linkert et al., 2010) – the solution for reading proprietary microscopy image data and metadata.
3. OpenCV (https://opencv.org/) – a set of programming functions mainly aimed at real-time computer vision.
4. Scikit-learn (https://scikit-learn.org/) – a Python machine learning library.
5. TensorFlow (https://www.tensorflow.org/) – a library for machine learning by Google that is easily combinable with Google Drive and Google Colab.

The most popular ready-to-work programs are:

1. ImageJ (Schneider et al., 2012). Released in 1997, it is the best known open-source software for biomedical image analysis with a wide variety of plugins and manuals that can display, edit and perform the analysis of varying complexity as well as save the majority of image formats; with the exception

of some WSI (as .mrxs), the format is essential for the current thesis. It requires significant modifications to cover the needs of the modern DP fully.

2. QuPath (Bankhead et al., 2017). A powerful open-source OpenSlide and OpenCV-based desktop bioimage analysis software. The only solutions in the list which initially were oriented to work with WSI images. It has flexible biomarker evaluation tools, provides batch-processing and scripting functionality, and allows to development and share of new algorithms to analyze complex tissue images. The image analysis is partially performed by exporting the image area to ImageJ. It cannot generate datasets and run third-party trained models.
3. CellProfiler (Lamprecht et al., 2007) enables a user without skills in programming to measure the phenotype from the thousands of images simultaneously; lacks a fully functional WSI support.

4. SUMMARY OF THE LITERATURE REVIEW

PCa is one of the most frequent malignancy diagnoses and makes a significant part of pathologists' work. Despite the recent improvements, the discrepancy in histology reports between the biopsy and RP is still high. This can potentially lead to inappropriate prognosis and treatment modalities. One practical consideration to improve the concordance of diagnosis is to quantify microenvironmental changes around the cancerous glands. Stroma is nearly always found in all biopsies; stromogenic reaction has already been proven to be a significant prognostic and diagnostic feature in different carcinomas as breast or colon and is actively studied in PCa.

Of two selected stainings to describe the stromogenic reaction, one is well known Masson`s trichrome, with controversies addressing its additional value in PCa diagnosis. The second one is relatively novel FANCM, which was not previously systematically evaluated in the prostate.

Precise quantification of the microenvironmental changes even highlighted with additional markers, may be challenging and time-consuming if performed with routine microscopy. At the same time, image analysis programs can perform color quantification objectively.

Machine learning algorithms can already do tissue segmentation at a high precision rate.

With a combination of digital pathology solutions, machine learning, and bioimage analysis algorithms, the stromogenic reaction can theoretically be evaluated in a semi- or fully automatic manner. The result should be quick and unbiased, which is especially important in terms of the descrtiption of new histological markers.

5. AIMS OF THE STUDY

The main aim of the work is to quantify and evaluate the diagnostic significance of carcinoma-associated microenvironmental changes around different Gleason grades and the applicatory use in biopsies.

This task first requires resolving a more general methodological issue as the development of a DP solution that is easy to use, accurate, and which working principle would mimic the pathologist's routine diagnostic process when working with a light microscope.

Specific tasks in the logical chronology to perform an objective biopsy analysis are as follows:

1. Create a WSI oriented open-source set of tools allowing to perform:
   - 1.1. Fundamental color analysis (K-means, color thresholding) in the region of interest (ROI).
   - 1.2. Quantification of diaminobenzidine (DAB) positive and negative cells in the ROI
     - 1.2.1. Using provided tools, evaluate DAB positive cell counting precision by quantifying Ki67 (as one of the most popular IHC markers) in PCa-s of different ISUP grades.
   - 1.3. Generation of image dataset for ML from digital slides.
   - 1.4. Visualization and validation of the trained model.
2. Create and validate a multiclass model, segmenting the prostate into five components – glands, stroma, nerves, fat, gaps for further independent analysis.
3. Using provided software tools, quantify stromal changes correlation with ISUP grade in MT and FANCM stained samples:
   - 3.1. Systematically evaluate FANCM staining in the prostate.
   - 3.2. In RP samples, objectively evaluate the significance of PCa associated microenvironmental changes and determine the rationality of further studies in the limited volume of biopsies.
   - 3.3. In biopsies, to evaluate the possibilities of practical diagnostic application of PCa associated microenvironmental changes.

The methodology is expected to be somewhat universal and serve as a manual for anyone willing to understand the basics of computer-assisted patohistological diagnostics.

6. MATERIALS AND METHODS

6.1 Ethics

The study was approved by the Ethics Review Committee of Human Research of Tallinn, Estonia (approval No 2173, issued on 12 May 2017) and the Estonian Data Inspection Protectorate (approval No 2.2.-1/17/50, issued on 19 Dec 2017). The nature of the study is retrospective. Patients remain anonymous.

6.2 General workflow

The methodology of the work resembles the routine workflow of a pathologist: studying histology on an H&E stained glass, distinguishing learned information on a new H&E slide, finding the corresponding region on slides with other stains, and analyzing the area. The main steps of the methodology are provided in **Figure 1.** The steps are universal and can be extrapolated to different tissues.

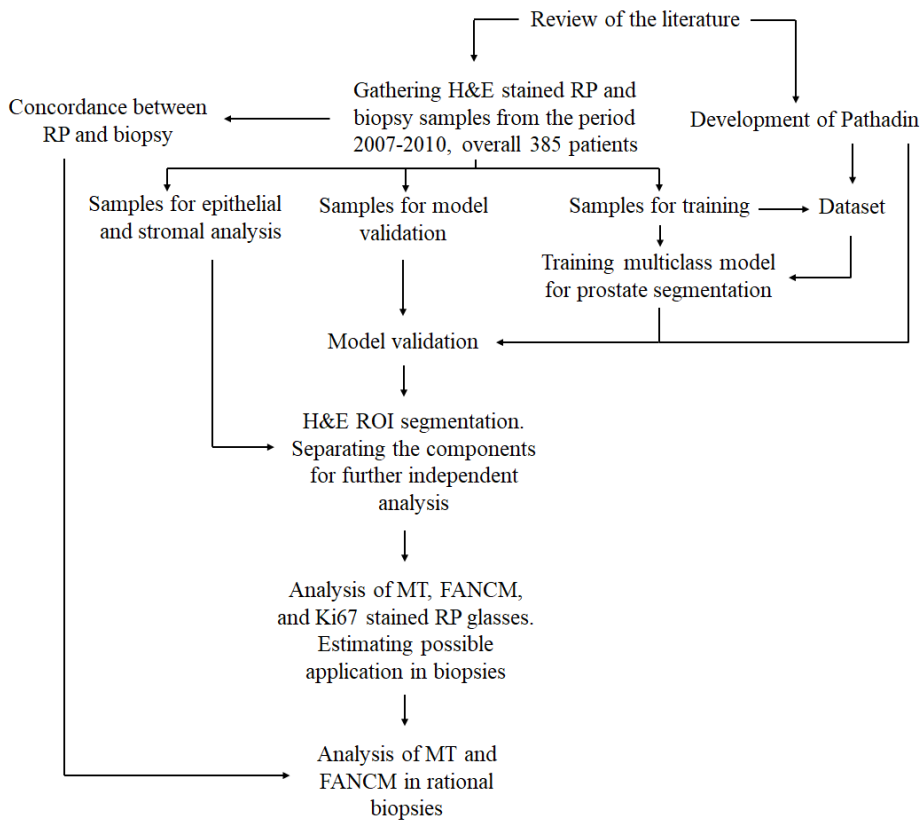

Figure 1. The main steps of the methodology.
(abbreviations: G- grade group, MT- Masson`s trichrome, ROI-region of interest, RP- Radical prostatectomy)

6.3 Samples

The material for the studies was acquired from East Tallinn Central Hospital from the period of 2007–2010. The inclusion criteria were a biopsy and RP performed at the same hospital to maintain the standard of the material and a pathology report. Overall, consecutive samples from 385 patients were analyzed, with a mean age of 65 (40–80) years at prostatectomy (Dzaparidze et al., 2021). The ISUP grade was reevaluated in both biopsies and RP according to 2016 WHO criteria. The distribution of patients according to ISUP grade in RP and biopsy is provided in **Table 1**.

Table 1. Distribution of patients according to ISUP grade in biopsy and RP.

		Biopsy G				
		G1	G2	G3	G4	G5
RP G	G1	136	2			
	G2	59	50	12	2	
	G3	16	27	28	6	2
	G4	7	2	9	14	1
	G5		1	1	6	4

(abbreviations: G- grade group, RP-Radical prostatectomy)

In 232 cases (60%), biopsy and RP ISUP grades were equal, upgraded in 128 (34%) RP, and downgraded in 25 (6%) cases. Among upgraded samples, the most frequent was, as expected, in G1 carcinomas in 82 patients. G2 was upgraded in 30, G3 in 10, and G4 in 6 cases.

Of 385 patients, 288 were in stage pT2, 94 pT3, and 3 pT4. Only five had metastases in regional lymph nodes (pN1). No patients with distant metastases were included.

In addition to the analytical set, 25 RP samples (5 per each grade group) were acquired from the West Tallinn Central Hospital to increase the diversity and minimize the batch effect in machine learning. All the patients were pT2 pN0 cM0.

For control, 11 autopsy samples were harvested. The mean age of the patients was 67 years (47- 89) with other causes of death than cancer and no previously diagnosed prostatic diseases. The majority of deaths had been caused by cardiovascular diseases (9/11). An autopsy was performed within 24 hours after death to minimize autolysis effects. The post mortem diagnoses are listed in **Table 2**.

Table 2. Information on autopsy controls.

Patient	At death (yrs)	ICD 10	Specification
1	83	I71	Aortic aneurysm and dissection
2	83	K85	Acute pancreatitis
3	54	I25	Chronic ischemic heart disease
4	69	I71	Aortic aneurysm and dissection
5	82	I13	Hypertensive heart and chronic kidney disease
6	57	I25	Chronic ischemic heart disease
7	89	I25	Chronic ischemic heart disease
8	70	T84	Complications of internal orthopedic prosthetic devices
9	47	I11	Hypertensive heart disease with heart failure
10	47	I42	Cardiomyopathy
11	53	I42	Cardiomyopathy

6.4 Staining protocols

H&E was stained using validated East-Tallinn Central Hospital protocols.

MT, FANCM, and Ki67 stained glasses were prepared from the same paraffin block. The staining protocols for MT and Ki67 are frequently used and can be found based on the catalog number.

1. For MT, Trichrome III Green Staining Kit (catalog n.r 860-031), a modification of Masson's Trichrome Stain by Ventana with Bouin's Solution application to intensify the final coloration; all deparaffinization and staining processes were carried out in Benchmark Special Stains by Ventana (Arizona, USA).
2. For Ki67 nuclear stain (catalog n.r 790-4286, rabbit monoclonal antibody (IgG)), all chemicals used were the products of Ventana), all deparaffinization and staining processes were carried out in BenchMark Ultra automated stainer (Ventana).
3. FANCM in the prostate was not previously systematically evaluated in the prostate, only in single non-cancerous samples (Kasak et al., 2018). All deparaffinization and staining processes were carried out in BenchMark Ultra automated stainer (Ventana); all chemicals used were the products of Ventana. The conditions and solutions used in IHC of the FANCM protein were as follows: deparaffinization of tissue sections with EZ Prep solution pH 8.4 at 72°C, heat pretreatment for antigen retrieval in Tris/ Borate/

EDTA buffered Cell Conditioning 1 (CC1) solution pH 8.4 at 100°C for 32 min and incubation with anti-human FANCM primary antibody (aa 1507-1679; x; CV5.1; Novus Biologicals, Abingdon, UK) at a dilution of 1:2000 for 24 min at 37°C. Primary antibody concentrations for the detection of the FANCM protein had been titrated to gain optimal staining of stromal compartments. During the optimization of the protocol, dilutions of 1:100 and 1:500 were also tested, in which weak positivity of FANCM staining was also detected in the glandular compartments. At these higher dilutions, the stromal compartment became overstained and indistinguishable from the background. The slides were incubated with secondary HQ Linker antibodies, followed by the application of HRP Multimer and the visualization via incubation with the OptiView DAB Kit, each step lasting 8 min. Tris-based buffer pH= 7.6–7.8 was used for the incubation of antibodies and the washing steps. Finally, the slides were counterstained with Hematoxylin II and post-counterstained with Bluing Reagent for 8 min each. Before mounting, slides were dehydrated through 70%, 96%, and 100% alcohols, cleared with xylene and covered using the permanent LCS- Liquid Coverslip mounting media and cover glass (Dzaparidze et al., 2020).

6.5 Slide digitalization

All analyzed slides were scanned using a 3DHistech Pannoramic Flash III 250 scanner (3DHistech, Budapest, Hungary) at a 20x magnification (resolution 0.24 μm / pixel, .mrxs format). Similarly to routine work, the magnification depends on the expected outcome: if the predicted outcome is on a cellular level, 40x or higher might be preferred. Otherwise, due to a drastic increase in the size of the slide, it is somewhat irrational.

The average size of a RP slide at mentioned resolution was 3.21 Gb, a biopsy – 0.78 Gb.

6.6 Pathadin

The software created for a digital analysis was named Pathadin *(Pathology + Paladin)* (Dzaparidze et al., 2020). The source code, original datasets used in the study, slicing, and training pipelines, as well as trained models, are provided at the open repository: https://gitlab.com/Digipathology/Pathadin
https://github.com/geodza/Pathadin

Minimum system requirements for adequate experience for provided binaries include monitor resolution of 1280 × 720, operation system Windows 7 SP1 or newer, CPU Intel DualCore, RAM 4 GB.

Among Java solutions, Pathadin is Python 3.6 software built with PyQT5 graphical user interface (GUI). Pathadin is based on the OpenSlide library. Central analytic libraries include Keras, Skimage/ Sklearn, and Histomics TK (Nalisnik et al., 2017). The interface of Pathadin is represented in **Figure 2.**

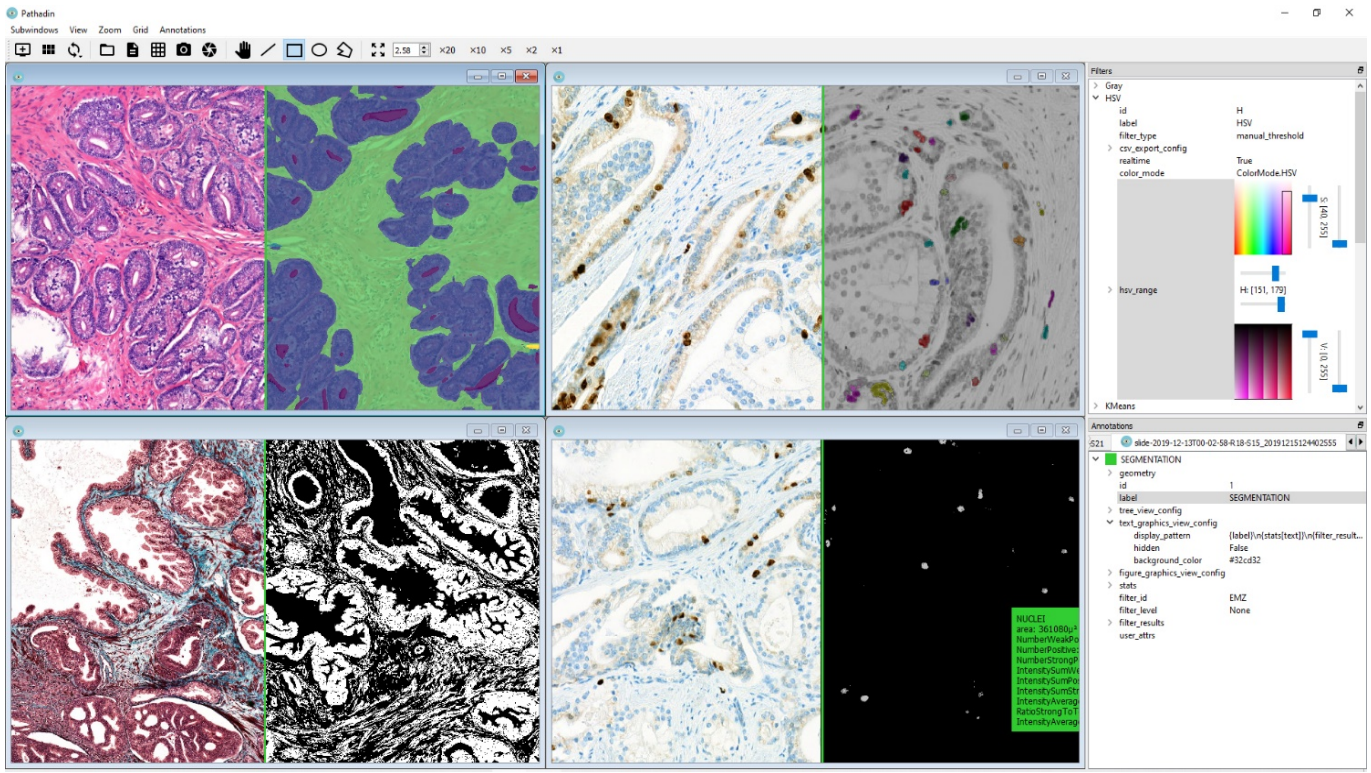

Figure 2. The interface of Pathadin, with simultaneous prostate segmentation on H&E slide, quantification of cytoplasm (red) stain in MT, and nuclei count in Ki67.

Pathadin is oriented to work with digital slides but includes all the main image formats. The concept of Pathadin differs from other alternatives listed previously. In contrast to unitary solutions, which require rather powerful machines, it is a combinatory set of tools, where each part can be modified separately. Such an approach should give a better understanding of functional elements of modern computer-assisted image analysis, make the program more flexible in the context of updates, and try different machine learning algorithms.

Pathadin performs routine tasks as color thresholding and K- means, significant for stroma quantification, are inside the software.

Currently, Pathadin provides the basic set of tools to begin with modern digital pathology:

1. Intuitive GUI: the application includes both basic image analysis algorithms, such as color thresholding, and advanced modules for IHC quantification by Histomics serving as an example of an integrated solution.
2. An advanced tool for slicing digital slides – used for a simple image dataset generation and augmentation for machine learning.
3. Reproducible example/pipeline for dataset generation and model training (U-net) with further integration to Pathadin.
4. All the generated data can be easily exported into a table for further analysis in statistical software.

Machine learning models' training is computationally heavy and excessively dynamic and requires rather powerful machines, thus frequently irrationally to be enclosed by GUI.

In the manuscript, the example of U-net training was based on Pathadin generated datasets and performed separately from GUI. The trained model was then imported back to the software.

All the analysis, model testing, and validation were performed with the following systems: Core i7-9760H, 2.6 GHz, 16 GB DDR4-2666 SDRAM / Ryzen 7 2700, 3.2 GHz, 16 GB DDR4-2066 SDRAM.

6.7 Multiclass model training and validation

The next step after the release of Pathadin was the creation of a working ML model.

The creation of a model includes the following steps:

1. Formulation of the expected outcome.
2. Creation of a dataset — a set of images for machine learning:
   2.1 Gathering of samples for training and validation.
   2.2 Annotation of regions of interest (something one wants to teach) to create a dataset for training and further validation.
3. Selection of an appropriate ML algorithm for training.
4. Testing and validation of the model.

If the outcome is unsatisfactory, additional samples, annotations, or choosing a different model might be required.

6.7.1 Selecting samples for the ML

Results of training and model universality are sensitive to the quality of samples. Homogenous samples gathered from the same lab during a short period of time may result in a batch effect- artificial sources of variation (systematically too light or uneven eosin, specific to one lab, etc.), which may confound the discovery of actual explanatory variables from data (Schmitt et al., 2021). There are computational methods for controlling the quality and increasing the heterogeneity of images (Janowczyk et al., 2019), but one of the most reliable methods for reducing the batch effect is by gathering samples from different labs. For the current study, the material was provided by the pathology departments of the East and West Tallinn Central hospitals. Focusing on the sufficient level of variation, samples of different quality were acquired, including the old ones with such artifacts as uneven H&E staining and thickness and stretches. The slides with diverse histological patterns in terms of pathology were preferred. Overall, H&E stained samples of 73 patients, including 38 RP and 35 biopsies, were harvested and divided into training and validation groups. The number of samples is the result of repetitive training and testing of the model, as described further.

RP's inclusion criterion was the presence of all five components: stroma, glands, nerves/ganglia, fat, and empty areas (as inside glands). All slides had a portion of non-cancerous regions and PNI of different extensions. Eleven had the presence of benign stroma and glandular hyperplasia. All ISUP grades, with the exception of the patterns, were covered. Inclusion criteria for biopsies were less strict due to the limited size of the tissue: all slides had stromal and glandular components, empty areas, and, most importantly, nerves/ganglia as assumably the most challenging, thus a component of the initial focus.

If microarray samples are used for training tissue, the annotation of the whole image due to its small size is appropriate. In the case of RP, only some areas are selected since it is better to get more RP samples than to increase the number of annotations on the sample. All slides were partially annotated to the stroma, glands, nerves/ganglia, fat, or gaps by two pathologists (**Fig. 3A**).

6.7.2 Dataset generation

For training (TRG), 38 slides, including 13 RP and 25 biopsy samples, were annotated with 1166 areas of different sizes, with the areas further sliced into smaller patches to create a dataset for machine learning. Depending on the expected outcome, variation in the patch size and magnification may result in different effects. In the manuscript, the magnification levels of 5x, 10x, and 20x were alternately tested with 256×256, 512×512, and 1024×1024 px patches. The optimal model appeared to be 256×256 px patches magnified to 5x since, for example, an extremely high magnification or small patches could not distinguish fat from empty gaps.

Of 1166 annotations, 114189 patches were generated. The resulting dataset consisted of multiple .zip archives consisting of the patch and a matching mask **(Fig. 3B)**. The mask represented pathologists' annotations meaning that each pixel had an integer value corresponding to one of the following classes: 0 – gaps, 1 – glands, 2 – nerves, 3 – stroma, 4 – fat. The majority of patches had an admix of at least two components; images were grouped by class by determining the dominating element for each mask:

0. gaps, 3865
1. glands, 7600
2. nerves, 20689
3. stroma, 48626
4. fat, 33409

The training process requires rather powerful machines; it can be done locally, but there are openly available and convenient cloud solutions. The patches were uploaded to Google Drive; the drive was then mounted in Google Colaboratory.

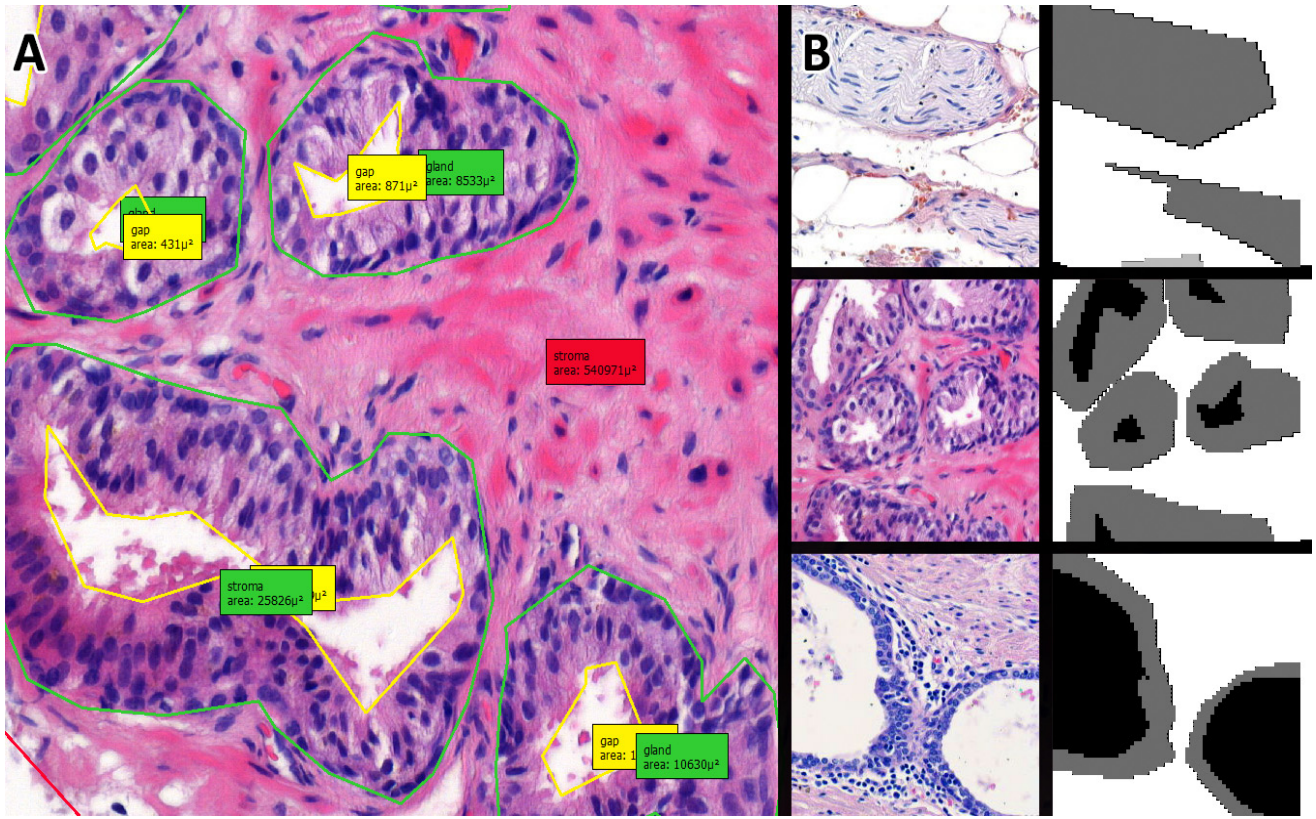

Figure 3. Preparation of the dataset.
A. An example of sample annotations for further dataset generation.
B. The dataset consists of multiple pairs of H&E images and corresponding black & white masks. Patches are 256×256 px**.**

6.7.3 Training

As can be seen from the above mentioned, the number of patches between groups varied significantly, which is evident since almost all patches had a stromal component. The different proportion of patches impacts the predictive value of the model. Because of the problem with class imbalance, the training dataset had to be balanced with both oversampling and undersampling techniques. 1000 samples were taken out from each group to build the intermediary validation dataset; remaining images were used for training, resulting in the following dataset:

0. gaps, 19689 (random oversampling)
1. glands, 19689 (random oversampling)
2. nerves, 19689 (base count, the main point of interest)
3. stroma, 19689 (random undersampling)
4. fat, 19689 (random undersampling)

Oversampling duplicates samples and can result in overfitting, making the model's predictions less accurate in new data. Undersampling removes samples from the dataset, which can result in the loss of important information required for training. In our case, the information in stroma and fat samples was repetitive and could be undersampled without valuable information loss. Samples with gaps are nearly identical and can be heavily oversampled. There was a risk of overfitting gland samples, but it did not turn out to be a problem.

The augmentation of the histological image is currently a topic of interest for data scientists in DP since usual techniques such as width shifts, height shifts, and zoom changes, which make images blurry on the outer sides, result in loss of valuable information in medical images. In the current manuscript, only vertical and horizontal flips were applied.

A Fully Convolutional Network Model model with the architecture that proved its efficiency in multiple biomedical studies was used for the multiclass semantic segmentation task (Falk et al., 2019). The architecture has a symmetric U-shape with the contraction path (encoder) on the left-hand side, where regular convolutions and max-pooling layers are applied. On the right-hand side is the expansion path (decoder), where we apply transposed convolutions with regular convolutions. The size of the input image is 256×256×3. The model has 5 classes with a Softmax activation layer, resulting in the 256×256×5 output size.

The model was trained for 13.2 hours in Google Colaboratory using the Tesla K80 GPU. The training was performed with a validation set using the sparse_categorical_crossentropy loss function since the mask pixel values are integer class values. The training process consisted of 30 epochs (1586s per epoch) and resulted in a validation loss of 0.0742.

Moreover, we attempted to train a model without a validation set. The trained model had a loss value of 0.0497. Although the loss value was lower, the model had worse performance in the production due to overtraining.

6.7.4 Validation

For validation, 50 of 1×1 millimeter ROI from 10 biopsy samples and 25 RP were analyzed. The ROI had at least two components and diverse structural complexity. The pathologists were asked to measure the area of the structural elements inside the ROI on the H&E stained sample; afterward, the trained model was applied to the ROI. The following parameters were calculated for each of five components per ROI:

1) Real composition of the ROI, as measured by the pathologist (R), mm^2
2) ML measured composition (M), mm^2
3) False-positive area (FP), mm^2
4) False-negative area (FN), mm^2
5) Error, FP+FN, mm^2
6) The true-positive area by ML (TP), mm^2
7) Precision, defined as the number of correct positive predicts = TP/(TP+FP)
8) Recall defined the number of predictions made out of all positive examples in the testing dataset = TP/(TP+FN).
9) F1, a harmonic mean of precision and recall = 2 × Precision × Recall/ (Precision+Recall).

Precision, recall, and F1 are the most important results in the context of model applicability.

Such an approach has become a standard for the validation of machine learning algorithms (Enomoto et al., 2006; Mäkelä et al., 2021)

6.8 Quantification of MT, FANCM, and Ki67

6.8.1 MT and FANCM in RP

After the main feature of Pathadin was ready for use, it was tested for practical application.

As the review of literature displayed controversies addressing stromal changes around PCa, the quantification of microenvironmental changes to establish general trends around carcinomatous nests was first performed on RP: there is more material in RP, and cancerous areas and the differentiation are clearly distinguishable; thus, the impact of the glandular component to the surrounding microenvironment could be evaluated precisely.

For FANCM, RP samples of 60 patients were analyzed. The ISUP grades were as follows:

- G1= 13; G2= 9; G3= 11; G4= 15, and G5= 12.
- MT: G1= 15, G2= 15, G3= 15, G4= 15, and G5= 12.
- Ki67: G1= 15, G2= 15, G3= 15, G4= 15, and G5= 12.

In addition to radical prostatectomy, 11 autopsy samples were retrieved for control (CTRL) from patients with no previously known or discovered autopsy prostatic diseases and stained with all three markers.

All the slides were divided into 1000x1000 μm (1 mm^2) regions of interest (ROI). From each cancerous slide, five ROIs from the normal non-cancerous (NCT) and five from the cancerous tissue were randomly selected for the analysis. In the case of the ROI consisting mainly of confluent epithelial nests (as in G4–5) and almost devoid of detectable stroma, the selection was manually drifted by one grid frame to include the closest stromal area adjacent to the cancer nest. 655 FANCM, 775 MT, and Ki67 1 mm^2 ROI were analyzed to evaluate the mean change per patient.

The covered area of 10 mm^2 per slide is approximately equal to the total surface of a single biopsy, consisting of both cancerous and cancer-free components.

As the ROI was selected and segmented into components by the trained ML algorithm, for FANCM and MT, the stromal staining index (SSI), defined as the percentage of the staining positive stroma over the total stroma in the ROI, was calculated. The HSV (hue, saturation, value) color model, an alternative to RGB with more precise alignment with the way human vision perceives color-making attributes, was used:

- For MT, the stromal staining index (SSI), a percentage of the collagen amount (green staining) of stroma over the total, was automatically calculated using the following settings H (50–135), S (0–255), and V (0–255) for green/blueish color.
- For FANCM, to quantify SSI of brownish DAB, settings were as follows: H (0–35), S (30–255), and V (0–220).

The selection of settings and analyses were performed under the visual control of two pathologists.

For Ki67, the validation method described in part 4.6.4 was applied. For DAB positive cell detection in the separated glands, the integrated module by HistomicsTK ver. 1.1.0 was used.

The settings for HSV and Histomics were defined empirically by two pathologists. All the analysis was performed under the visual control of pathologists. The main steps of the workflow are demonstrated in **Figure 4**.

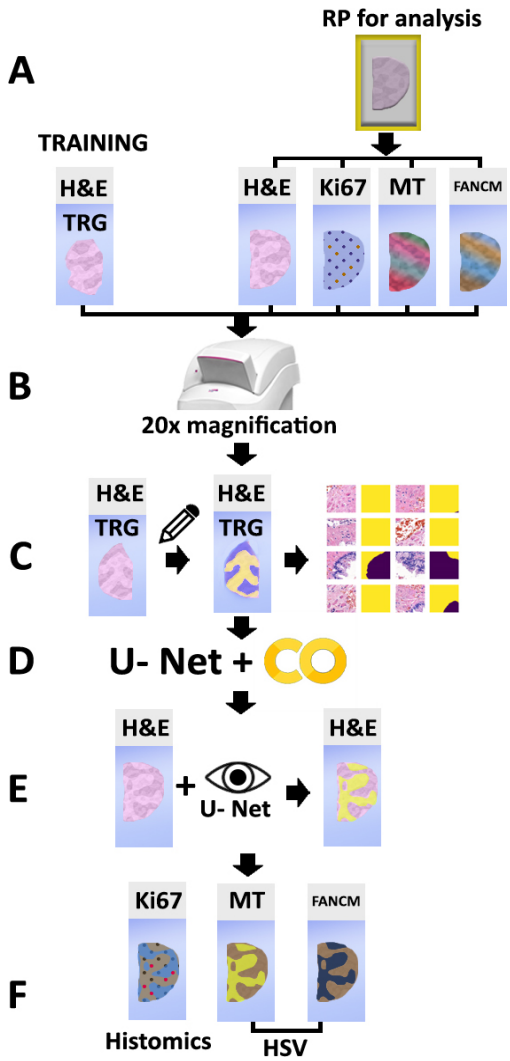

Figure 4. The workflow of image analysis.

A. FANCM, MT, and Ki67 stained glasses were prepared.
B. The set of glasses for training (H&E) and analysis (H&E, Ki67, MT, FACM) were scanned at 20x magnification with a resolution of 0,24 µm/px.
C. The training set was annotated by pathologists into stroma and glands and sliced into tiles.
D. The U-net model, in combination with Google's Colab, was trained for gland and stroma segmentation.
E. The trained model was applied to highlight glands and stroma on the 1 mm^2 ROI on the set of analytical H&E, facilitating the selection of these components by pathologists.
F. The selection of glands or stroma on the ROI was placed to the corresponding area on MT, FANCM, and Ki67 stained glasses. The amount of collagen in ROI was evaluated using the HSV color threshold. The expression of Ki67 defined as DAB positive nuclei to all glandular nuclei per 1 mm^2 (%) was quantified using HisomicsTK.

(abbreviations: MT-Masson˙s Trichrome stain, RP-Radical prostatectomy, TRG- training)

6.8.2 MT and FANCM in the biopsy

First of all, grade-associated changes have to be evaluated in RP samples to describe general trends in staining behavior. The next step is to determine if these changes can be extrapolated and have any value in the limited volume of biopsy samples. As the quantification of Ki67 in glands would not be different in biopsies, only MT and FACM were used in further analysis.

Unlike RP, the whole biopsy was analyzed. The HSV parameters were left the same. It is essential to articulate that analyzed samples were only from the peripheral part, excluding anterior fibromuscular stroma. Thus, the zone-dependent stromal composition did not impact the final result.

6.9 Statistics

Pairwise Wilcoxon Rank Sum test was used to compare SSI of FANCM, MT, and Ki67 among different Gleason grade groups, and controls in RP two-one-sided t-tests (TOST) was used to demonstrate the equivalence between cadaveric samples and non-cancerous tissue in RP A Wilcoxon signed-rank test was used in biopsies to establish if there is a statistically significant difference between the test and control groups.

A p-value of less than 0.05 was considered statistically significant after the Bonferroni correction. Spearman's ρ was used to show the dependence of FANCM of the age group. The charts were made using Excel, statistics were performed in R ver. 3.6.3.

7. RESULTS

7.1 The trained U-net model can quickly and reliably segment histological slides into components

Prior to the analysis of PCa associated changes, the computer was trained to distinguish five components of the prostate: glands, stroma, nerves, fat, and gaps.

Two pathologists evaluated ML results' quality; examples of H&E ROI and the corresponding mask are demonstrated in **Figure 5.**

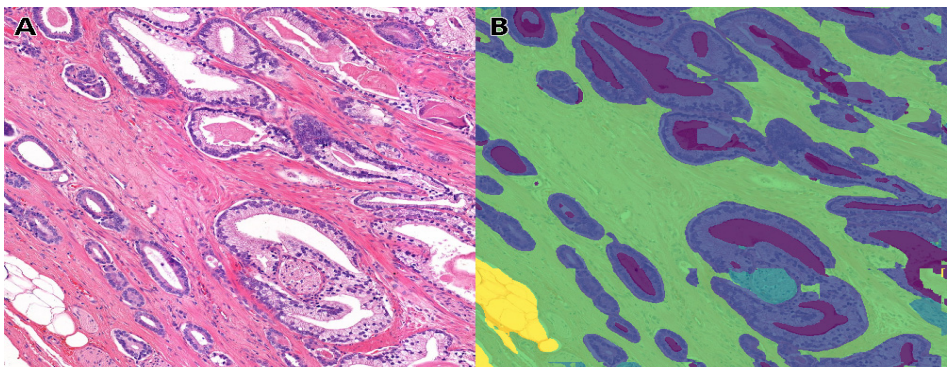

Figure 5. Sample of ML performed tissue segmentation.
A. Validation of ROI sized 1x1 mm^2, H&E staining.
B. ML analysis results. Stroma is highlighted green, nerves bluish-green, glands dark-blue, gaps violet, and fat yellow. The color scheme can be easily modified.
(abbreviations: ML- Machine Learning, ROI- region of interest)

The average time of the ROI analysis was 3.4 seconds. Cumulative model efficiency, covering all the five components: error was 4.598 mm^2, precision was 95.3%, recall 95.5%, F1 95.4%,

Stroma was present in all the 50 ROI, with 22.404 mm^2 annotated by pathologists. Efficiency of ML: error 1.845 mm^2, precision 95.7%, recall 96.1%, F1 95.9%. It is important to emphasize that the error, both false-positive and -negative, was mainly caused by the misinterpretation of nerves.

Neural tissue, including ganglia, was present in 38 ROI, with 4.391 mm^2 annotated. Efficiency: error 1.382 mm^2, precision 80.5%, recall 90.5%, F1 85.2%. Nerves posed a major challenge for ML, especially in the desmoplastic stroma, being frequently false-positive. In a single ROI, pale-colored sheets and scattered carcinoma cells were also wrongly interpreted as nerves, mimicking ganglion cells.

The glandular component was present in 31 ROI, covering an area of 10.950 mm^2. Efficiency: error 0.726 mm^2, precision 98.9%, recall 94.5% and F1

96.6%. No consistent pattern in mistakes was found, with the main cross-reaction with neural and stromal tissue.

Fat presented in 15 ROI with a total area of 4.460 mm^2. Efficiency: error 0.276 mm^2, precision 98%, recall 97.2% and F1 97.6%. As expected, the primary mismatch was due to the fragmentation and deformation of adipocytes, interpreted as empty areas or secretion components, and artificial masses inside the gaps interpreted as fat.

Empty areas (gaps), represented mainly as lumens of glands and blood vessels, were annotated in 44 ROIs, covering the area of 7.95 mm^2. Efficiency: error 0.368 mm^2, precision 98%, recall 97.2 and F1 97.6%.

The summary of calculated parameters per component is provided in **Table 3**.

Table 3. The result of prostate tissue segmentation.

	Stroma	**Nerves**	**Glands**	**Fat**	**Empty**
Pathologist, mm^2	22.404	4.391	10.950	4.460	7.795
Machine, mm^2	22.483	4.949	10.464	4.463	7.640
False-neg. mm^2	0.878	0.417	0.606	0.137	0.213
False-pos. mm^2	0.967	0.965	0.120	0.140	0.155
Error, mm^2	1.845	1.382	0.726	0.276	0.368
True pos., mm^2	21.525	3.984	10.344	4.323	7.485
Precision	0.957	0.805	0.989	0.969	0.980
Recall	0.961	0.905	0.945	0.969	0.972
F1	0.959	0.852	0.966	0.969	0.976

7.2 PCa associated changes in radical prostatectomy

As the ML model was created to help the independent analysis of prostatic components, the next step was to quantify the PCa associated changes in RP and biopsies. Only biopsies have limited volume; thus, general tendencies in changes had to be first evaluated in RP to further extrapolate these in biopsies.

7.2.1 Masson's trichrome staining demonstrates the grade-dependent gradual increase of relative collagen amount in PCa

The Trichrome III Green Staining Kit stains collagen green, muscle and erythrocytes red, and cell nuclei blue-black. In CTRL and NCT, stroma was predominately red because of a high composition of smooth muscle found in thick

extensive bands. The mean SSI of CTRL and NCT was 28 ± 8.1 (2SD) and 26.9 ± 7.8, respectively **(Table 4, Fig. 6)**. The TOST equivalence test demonstrated the equivalence of SSI and CTRL, and NCT (p= 1). **Figure 7** demonstrates the stepwise increase of reactive stroma in PCa until it becomes almost fully green with some small areas of entrapped bundles of smooth muscle in G5. The increase in SSI was statistically significant between CTRL and G1 carcinoma (mean SSI= 28% *vs.* 40.5 %; p< 0.001). A statistically significant elevation in the collagen level was also detected between G1 (40.5 %) and NCT (26.9 %), p< 0.001, and G3 (50.3%) *vs*. G4 (83%), p< 0.001. The differences remained statistically insignificant between G1 (40.5 %) vs. G2 (44.2%), p= 1; G2 (44.2 %) *vs.* G3 (50.3 %), p=0.06; G4 (83.0%) vs. G5 (83.6%), p= 1.

Table 4. SSI of collagen depending on ISUP grade.

	CTRL (n=11)	NCT (n=72)	G1 (n=15)	G2 (n= 15)	G3 (n= 15)	G4 (n= 15)	G5 (n= 12)
Mean %	28	26.9	40.5	44.2	50.3	83	83.6
± 2SD	8.1	7.8	12.4	9.9	8.2	7	8.5
Median %	28.8	26.6	42.2	44	49.8	83.2	84.2
Min. value	22.4	18.8	21.8	37.2	43.6	78.4	75.4
Max. value	36.4	35.2	46.8	52.2	58.2	89.4	91.6

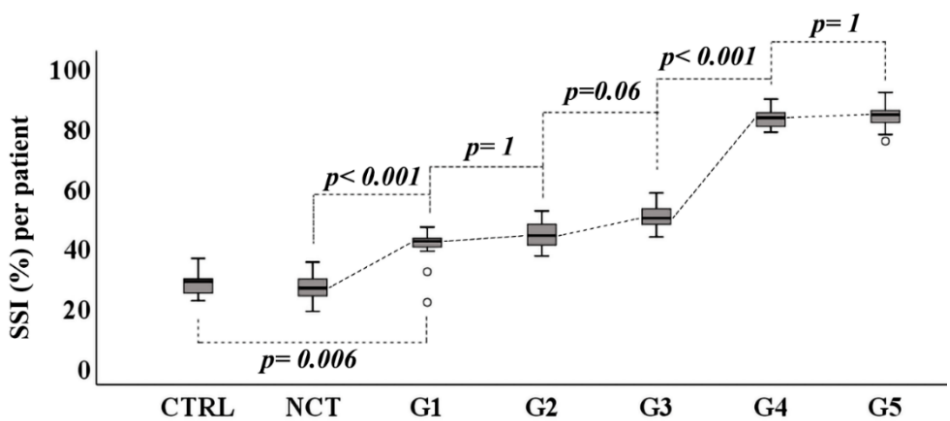

Figure 6. ISUP grade dependant stepwise increase of collagen SSI (green in MT). (abbreviations: CTRL- control group (autopsy), G- grade group, NCT- non-cancerous tissue, SSI- stromal staining index)

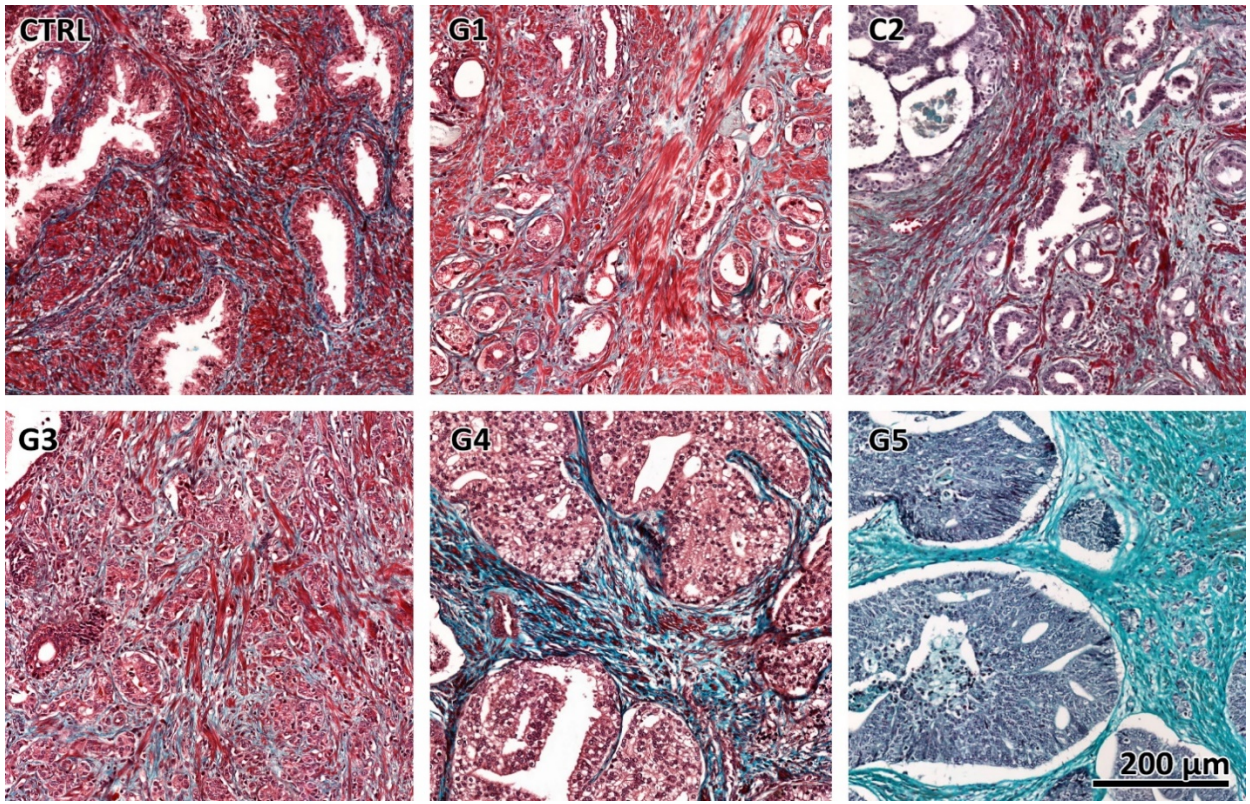

Figure 7. MT staining around different ISUP grade groups.
As demonstrated with Masson's Trichrome, the amount of collagen fibers (green) in stroma is minimal in non-cancerous tissue (CTRL) and gradually proportionally growing with ISUP grade groups. The change in muscles (red) is the opposite, being highly expressed in NCT, and only minimally in high-grade G5 cancer.

7.2.2 Stroma-specific strong expression of FANCM in autopsy prostate and non-cancerous radical prostatectomy areas

This work is the first one to evaluate FANCM staining in the prostate tissue systematically. The FANCM immunohistochemical expression was analyzed in 11 cadaveric prostates for controls and non-cancerous tissues from 60 radical prostatectomy samples with carcinoma diagnosis. Strong diffuse cytoplasmic expression of the FANCM protein was detected in smooth muscle cells in autopsy CTRL and NCT prostate tissues; a weak FANCM positivity was also observed in glandular compartments of either normal or cancerous epithelial nests, but only when incubating in a 20- fold increased antibody concentration. Furthermore, FANCM positive staining was detectable along the walls of blood vessels and, to a smaller extent, in nerve fibers.

TOST equivalence test demonstrated that FANCM expression between two non-cancerous control sample sets of CTRL and NCT were equivalent (p<0.001), the mean values of SSI being 39.1% and 41%, respectively (**Table 5, Fig. 8**). The patients' age at sampling (47–89 yrs.) did not show a strong association in correlation to the intensity of FANCM expression (Spearman's ρ= 0.136; p= 0.01).

7.2.3 FANCM staining demonstrates a grade-dependent gradual decrease in staining intensity PCa

In the controls, the intensely diffused FANCM positive stroma extended as close as to the basement membrane of normal prostatic glands; however, the cancerous glandular complexes appeared to be surrounded by a notably less intensely FANCM stained stromal rim already at the lowest G1 grade. The stepwise decline of FANCM staining intensity was apparent in each next grade until becoming barely visible in the highest G5. In G5 carcinoma, only the walls of blood vessels remained FANCM positive (**Fig. 9**).

SSI per patient demonstrated a statistically significant decline in the mean SSI (%) in G1 (27.7%) *vs.* CTRL (39.1%) and NCT (41%), p= 0.001 and p<0,001, respectively. A statistically significant drop in the FANCM expression level was also detected between G2 (24.7%) *vs.* G3 (17.6%), p=0.005. Differences remained statistically insignificant for declines G1 (27.7%) *vs.* G2 (24.7%), p= 0.3; G3 (17.6%) vs. G4 (14.2%), p= *0.06*; and G4 (14.2%) *vs.* G5 (12.4%), p= *1*.

The grade-dependent decline of staining intensity in the cancerous specimen was evident both per surface area and per individual stromal cells when the prostatectomy data were analyzed per each cancer patient with a spectrum of identified grade groups.

Table 5. SSI of FANCM depending on ISUP grade.

	CTRL (n=11)	NCT (n=60)	G1 (n=13)	G2 (n= 9)	G3 (n= 11)	G4 (n= 15)	G5 (n= 12)
Mean %	39.1	41	27.7	24.7	17.6	14.2	12.4
± 2SD	10.8	9	6.1	3.9	5	5.3	3.9
Median %	39	41.8	28.2	25	17.9	13.5	11.8
Min. value	32.4	32.1	23.9	22.1	13	11	9.4
Max. value	54.2	50.4	31.9	28.7	22.2	19.2	16

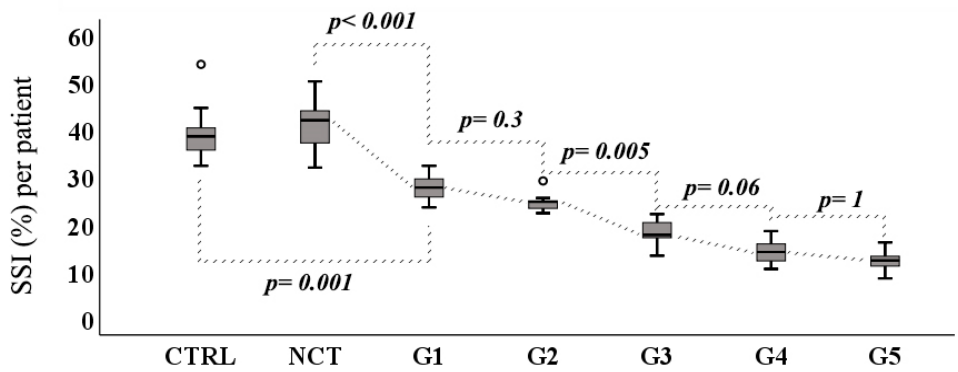

Figure 8. ISUP grade depending stepwise decrease of FANCM SSI.
(abbreviations: CTRL- control group (autopsy), G- grade group, NCT- non-cancerous tissue, SSI- stromal staining index)

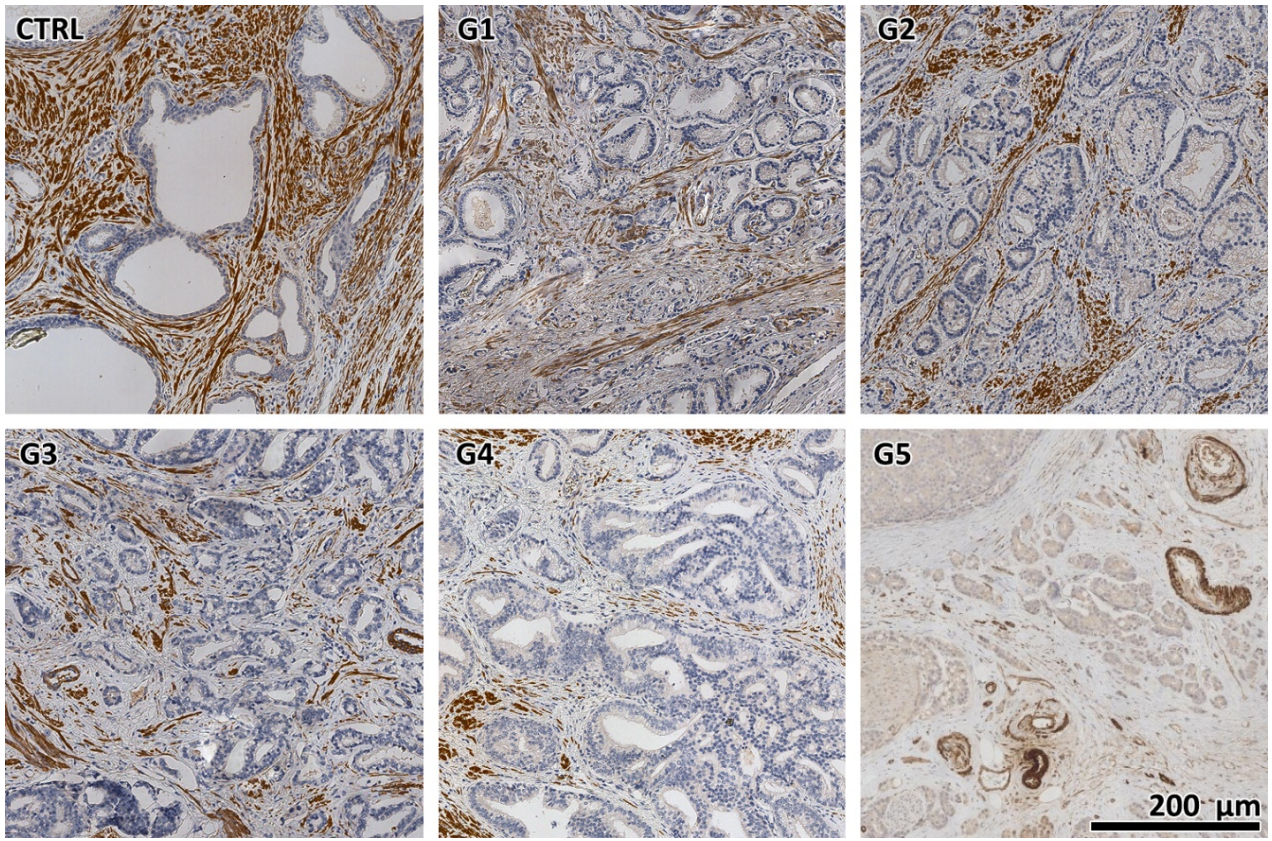

Figure 9. FANCM staining around different ISUP grade groups.
Already in G1, a decrease in FANCM expression over total stroma is seen if compared to CTRL. FANCM stromal staining intensity shows a progressive drop along with progression from lower to higher G. At G5, only the walls of blood vessels remained FANCM positive.

7.2.4 Ki 67 staining demonstrates ISUP grade-dependent gradual increase in PCa

Ki67 quantification (positive nuclei/all epithelial nuclei per 1 mm^2, %) was performed under the control of two pathologists: the percentage of DAB positive and negative cells was calculated using an open-source module by Histomics for cell counting. The module was integrated into Pathadin and counted cells according to empirically defined staining intensity and size (radius, area, the distance between cells). Overall, 775 1 mm^2 ROI were analyzed.

Averagely, the analysis of a single ROI was performed in 2 seconds (1–3 sec.). Based on all counted DAB positive and negative cells, the precision was 86.5%, recall 82.1%, and F1 84.2%. The algorithm failed in some cases of overlapping cells: this was especially prominent in high-grade carcinomas with many Ki67 positive nuclei of different staining intensity in G4 and G5 samples. 29% (39 of 135) of analyzed ROI taken from these areas had more than 25% of wrongly identified cells. In CTRL and G1-G3 samples with only single Ki67 positive cells, mistakes remained insignificant, with a failure rate of 4% (27 of 640) in the remaining ROI.

Ki67 expression, evaluated by computer and corrected by human vision, was almost undetectable in CTRL and NCT, with a mean value of 1.1% (±0.7) and 1 (±0.7%) per mm^2, respectively. The TOST equivalence test showed the equivalence of CTRL and NCT ($p=1$). The stepwise increase of Ki67 was seen in cancerous tissue: a statistically significant elevation in Ki67 was detected between CTRL (1.1%) and G1 (8.0%), $p<0.001$; NCT (1.0%) and G1 (8%), $p<0.001$; between G2 (8.9%) and G3 (14.5%) ($p<0.001$); G3 (14.5%) *vs.* G4 (23.5%) ($p<0.001$). Differences remained statistically insignificant between G1 (8.0%) vs. G2 (8.9%), $p= 1$; G4 (23.5%) *vs.* G5 (27.8%), $p= 1$. (**Table 6, Fig. 10 and 11**)

Table 6. Ki67 % per 1 mm^2 depending on ISUP grade.

	CTRL (n=11)	NCT (n=72)	G1 (n=15)	G2 (n= 15)	G3 (n= 15)	G4 (n= 15)	G5 (n= 12)
Mean %	1.1	1	8	8.9	14.5	23.5	27.8
± 2SD	0.7	0.7	3.3	3.1	6.5	10.6	16.2
Median %	1.2	1	7.8	9	13.8	22.4	27.1
Min. value	0.4	0.2	5.6	6.4	8.6	17.6	16.4
Max. value	1.6	1.8	11	11.6	20.8	38.6	42

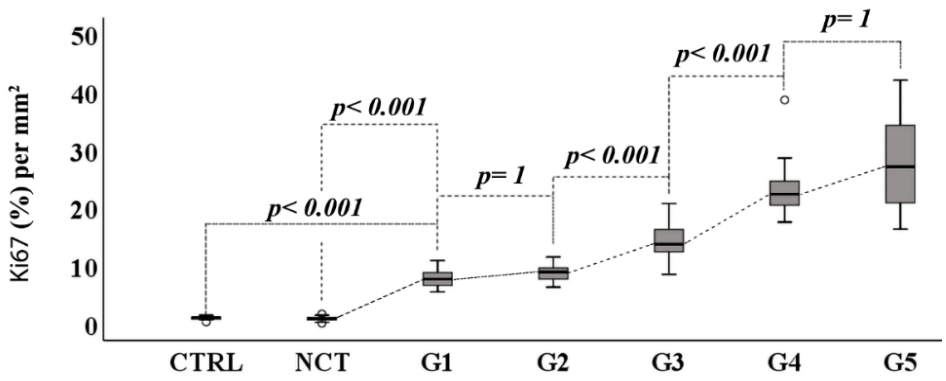

Figure 10. Stepwise increase in Ki67 depending on ISUP grade.
(abbreviations: CTRL- control group (autopsy), G- grade group, NCT- non-cancerous tissue, SSI- stromal staining index)

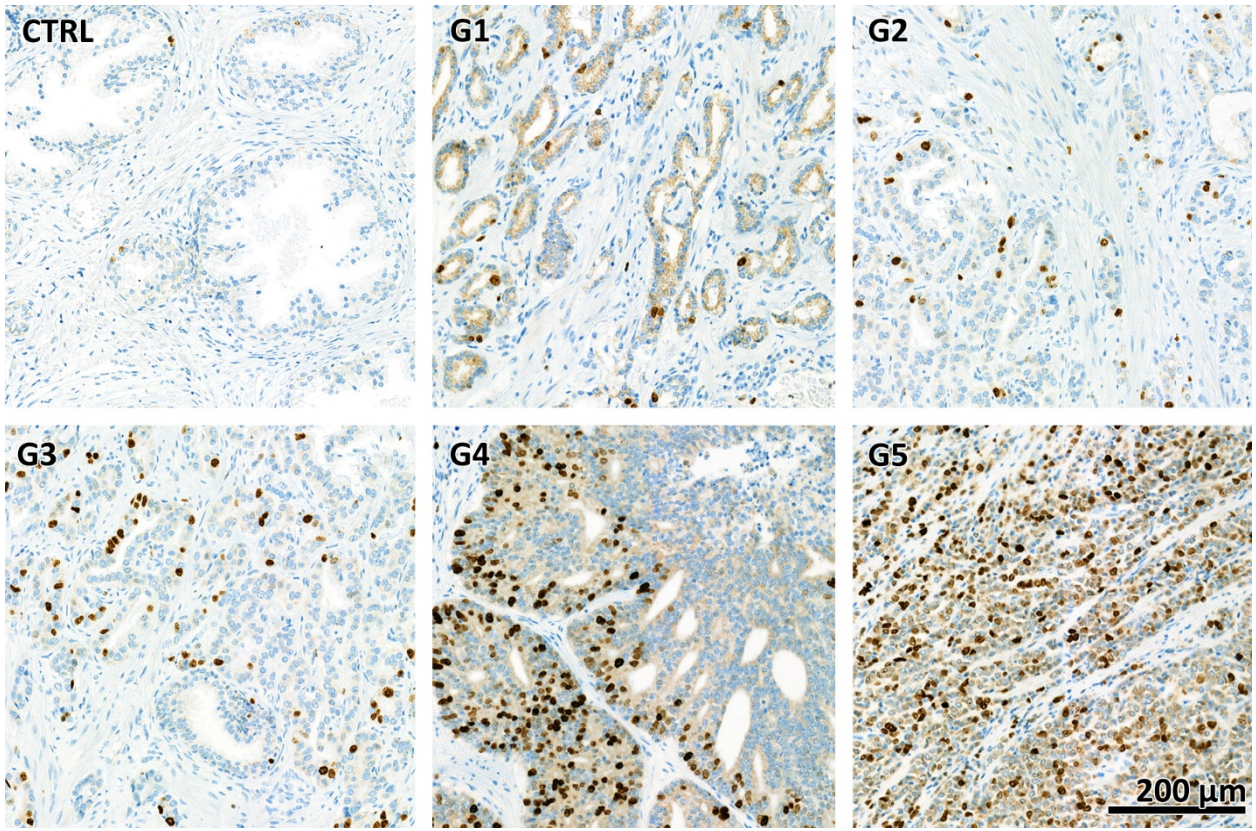

Figure 11. Ki67 expression in different ISUP grade groups.
Ki67 demonstrated only minimal nuclear expression in non-cancerous tissue; the number of DAB-positive cells is growing with increasing ISUP grade groups.

7.3 PCa associated changes in the biopsy

Following the analysis in RP, the MT and FACNM stainings combined with validated DP algorithms were applied to a limited volume of the biopsy.

7.3.1 G1 is most frequently upgraded and rationale for analysis in a biopsy

Taking into account the following facts:

1. There are markers to distinguish benign and cancerous changes (Alpha-methylacyl-CoA racemase, p63, and High Molecular Weight Cytokeratin cocktail).
2. G1 is the most frequently diagnosed differentiation grade (Eggener et al., 2015) and most frequently updated, as confirmed in our cohort – of 128 upgraded cases, 82 were G1: 59 changed to G2, 16 to G3, and 7 to G4.
3. False-positive G1 in biopsy may lead to a less radical treatment decision.
4. It was demonstrated on RP that stromal changes alone could not distinguish adjacent ISUP grades.

It was concluded that the only practical use of stromal changes in the current clinical paradigm would be in cancer-free samples to predict the existence of cancer at all and in G1 biopsies to predict less differentiated cancer nearby.

To test the hypothesis, the following groups of biopsies were formed:

(1) The control group (CG)- biopsies with G1 carcinoma, where no upgrade happened.
(2) The test group (TG), covering all patients with upgraded G1 biopsies. Test groups included samples with carcinoma (TGC) and samples without cancer (TGW) retrieved from the same patient.

As the prostate histology depends on the zone, the samples from the peripheral part were analyzed, excluding anterior fibromuscular stroma. In TGC, biopsies from the site of the highest ISUP grade in the RP were retrieved. In the case of several positive samples, the biopsy with the highest percentage of the area of the cancerous component was included. From the CG, biopsies with the highest percentage of the cancerous area were retrieved.

All the upgraded 82 G1 (TG) were stained with FANCM and MT and compared with 50 samples without the upgrade (CG). **Table 7** summarizes biopsy and RP cancer data along with available PSA values of study patients, including the extent of distribution in the prostate. Although some tumors were also present in the transitory and central zones, only biopsies from the peripheral zone were included for comparison.

Table 7. Information on included G1 patients and samples

	TG	CT
Age at biopsy	63.4 ± 6.5	62.5 ± 5.9
Total PSA (ng/ml)	6.41 ± 1.92	5.9 ± 1.6
Biopsy:		
Number of cores	9.6 (8–12)	9.4 (8–12)
Positive cores	2.3 (1–7)	2.6 (1–8)
Area of the core (mm^2)	6.1 ± 1.7	6 ± 1.8
% of microenvironment	66.9 ± 14.2	70 ± 14.1
% of cancerous glands	15 ± 3.3	14.8 ± 2.9
Tumor presence in RP:		
Central	2	0
Transitory	11	7
Peripheral	82	50
Anterior fibromuscular	5	1

(abbreviations: TG- test group, with Gleason upgrade; CT- control group, without upgrade)

7.3.2 Masson's trichrome displays a statistically significant change between cancerous and cancer-free samples but not between upgraded and non-upgraded

Biopsy samples with an upgrade in RP were compared with samples without the upgrade and samples without cancer. Using MT stain, the change in the quantity of collagen (bluish color) was analyzed with the SSI and expected to be higher in carcinomas. The mean SSI in non-upgraded (control group, CG) biopsies was 41% (20–78); 44% (23–89) in samples from upgraded cancerous group (TGC) and 37 % (15–57) in samples without cancer (TGW) (**Fig. 12**).

No statistically significant difference was found between non-upgraded and upgraded groups (*p=0.84*). SSI of 31 samples in the TGC group was higher than 95 CI of the CG (38–44 %), with 4 of 7 samples from the region of G4 carcinoma being among these samples.

The difference between TGC and TGW appeared to be statistically significant (*p=0.012*) despite the major overlap in SSI between groups.

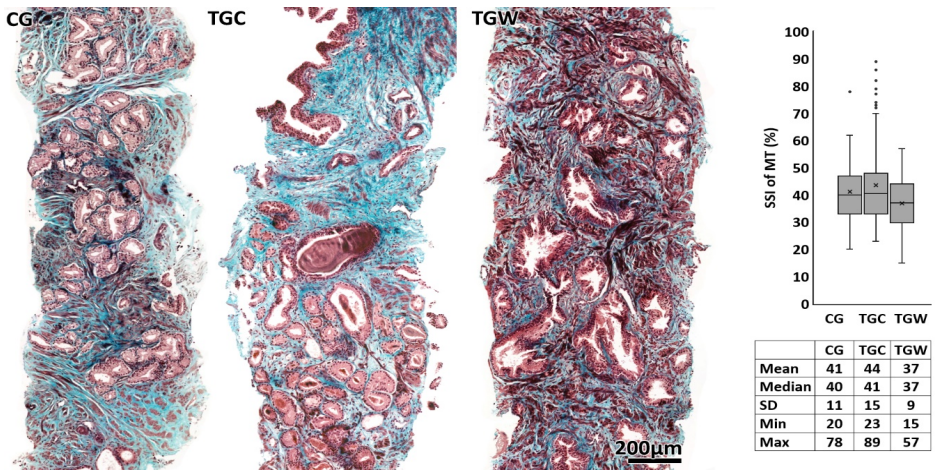

	CG	TGC	TGW
Mean	41	44	37
Median	40	41	37
SD	11	15	9
Min	20	23	15
Max	78	89	57

Figure 12. Masson's trichrome staining in different biopsy samples.
Compared to samples without cancer (TGW), in cancerous samples (CG and TGC), the number of collagen fibers is higher (bluish), the muscles are fragmented and thinner. In some cancerous samples taken from the area where the ISUP upgrade happened, there is only a minimal residual muscular component. On the right, an overview of SSI distribution in different samples is presented; a significant overlap between the groups is seen. The "X" on the barplot indicates the mean value of SSI.

7.3.3 FANCM displays a statistically significant change between cancerous and cancer-free samples but not between upgraded and non-upgraded

Biopsy samples with an upgrade in RP were compared with samples without upgrade and samples without cancer. With FANCM, the quantity of DAB positive stromal elements was evaluated, with the SSI expected to be lower in carcinomas. The mean SSI in the non-upgraded (CG) was 36% (13–59); 34% (9–58) in samples from the upgraded cancerous group (TGC), and 44% (22–69) in the group without cancer (TGW) (**Fig. 13**).

No statistically significant difference between the non-upgraded (CG) and the upgraded (TGC) specimen was found ($p=0.5$). SSI of 37 samples in the TGC group was higher than 95 CI of the CG (33–40%), with 5 of 7 samples from the region of G4 carcinoma being among these samples.

The difference between TGC and TGW appeared to be statistically significant ($p<0.001$) despite the major overlap in SSI between the groups.

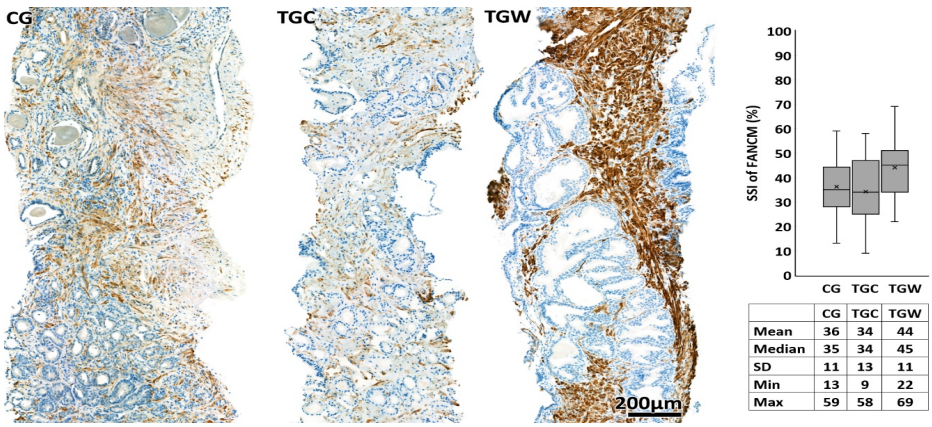

	CG	TGC	TGW
Mean	36	34	44
Median	35	34	45
SD	11	13	11
Min	13	9	22
Max	59	58	69

Figure 13. FANCM staining in different biopsy samples.
Compared to samples without cancer (TGW), in cancerous samples (CG and TGC), the amount of DAB is significantly lower. In some cancerous samples taken from the area where the ISUP upgrade happened, there is almost only hematoxylin. On the right, an overview of SSI distribution in different samples is presented; a significant overlap between the groups is seen. The "X" on the barplot indicates the mean value of SSI.

8. DISCUSSION

8.1 FANCM and MT in radical prostatectomy samples

FANCM immunohistochemical expression in stroma has been previously described in a few normal prostate samples, but this larger cohort analysis was the first systematic comparison of FANCM immunohistochemical expression in normal and cancerous prostate samples. The analysis was performed with a simultaneous evaluation of stromogenic changes in MT, straining muscles, and collagen, to display a simultaneous decrease in smooth muscle cells and increase in collagen composition proportionally to the ISUP grade. The current study confirmed FANCM expression to be highly stroma-specific in the normal prostate and showed a grade-dependent gradual decline in prostate carcinoma. Per patient, the difference remained statistically insignificant between adjacent ISUP grade groups, except G2 vs. G3 and G1 vs. controls.

This morphological study demonstrated there was no difference in FANCM expression between unaltered stromal areas from cancer patients and the stroma of the prostate from cancer-free controls, thus indicating the absence of underlying baseline alterations in FANCM protein expression, which could potentially affect susceptibility to PCa in our entire cohort.

The studies in animal models and human PCa report the phenotype change in reactive tumor stroma with loss of myoepithelial cells and an increase in the proportion of CAFs (Gravina et al., 2013; Yang et al., 2017). It suggests that FANCM depletion is a secondary change, corresponding to the formation of the reactive tumor stroma.

Prior to the current paper, there have been no reports on the role of homologous recombination DNA repair pathway protein expression in the cancer stroma. Various other expression pattern changes of these proteins have been reported in the epithelial compartment of PCa: BRCA1 was increasingly expressed in cancer cell nuclei in higher grade PCa, heralding worse clinical outcomes (Fiorentino et al., 2010; Schayek et al., 2009). BRCA2 has revealed a much more sophisticated response as membranous staining declined, but cytoplasmic expression increased with higher grade, and, notably, lack of C-terminal expression in the cytoplasm was associated with a reduced risk of rapidly fatal prostate cancer (Thorgeirsson et al., 2016). Results of FANCM expression in the prostate draw attention to the potential role of the homologous recombination DNA repair pathway in cancer-associated stromal changes and their further research. Of notice, if used in ultra automated stainer, the FANCM antibody from Novus Biologicals appeared highly cost-effective, gaining optimal stromal staining at 1:2000 dilution.

Even though Masson’s trichrome being a widely available staining, we didn’t find a simple method of precise quantifying collagen. In this manuscript, an HSV color model was applied, providing the results in seconds. An alternative solution would be K- means color clustering, included in Pathadin: an objective yet straightforward and difficult to manipulate method, less precise

in some cases. As with FANCM, Masson's trichrome staining demonstrated a statistically significant gradual increase in the collagen amount in PCa, depending on ISUP grade, but not between the adjacent groups – there was considerable overlap in 95 Cl. On the other side, there was only a minor overlap between low and high-grade carcinomas.

In conclusion, both markers displayed insufficiency in distinguishing adjacent grade groups or detecting stromogenic reactions in non-affected parts of the prostate. On the other hand, it is essential to emphasize that there is evidence that mortality in the G2 group is only slightly higher than G1 (Rider et al., 2013), while men with high-risk localized PCa or more advanced disease have substantially higher mortality compared with G1 and G2; there is some overlapping in SSI between adjacent grade groups, but there is only minor overlapping between low- and high-risk carcinomas defying clinical prognosis.

8.2 FANCM and MP in biopsy: diagnostic significance and practical application

The essential part of the work was to evaluate whether microenvironmental changes found in RP are applicable to biopsies. For this purpose, biopsy and RP samples of 385 patients were reevaluated.

Results of the biopsy analysis showed that G1 carcinomas are most frequently diagnosed and further upgraded in RP. In G1 carcinomas, stromal staining indices appeared to overlap with ones from RP with upgraded PCa. However, the difference between cancerous and non-cancerous samples bore statistical significance.

The amount of stromogenic reaction is traditionally graded qualitatively: minor, moderate, and extensive, for example, as there is no simple way for a quantitative analysis of stroma using only human vision. Such gradation is easy to use; however, it loses its precision and is not applicable in new markers and experimental works. Digital pathology analysis performed in this work allows performing stromal staining quantification of the entire biopsy material rapidly.

As biopsies cover only a tiny part of the prostate and provide limited information, which can be significantly impacted by preanalytical procedures, stromal changes could potentially predict the presence of higher grade carcinomas. Two markers, MT and FANCM, which in previous publications demonstrated the grade-dependent change of expression in RP, were analyzed in biopsies to test two hypotheses.

First, stromal statistically significant composition differences could be revealed between cancerous and non-cancerous areas from the same anatomical locations both by FANCM and MT stain.

The moderate sample size and inclusion of G1 in this study represented a realistic clinical setting, and as it showed overlap in SSI between the G groups, the routine use as a discriminative marker can't be advised. Also, it should be kept in mind that in the case of elderly patients, stromal changes can be caused

by other conditions, such as, for example, stromal hyperplasia or inflammation, which in terms of the limited size of the sample could be challenging to distinguish.

Secondly, a difference in the stromal compound between samples with and without ISUP upgrade in RP was analyzed, as, presumably, stromogenesis is correlated with cancer differentiation. We found no statistically significant difference between these groups. To some extent, this can also be caused by a consciously original routine cohort with the predominant upgrade from G1 to G2. The expectation to distinguish adjacent groups with stromogenetic changes in biopsies is somewhat optimistic, especially, taking into count that the stromogenic changes are apparent only on a limited distance. Promisingly, some SSI values were outside the 95% interval of the control group, meaning that there can be found a cutoff value for SSI in G1 carcinomas, which could help predict changes to a higher grade in the area of the biopsy.

In conclusion, despite somewhat similar results in MT and FANCM stainings, it could be seen that the overlap in SSI expression in FANCM was slightly less. Taking into account the availability of different stromal markers, which could potentially show higher specificity and sensitivity, and modern solutions in image analysis, it can be encouraged to study the composition of stroma with new emerging stains.

8.3 Ki67 in radical prostatectomy samples

The quantification of nuclear IHC is no longer an experiment, rapidly becoming a routine solution, provided by commercial (e.g., CellQuant by 3DHistech) and open-source tools, such as Histomics. Although Ki67 is not frequently used in PCa, it is one of the most popular stains, which requires precise and time-consuming calculations; for this reason, it was decided to be included in the current work. The module showed its effectivity, calculating the % of Ki67 staining in PCa, only struggling with overlapping cells of G4 and G5 carcinomas. It should be articulated that better precision could be achieved with algorithms oriented for a single task, explicitly (Acs et al., 2018; Saha et al., 2017); Histomics was selected for its simplicity in use and universality.

Under the visual control of pathologists, results demonstrated the correlation between Ki67 expression and Gleason score in numbers similar to the large Ki67 studies (Richardsen et al., 2017; Tretiakova et al., 2016b).

8.4 Application of digital pathology and machine learning in the prostate histology

The critical part of PhD studies was to create an easily reproducible multiclass model for PCa compartments analysis to see if advanced digital pathology solutions can already be helpful in daily routine. For this purpose, the segmentation of prostatic tissue into five universal components, meaning it can be adapted to samples of many different types, was created.

Although the model was quick and displayed a high predictivity rate as well as was seemingly simple, it posed some challenges we struggled to overcome.

Distinguishing fat tissue and empty areas is essential in the theoretical paradigm of fully automated analysis in order to avoid a false-positive pT3a stage. In single ROIs, gaps included processing caused artifacts, such as eosinophilic stripes or thin tissue fragments. The algorithm counted them as adipocytes. Fortunately, the problematic areas were small, and the background remained genuinely true.

Significantly more challenging was to distinguish between stroma and nerves. Areas of fibrous proliferate, such as stromal hyperplasia or desmoid reaction, especially in older, manually-stained slides specifically found from the archives, were occasionally interpreted as nerves. These slides may have grayish areas with lesser eosin and, especially if stretched in a biopsy, can indeed mimic nerves even for an experienced eye; at this point, only IHC can be decisive. Neither the dataset enlargement nor manipulations with magnifications or patch size impacted the outcome; the model fluctuated between false-negativity and false-positivity in nerve detection. For such cases, IHC cannot be replaced.

In some ROIs, the ML segmentation mask appears to be prominently angular and square. This effect is due to the final image being composed of smaller 256x256 px patches, generated using a step size that is equal to the patch size, making the patches non-overlapping. For ML, a tissue element, such as a nerve, extending between several patches and recognized as a single structure by the pathologist, is composed of independent images. The residual part of an element, extending across the border of an adjacent patch, loses prominent features required for the model to assign it to the same class as the main body, resulting in the sharp demarcation between adjacent mask elements. This can be easily fixed by changing the step of ML and thus creating an overlay of the patches. It will make a better visual outcome but results in a slightly increased analysis time.

On the other hand, as concluded from experiment results, ML can be reliably used to quantify secondary features before the sample gets to the pathologist, thus simplifying their work. These features are not as sensitive and pathologist-dependant as Gleason's grade but still essential and time-consuming to report. The model can be combined with the cellular analysis, as, for example, the IHC quantification or detection of inflammatory cells; these algorithms are available in many open-source solutions, including Pathadin.

Currently, Pathadin includes only a few features but is rapidly evolving, aiming to make use of computer-assisted analysis as convenient as possible. It demonstrates that there is no need for significant resources to experience the advantages of modern computer-assisted analysis. WSI analysis is a relatively new world, full of new ideas. A pathologist should be encouraged to test experimental open-source algorithms, both by individual developers and giants, such as Google, as well as give feedback and advice on the provided solutions. Such collaborations will help to make science transparent and precise in all its manifestations.

9. CONCLUSIONS

The main task of the work was to objectively analyze the amount and diagnostic significance of carcinoma-associated microenvironmental changes around different Gleason grades and the practical use of such changes, especially in biopsies.

Given that the microscope has limitations to perform the precise evaluation of histological changes, a tool based on modern digital pathology solutions was developed and tested.

The results in logical chronology are as follows:

1. The created open-source tool for WSI-oriented analysis, Pathadin, performed successfully in:
   - 1.1. Quick, objective, and reproducible research of staining on histological samples using color analysis algorithms (HSV thresholding).
   - 1.2. Quantification of DAB positive nuclei in Ki67 stained samples. The analysis performed under the visual control of pathologists showed that despite Gleason-dependent differences, the overlap between the adjacent grade groups limits the clinical application.
   - 1.3. Preparation of image datasets for the training of the machine learning algorithms.
   - 1.4. Testing, visualization, and validation of trained machine learning model.
2. A U-net model distinguishing glands, stroma, nerves, fat, and gaps was created and validated for further independent analysis of the experimental material.
3. The combination of the trained model and color analysis algorithms used in the Pathadin environment was applied to evaluate the microenvironmental changes around different cancer grade groups: firstly, in radical prostatectomy samples, afterward – in biopsies to understand the practical value for diagnostics.
   - 3.1. In radical prostatectomy samples:
     - 3.1.1. FANCM, a novel marker, was for the first time systematically described in prostate adenocarcinoma. It showed stromal specificity and grade-dependent decline in the carcinoma microenvironment and indicated the potential role of the homologous recombinant pathway in cancer stroma. FANCM protein baseline expression in normal prostate stroma did not affect the susceptibility to adenocarcinoma.
     - 3.1.2. Masson's trichrome (the analyzed staining of collagen) also demonstrated a grade-dependent change in expression and a difference between cancerous and non-cancerous areas.
     - 3.1.3. Both markers had a significant overlap in expression between the adjacent grade groups. The overlap was minimal between low (G1)- and high-grade (G4 and G5) carcinomas and between cancerous versus cancer-free areas.

3.2. In biopsies:
    3.2.1. It was confirmed that G1 prostate carcinoma is diagnosed and upgraded most frequently.
    3.2.2. Stromal composition quantification based on FANCM and Masson's trichrome stainings showed a statistically significant difference between non-cancerous and cancerous areas with G1 differentiation.
    3.2.3. Despite the confirmed statistical significance, considerable overlap in expression between G1 and non-cancerous tissue is a limitation for FANCM and Masson`s trichrome differential diagnostic use in biopsies a thus in clinical practice.

The created methodology is universal. Using the guidelines and samples provided in the repository (https://gitlab.com/Digipathology/Pathadin; https://github.com/ geodza/Pathadin) can serve as a manual for anyone willing to understand the basics of computer-assisted pathohistological diagnostics as well as assist in the creation of one's own model or quantification of microenvironmental changes in different tissues.

10. IMPLICATIONS FOR PRACTICE

1. FANCM, a homologous recombinant pathway protein, appears to be a novel, highly stroma-specific immunohistochemical marker in the prostate, showing the grade-dependent decline in the carcinoma microenvironment. This outlines the potential role of homologous recombinant pathway proteins in cancer stromogenesis.
2. In biopsies, FANCM and Masson's trichrome demonstrated a statistically significant difference between G1 cancerous stroma and non-cancerous areas, but with considerable overlap in staining intensity between the groups. Thus, the use of these markers or similar (such as Van Gieson) should be avoided in the analysis of stromogenic reaction of PCa despite being recommended by some practitioners.
3. Ki67 gains more and more attention in PCa diagnosis. This study displayed grade dependant increase in DAB-positive cells, but adjacent groups are indistinguishable; thus, the stain cannot be used in Gleason grading. At the same time, Ki67 is one of the most frequently used IHC markers and has proved diagnostic value in some neoplasms (as neuroendocrine tumors). Precise quantification of Ki67 using microscopes is time-consuming if done correctly. Results prove that a reliable analysis can be performed by computer within seconds. The integrated algorithm provided by Histomics has flexible settings, thus is universal, and can be used not only for nuclear but also for cytoplasmic and membrane stains.
4. Pathadin software allows experiencing almost all benefits of computer-assisted analysis of different complexity without any cost: the creation of models for any purpose, an independent quantification of stromal and epithelial changes. The concept should give an understanding of what modern DP and ML are and how enormous their applicatory function in medicine can be. Even a basic multiclass model for prostate segmentation is a time-saver for pathologists simplifying detection of extraprostatic or perineural invasion.
5. Following provided manuals, a similar model can be created for more precise prostate analysis or entirely different tissues.

11. FUTURE DIRECTIONS

Microenvironmental changes in carcinomas are starting to gain more attention in many organs, including the prostate. While it was demonstrated that the FANCM and MT's clinical use is somewhat limited, the difference between cancer-free, low, and high-risk carcinomas was seen and is worthy of further research. The study also outlined the potential role of homologous recombinant pathway proteins in cancer stromogenesis with the necessity of further investigation.

Pathadin will be further improved and reformated depending on the understanding of the current and future trends: the updates constitute the addition of new formats, such as DICOM (a possible new standard for digital pathology), testing new neural networks, and adding features as stereological analysis. When combined with clinical data, the described workflow can be used to reliably test new histological markers and evaluate possibilities for application in daily practice.

Currently, coexisting, at some point, digital pathology will inevitably replace the microscope. Both the College of American Pathologists and the Royal College of Pathologists already provide the guidelines for the implementation of digital pathology. The fast spread is synergic with the constantly evolving machine learning algorithms. At the same time, the quality of histological slides is continuously improved and standardized, meaning that some machine learning-related issues described in the manuscript will soon become archaic.

Today any histologist with access to a scanning device can collaborate with a data scientist and train a model without significant expenses. It will lead to a point where experts will create models equal to or outperforming the average pathologist. It can be imagined how the trained algorithms will also be provided and used by the validated labs along with the classical diagnostic manuals.

Estonia has a perfect potential to become the first fully digital country: high quality of histological samples, advance in IT, a small population, and lack of pathologists. In this paradigm, the national digital archive covering all country hospitals seems reasonable: easy access to morphology in combination with clinical data will improve both clinical and scientific routine for pathologists, oncologists, and genetics, resulting in benefits for the patient.

The manuscript's author will continue spreading the ideas of computer-assisted diagnostics by reviewing the latest solutions and consulting anyone willing to start with such an approach.

12. SUMMARY IN ESTONIAN

Adenokartsinoomi mikrokeskkonna muutuste kvantifitseerimine ja diagnostilise tähenduse hindamine eesnäärmes, rakendades uuemaid digipatoloogilisi programmiarendusi

Sissejuhatus

Maailmas on eesnäärme adenokartsinoom sageduselt teine pahaloomuline kasvaja meestel. 2018. aastal diagnoositi 1 276 106 uut eesnäärme adenokartsinoomi juhtu moodustades 3.8% meeste vähisurmade põhjustest. Eestis moodustas 2017. aastal eesnäärmekartsinoom 25.2% kõigist vähijuhtudest meestel. Eesnäärmevähi diagnostika standardiks enne raviotsust on histoloogiline uuring nõelbiopsiatest. Histoloogilise diagnoosi lahknevusi biopsiate ja radikaalse prostatektoomia (RP) vahel esineb kirjanduse andmetel 23–43% juhtudest.

Eesnäärmevähi biokeemilise retsidiivi riski alusel, mis on ravivaliku aluseks jaotab Uroloogilise Patoloogia Ühing, eesnäärmevähi kolme astmesse G1, G2 ja ≥G3. Kuna mõned ravivõimalused on rakendatavad vaid madala riskiga haigetel, siis on ülimalt oluline viia miinimumini diagnooside lahknevused biopsias ja RP-s, eriti G1 astmesse kuuluva vähi korral.

Üheks võimaluseks vähendada diagnooside lahknevusi pakub Ameerika Patoloogide Kolleegium välja strooma hindamist näärmeliste vähikollete vahel biopsiates. Vähi mikrokeskkonna muutused on kliiniliste uuringute andmetel olulise prognostilise tähtsusega rinna, jämesoole ja teiste organite kartsinoomides. Eesnäärmevähil korreleerub strooma rakulise koostise fenotüübiline muutus kasvaja Gleasoni astmega.

Strooma muutuste hindamiseks on vajalik eristada selle rakutüüpe: normaalsed silelihasrakud, vähi fibroblastid ja müofibroblastid. Selles töös kasutati Masson'i trikroom (MT) värvingut ja immunohistokeemilist (IHK) uuringut Fanconi aneemia komplementaarse rühma M (FANCM) antikehaga. FANCM osaleb DNA homoloogilise rekombinatsiooni (HR) protsessis ja selle avaldumist normaalses eesnäärme stroomas on varem täheldatud, kuid antud uuring oli selle esimeseks süstemaatiliseks hindamiseks eesnäärmevähis.

Senini strooma hindamiseks kasutatud kvalitatiivsed meetodid on ebapiisava täpsusega tuginedes uurija subjektiivsele hinnangule valgusmikroskoobi piiratud vaateväljades. Digipatoloogia (DP) võimaldab alusklaasil olevaid histoloogilisi preparaate skaneerides saada digipreparaadid, mida on võimalik täies ulatuses automaatselt arvuti-assisteeritult analüüsida ja isegi diagnoosida. Selleks on viimastel aastatel arendamisel masinõppe algoritmid (ML). Lõplikku diagnostikat ML praegu veel päriselt ei asenda, kuid neil on potentsiaali igapäevases rakendustes, näiteks erinevate koeliikide eristamiseks või vähikahtlaste kollete automaatseks avastamiseks. ML võimaldab täpselt eristada strooma komponenti näärmetest ja analüüsida kumbagi eraldi olenevalt kasutatud värvimismetoodikast.

Ehkki viimasel ajal lisandub uusi DP lahendusi, ka vabavarana, pidevalt juurde, siis ei olnud väitekirja alustades saada programme, mis võimaldaksid ML lihtsal teel rakendada alates esimestest etappidest nagu digipreparaadi annoteerimine, erinevatest koetüüpidest andmekogumite loomine ja tulemuste visualiseerimine.

Töö eesmärgid

Töö eesmärgiks on kvantifitseerida ja hinnata kartsinoomiga seotud mikrokeskkonnamuutuste diagnostilist olulisust erinevate Gleason'i astmete ümber ning nende praktilist kasutusvõimalust biopsiate puhul.

Ülesanne nõuab esmalt üldisema metodoloogilise probleemi lahendamist lihtsalt kasutatava, täpse DP-lahenduse väljatöötamisel, mille tööpõhimõte jäljendaks valgusmikroskobiga töötava patoloogi rutiinset diagnostilist protsessi.

Loogilises kronoloogilises järjekorras reastatuna on konkreetsed ülesanded objektiivse biopsiaanalüüsi tegemiseks järgnevad:

1. Luua WSI-orienteeritud avatud lähtekoodiga tööriistakomplekt, mis võimaldab teha järgmist:
   1.1. Põhivärvianalüüs (K-keskmised, värvikünnised) huvipakkuvas regioonis (*region of interest*, ROI).
   1.2. Diaminobensidiini (DAB) positiivsete ja negatiivsete rakkuda kvantifitseerimist huvipakkuvas regioonis.
      1.2.1. Pakutavate tööriistade abil hinnata DAB-positiivsete rakkude loendamise täpsust, kvantifitseerides Ki67 (üks populaarsemaid immunohistokeemilisi markereid) erinevate ISUP-klasside PCades.
   1.3. Pildiandmestu komplekteerimist ML-i jaoks digitaliseeritud preparaadiklaasidelt.
   1.4. Treenitud mudeli visualiseerimist ja valideerimist.
2. Luua ja kinnitada mitmeklassiline mudel, segmenteerides eesnäärme viieks komponendiks – näärmed, strooma, närvid, rasv, tühimikud edasiseks sõltumatuks analüüsiks.
3. Kvantifitseerida stromaalsete muutuste korrelatsioon ISUP-klassidega MT ja FANCM värvitud proovides, kasutades kaasasolevaid tarkvaratööriistu:
   3.1. Süstemaatiliselt hinnata FANCM värvingut eesnäärmes.
   3.2. Objektiivselt hinnata RP-proovides PCa-ga seotud mikrokeskkonnamuutuste olulisust ja selgitada edasiste uuringute teostamise ratsionaalsus piiratud biopsiate mahul.
   3.3. Hinnata biopsiates PCa-ga seotud mikrokeskkonnamuutuste praktilise diagnostika rakendamise võimalusi.

Metodoloogiat peetakse mõnevõrra universaalseks ning sobivaks kasutamiseks juhendina kõigile, kes soovivad mõista arvutipõhise patohistoloogilise diagnostika põhitõdesid.

Materjalid ja metoodika

Uuringus kasutati histoloogilisi koematerjale 385 patsiendilt, kellele ajavahemikus 2007–2010 teostati Ida-Tallinna keskhaiglas nii eesnäärme biopsiad kui radikaalne prostatektoomia (RP). Uuritavatest 232 juhul (60%) olid biopsia ja RP G astmed samad, biopsiates diagnoositud G astme hilisem suurendamine RP alusel esines 128 (34%) ja vähendamine 25 (6%) korral. Biopsiad, mille diferentseerumise aste RP uuringul suurenes, olid kõige sagedamini G1 kokku 82 juhul. Negatiivse kontrollina on kasutati 11 lahangu materjali, mille puhul ei esinenud eesnäärmehaigusi ega muid pahaloomulisi kasvajaid.

Histoloogiliste preparaatide värvimismeetoditest kasutati G astme hindamisel, selekteerimisel ja MA tarvis koetüüpide märgistamisel rutiinset hematoksüliin-eosiin värvingut (H&E), strooma koostise hindamiseks histokeemilist MT meetodit ja IHK värvingut inimese FANCM-vastase primaarse antikehaga. Mitootilist aktiivsust hinnati IHK värvingu alusel Ki67 monoklonaalse antikehaga. Mikropreparaadid digitaliseeriti kasutades 3DHistech Pannoramic Flash III 250 skannerit 20x suurendusega (eraldusvõime 0,24 μm/pikselit).

Digianalüüsiks loodi ja valideeriti tarkvara Pathadin *(Pathology + Paladin),* mille lähtekood, kasutatud andmekogud ja mudelid on esitatud repositooriumis: https://gitlab.com/Digipathology/Pathadin (https://github.com/geodza/Pathadin)

Rakendades Pathadin valideeritud ML mudelit, sai eesnäärme preparaatides automaatselt eristada strooma komponente näärmetest paralleelselt kõigis kasutatud värvingutega preparaatides ja kvantifitseerida nende koostist algul RP ja seejärel biopsiates. FANCM ja MT hindamisel kasutati strooma värvumisindeksit (SSI, stromal staining index), positiivselt värvunud strooma osakaalu (%) kogu strooma pindalast. Kollageeni osakaalu hinnati MT värvingul seadistatud HSV (hue, saturation, value) värvilävendi alusel. Ki67 avaldumist määratleti positiivselt värvunud näärmeliste rakutuumade suhtega kõigi epiteelsete rakutuumade arvu 1 mm^2 (%) kohta.

Tulemused ja arutelu

MT värving RP preparaatides näitas ilmekalt astmelist kollageeni hulga suurenemist eesnäärmevähi ümbruse stroomas, mille suhteline hulk hinnatuna SSI alusel kasvas sõltuvalt vähi G astmest. Keskmine SSI oli statistiliselt kõrgem juba G1 astme vähis (40.5 %) võrreldes kontrolliga (28%; $p< 0.001$). Statistiliselt oluline kollageeni hulga suurenemine ilmnes kui võrreldi keskmisi SSI väärtusi kasvajavabas koes samast prostatast (26.9 %) pärineva vähi stroomaga: G1 (40.5 %), G3 (50.3%) või G4 (83%; kõigil $p< 0.001$).

FANCM immuunohiostokeemiline värving RP normaalsetes eesnäärme stroomarakkudes on tugev ja difuusne, olles seega nende spetsiifiline marker. FANCM avaldumine väheneb proportsionaalselt eesnäärmevähi G astme suurenemisega. Keskmine SSI vähenes statistiliselt oluliselt juba G1 vähis (28%) võrreldes kasvajavaba kontrolliga (39%) ja koega sama kasvaja kõrvalt (41%),

p <0,001 mõlemal. FANCM avaldumistaseme statistiliselt oluline langus tuvastati ka G2 (25%) võrreldes G3 vähiga (18%), p = 0,005. Spearman'i korrelatsioonikordaja SSI ja G astmegruppide vahel oli −0,9 (p <0,001). FANCM SSI muutused stroomas erinevates vähi G astmegruppides olid vastupidised MT SSI muutustele, seega on mõlemad markerid strooma rakulise koostise näitajad.

FANCM avaldumistase vähi naabruses olevas normaalses stroomas ei erinenud tasemest vähivabas kontrollis, mis viitab, et puudub potentsiaalselt eesnäärmevähi riski suurendav FANCM baasavaldumise muutus uuritavas valimis. FANCM tulemused osundavad DNA HR, mille tähtsus on varasemast teada näärmetes, võib omada tähendust ka vähi stroomas.

MA programm suutis tõhusalt eristada ja arvutada strooma markerite MT ja FANCM SSI kui ka Ki67 avaldumisprotsenti vähikoes. Pärast RP analüüsi rakendati MT ja FACNM värvingut koos valideeritud DP algoritmiga biopsiate analüüsil, mille koemaht on RP-ga võrreldes piiratud. Kuna praktilises kliinilises olukorras tuli G1 vähiga biopsiates kõige sagedamini ette diagnoosi muutmist RP alusel (82 korral), siis kujunes tööhüpoteesiks, kas strooma muutuste alusel oleks võimalik ennustada biopsias G1 vähi naabruses kõrgema G astmega vähi esinemist või vähivabas biopsias mistahes astmega vähi esinemist. Arvestades, et eesnäärme strooma histoloogiline ehitus sõltub anatoomilisest tsoonist, kaasati analüüsi ainult perifeerse tsooni biopsiad, mis moodustasid valimist enamuse.

Kontrollgrupi (CG) moodustasid G1 vähiga biopsiad, mille diagnoos RP alusel ei muutunud. Testgruppi (TG) kuulusid kõik üles gradeeritud G1 biopsiad, hõlmates nii vähiga (TGC) kui vähivabasid bioptaate (TGW) samalt patsiendilt.

Gruppide kollageeni hulga võrdlus MT värvingu alusel näitas, et keskmine SSI kontrollgrupi (CG) biopsiates oli 41% (20- 78%, SD= 11)) üles gradeeritud vähiga grupis (TGC) 44% (23–89%, SD= 15) ja vähivabades bioptaatides37 % (15–57%, SD= 9). Kontroll-testgruppide vahel esines osalist kattuvust ja seega puudus statistiline erinevus (*p=0.84*). Erinevus TGC ja TGW rühmade vahel oli statistiliselt erinev (*p=0.012*).

FANCM värvingu alusel positiivsete strooma elementide võrdlus gruppides näitas, et keskmine SSI CG grupis oli 36% (13- 59%, SD= 11); 34% (9–58%, SD= 13) TGC grupis ja 44 % (22–69%, SD= 11) TGW grupis. CG ja TG gruppide vahel esines osaline kattuvus ja seega puudus statistiline erinevus (*p=0.5*). Erinevus TGC ja TGW rühmade vahel oli statistiliselt erinev (*p<0.001*).

Tulemused näitavad, et MT ja FANCM värvingud võimaldavad mõlemad eristada olulisi strooma koostise erinevusi vähi ümbruses võrreldes samast anatoomilisest piirkonnast pärineva vähivaba koega. G1 vähk gradeeriti RP-s kõige sagedamini G2 astmeks, mis võib olla põhjuseks, et üles gradeeritud grupis esinevad muutused võrreldes G1 grupiga olid liiga vähesed, et oleksid kummagi värvinguga usaldusväärselt ennustatavad, et neid võiks soovitada rutiinses diagnostikas. Siiski, kuna TG grupis esines ka kõrgema G astme vähki ja üle 95% intervalli SSI väärtusi, oleks mõeldav leida G1 vähis SSI lävend, mis ennustaks kõrgema astme vähi võimalikku esinemist bioptaadi naabruses.

Kuigi MT ja FANCM värvingu tulemused olid sarnased, oli FANCM värvinguga SSI kattuvus gruppide vahel väiksem.

Järeldused

Töö põhieesmärgiks oli objektiivselt analüüsida kartsinoomiga seotud mikrokeskkonnamuutuste hulka ja diagnostilist olulisust erinevate Gleason'i astmete ümber ning selliste muutuste praktilist kasutusvõimalust, eelkõige biopsiate puhul.

Võttes arvesse mikroskoobil olevaid piiranguid histoloogiliste muutuste täpseks hindamiseks, töötati välja ja katsetati kaasaegsetel digitaalsetel patoloogialahendustel põhinevat tööriista.

Loogilises kronoloogilises järjekorras on järeldused järgnevad:

1. Avatud lähtekoodi baasil loodud tööriist WSI-orienteeritud analüüsiks, Pathadin, toimis edukalt järgmistes valdkondades:
   1.1. Kiire, objektiivne ja korratav histoloogiliste proovide värvingute uurimine, kasutades värvianalüüsi algoritme (HSV lävend).
   1.2. DAB-positiivsete tuumade kvantifitseerimine Ki67-ga värvitud proovides. Analüüs näitas, et vaatamata Gleason'i astmetest sõltuvatele erinevustele piirab külgnevate klassigruppide kattumine kliinilist rakendust.
   1.3. Pildiandmestu ettevalmistamine masinõppe algoritmide treenimiseks.
   1.4. Treenitud masinõppemudeli testimine, visualiseerimine ja valideerimine.
2. Katsematerjali edasiseks sõltumatuks analüüsiks loodi ja valideeriti U-Net mudel, mis suudab eristada näärmeid, stroomat, närve, rasva ja tühimikke.
3. Pathadin'i keskkonnas kasutatud treenitud mudeli ja värvianalüüsi algoritmide kombinatsiooni kasutati mikrokeskkonna muutuste hindamiseks erinevate vähkkasvajate klassifitseerimise rühmade ümber: esiteks radikaalse prostatektoomia proovides ning seejärel biopsiates, et mõista praktilist väärtust diagnostikale.
   3.1. Radikaalse prostatektoomia proovides:
      3.1.1. Uudne marker FANCM, mida süstemaatiliselt kirjeldati esmakordselt eesnäärme adenokartsinoomi korral. See näitas stroomaspetsiifilisust ja kartsinoomi klassist sõltuvat langust kartsinoomi mikrokeskkonnas ning viitas homoloogse rekombinantse raja võimalikku mõju vähi stroomas. FANCM valgu algtaseme ekspressioon normaalses eesnäärme stroomas ei mõjutanud tundlikkust adenokartsinoomi suhtes.
      3.1.2. Massoni trikroom (kollageeni analüüsitud värvimine) näitas samuti kartsinoomi klassist sõltuvat muutust ekspressioonis ning erinevust vähkkasvajast mõjutatud ja normaalsete piirkondade vahel.

3.1.3. Mõlemal markeril esines märkimisväärne kattumine ekspressioonis külgnevate klassigruppide vahel. Kattuvus oli minimaalne madalate (G1) ja kõrge astmega (G4 ja G5) kartsinoomide ning vähkkasvajast mõjutatud ja normaalsete piirkondade vahel.

3.2. Biopsiates:

3.2.1. Leidis kinnitust, et G1 eesnäärme kartsinoomi diagnoositakse ja hinnatakse kõrgemale astmele kõige sagedamini.

3.2.2. Strooma koostise kvantifitseerimine FANCM-i ja Massoni trikroomvärvingu põhjal näitas statistiliselt olulist erinevust G1 diferentseerumisega vähkkasvajast mõjutatud ja normaalsete piirkondade vahel.

3.2.3. Vaatamata kinnitatud statistilisele olulisusele, on G1 ja normaalsete piirkondade ekspressiooni märkimisväärne kattumine piiranguks FANCM-i ja Massoni trikroomvärvingu diferentsiaaldiagnostika kasutamisel biopsiates ja seeläbi ka kliinilises praktikas.

Loodud metodoloogia on universaalne. Andmehoidlas (https://gitlab.com/Digipathology/Pathadin või https://github.com/geodza/Pathadin) olevate juhiste ja näidiste kasutamine võib toimida juhendina kõigile, kes soovivad mõista arvutipõhise patohistoloogilise diagnostika põhitõdesid. Samuti võib see aidata kaasa uute mudelite loomisele või mikrokeskkonnamuutuste kvantifitseerimisele erinevates kudedes.

Praktilised soovitused

1. FANCM, homoloogse rekombinantse raja valk, paistab olevat uudne, kõrgelt strooma-spetsiifiline immunohistokeemiline marker eesnäärmes, mis näitab astmest sõltuvat langust kartsinoomi mikrokeskkonnas. See annab ülevaate homoloogse rekombinantse raja valkude potentsiaalsest rollist kartsinoomi stromogeneesis.
2. Biopsiates demonstreerisid FANCM ja Massoni trikroomvärving statistiliselt olulist erinevust G1 astme kartsinoomist mõjutatud strooma ja normaalsete regioonide vahel, kuid värvingu intensiivsuses esines gruppide vahel märkimisväärne kattumine. Seetõttu tuleks nende või sarnaste markerite (nt. Van Gieson) kasutamist vältida PCa stromogeensete reaktsioonide analüüsil, kuigi nende kasutamine on mõndade praktikute poolt soovitatud.
3. Ki67 püüab PCa diagnostikas järjest enam tähelepanu. Käesolevas uuringus leiti astmest sõltuv tõus DAB-positiivsete rakkude hulgas, kuid eristatavad ei ole lähedalpaiknevad grupid, seetõttu ei saa värvingut kasutada Gleasoni astmete määramisel. Samaaegselt on Ki67 üks enimkasutatavaid immunohistokeemilisi markereid, millel on tõestatud diagnostiline väärtus mõndade neoplaasiate puhul (nt. neuroendokiinsed kasvajad). Korrektselt teostatud Ki67 kvantifitseerimine valgusmikroskoopi kasutades on aga aeganõudev. Tulemused tõestavad, et arvutit kasutades on võimalik usaldusväärne analüüs

teostada sekundite jooksul. Näiteks vabavarana saadaval Histomics'i poolt pakutud integreeritud algoritmil on paindlikud sätted ning on seega universaalne, võimaldades kasutust mitte ainult rakutuuma värvingutel, vaid ka tsütoplasmaatiliste ja membraanivärvingute puhul.

4. Pathadin tarkvara võimaldab kogeda pea kõiki komplekse eritasemelise arvutipõhise analüüsi hüvesid ilma kahjudeta: mudeleid on võimalik luua igal eesmärgil, eelkõige strooma ja epiteliaalsete muutuste iseseisvaks kvantifitseerimiseks. Kontsept peaks andma ülevaate kaasaegsest DP-st ja ML-ist ning kui suurejoonelised võivad olla nende kasutusvõimalused meditsiinis. Patoloogide jaoks vähendab ajakulu ka lihtne mitmeklassiline mudel eesnäärme segmenteerimisest, lihtsustades ekstraprostaatiliste või perineuraalsete invasioonide detekteerimist.
5. Pakutud juhendeid järgides on võimalik luua sarnane mudel spetsiifilisemaks eesnäärmekudede analüüsimiseks või kasutada seda erisuguste kudede hindamisel.

ACKNOWLEDGMENTS

This study was carried out in cooperation with the East Tallinn Central Hospital.

I want to express my sincere gratitude and respect to:

- My supervisor, Ave Minajeva, MD, PhD, for providing valuable advice, encouragement, and assistance in all aspects of PhD studies while leaving me enough freedom for creativity and a nontraditional approach.
- Reviewers, Margus Punab, MD, PhD, and Peeter Ross, MD, PhD, for the constructive criticism, valuable advice, and the analysis of the manuscript.
- The whole pathology team of the East Tallinn Central Hospital represented by Eero Semjonov, MD, one of the pioneers of digital pathology in Estonia; Kristi Laht, MSc, and Heleri Taelma, BSc, for the support in all steps of sample preparations and integration of digital pathology.
- Dmitri Kazahonok, MSc, the main author of Pathadin's code, for practical, gratuitous, and indispensable support in the IT part of the work.
- Maris Laan, PhD, for reviewing the research paper and demonstrating high standards of critical analysis of scientific publications.
- Marika Tammaru, M.D, PhD, for assistance with maths and statistics, sample gathering, application for ethical approval and for being a great friend and adviser.
- Kaarina Ristmägi, MD, Tanel Vaas, MD, Karin Kalda, MSc, and Kaarel Reim, MD, for the assistance with text preparation and translation, but also for making my work routine brighter and unforgettable.
- Natalia Lapidus, MD, for providing control samples from West Tallinn Central Hospital.
- My friends, represented by Alexander Gvozdkov, BSc, who spent weeks altruistically helping me to resolve computational tasks.
- And most importantly, my beloved family.

The study is supported by the 'Higher education speciality scholarship in smart specialization growth areas' granted by SA Archimedes.

REFERENCES

1. Acs B, Pelekanou V, Bai Y, Martinez-Morilla S, Toki M, Leung SCY, Nielsen TO, Rimm DL. Ki67 reproducibility using digital image analysis: an inter-platform and inter-operator study. Lab Invest. 2019 Jan;99(1):107–117. doi: 10.1038/s41374-018-0123-7. Epub 2018 Sep 4. PMID: 30181553.
2. Alchin DR, Murphy D, Lawrentschuk N. What Are the Predictive Factors for Gleason Score Upgrade following RP? Urol Int. 2016;96(1):1–4. doi: 10.1159/000439139. Epub 2015 Aug 29. PMID: 26314299.
3. Arias-Stella JA 3rd, Shah AB, Montoya-Cerrillo D, Williamson SR, Gupta NS. Prostate biopsy and radical prostatectomy Gleason score correlation in heterogenous tumors: proposal for a composite Gleason score. Am J Surg Pathol. 2015 Sep;39(9):1213–8. doi: 10.1097/PAS.0000000000000499. PMID: 26274028.
4. Arias-Stella JA 3rd, Varma KR, Montoya-Cerrillo D, Gupta NS, Williamson SR. Does discontinuous involvement of a prostatic needle biopsy core by adenocarcinoma correlate with a large tumor focus at radical prostatectomy? Am J Surg Pathol. 2015 Feb;39(2):281–6. doi: 10.1097/PAS.0000000000000344. PMID: 25353288.
5. Arvaniti E, Fricker KS, Moret M, Rupp N, Hermanns T, Fankhauser C, Wey N, Wild PJ, Rüschoff JH, Claassen M. Automated Gleason grading of prostate cancer tissue microarrays via deep learning. Sci Rep. 2018 Aug 13;8(1):12054. doi: 10.1038/s41598-018-30535-1. Erratum in: Sci Rep. 2019 May 16;9(1):7668. PMID: 30104757; PMCID: PMC6089889.
6. Ayala G, Tuxhorn JA, Wheeler TM, Frolov A, Scardino PT, Ohori M, Wheeler M, Spitler J, Rowley DR. Reactive stroma as a predictor of biochemical-free recurrence in prostate cancer. Clin Cancer Res. 2003 Oct 15;9(13):4792–801. PMID: 14581350.
7. Bankhead P, Loughrey MB, Fernández JA, Dombrowski Y, McArt DG, Dunne PD, McQuaid S, Gray RT, Murray LJ, Coleman HG, James JA, Salto-Tellez M, Hamilton PW. QuPath: Open source software for digital pathology image analysis. Sci Rep. 2017 Dec 4;7(1):16878. doi: 10.1038/s41598-017-17204-5. PMID: 29203879; PMCID: PMC5715110.
8. Basbous J, Constantinou A. A tumor suppressive DNA translocase named FANCM. Crit Rev Biochem Mol Biol. 2019 Feb;54(1):27–40. doi: 10.1080/10409238.2019.1568963. Epub 2019 Feb 4. PMID: 30714416.
9. Bjurlin MA, Taneja SS. Standards for prostate biopsy. Curr Opin Urol. 2014 Mar;24(2):155-61. doi: 10.1097/MOU.0000000000000031. PMID: 24451092; PMCID: PMC4142196.
10. Bogliolo M, Bluteau D, Lespinasse J, Pujol R, Vasquez N, d'Enghien CD, Stoppa-Lyonnet D, Leblanc T, Soulier J, Surrallés J. Biallelic truncating FANCM mutations cause early-onset cancer but not Fanconi anemia. Genet Med. 2018 Apr;20(4):458–463. doi: 10.1038/gim.2017.124. Epub 2017 Aug 24. PMID: 28837157.
11. Bonk S, Kluth M, Hube-Magg C, Polonski A, Soekeland G, Makropidi-Fraune G, Möller-Koop C, Witt M, Luebke AM, Hinsch A, Burandt E, Steurer S, Clauditz TS, Schlomm T, Perez D, Graefen M, Heinzer H, Huland H, Izbicki JR, Wilczak W, Minner S, Sauter G, Simon R. Prognostic and diagnostic role of PSA immunohistochemistry: A tissue microarray study on 21,000 normal and cancerous tissues. Oncotarget. 2019 Sep 10;10(52):5439–5453. doi: 10.18632/oncotarget.27145. PMID: 31534629; PMCID: PMC6739211.

12. Boufaied N, Takhar M, Nash C, Erho N, Bismar TA, Davicioni E, Thomson AA. Development of a predictive model for stromal content in prostate cancer samples to improve signature performance. J Pathol. 2019 Dec;249(4):411–424. doi: 10.1002/path.5315. Epub 2019 Oct 16. PMID: 31206668; PMCID: PMC6900085.
13. Bray F, Ferlay J, Soerjomataram I, Siegel RL, Torre LA, Jemal A. Global cancer statistics 2018: GLOBOCAN estimates of incidence and mortality worldwide for 36 cancers in 185 countries. CA Cancer J Clin. 2018 Nov;68(6):394–424. doi: 10.3322/caac.21492. Epub 2018 Sep 12. Erratum in: CA Cancer J Clin. 2020 Jul;70(4):313. PMID: 30207593.
14. Browning L, Fryer E, Roskell D, White K, Colling R, Rittscher J, Verrill C. Role of digital pathology in diagnostic histopathology in the response to COVID-19: results from a survey of experience in a UK tertiary referral hospital. J Clin Pathol. 2021 Feb;74(2):129–132. doi: 10.1136/jclinpath-2020-206786. Epub 2020 Jul 2. PMID: 32616541; PMCID: PMC7841475.
15. Bulten W, Pinckaers H, van Boven H, Vink R, de Bel T, van Ginneken B, van der Laak J, Hulsbergen-van de Kaa C, Litjens G. Automated deep-learning system for Gleason grading of prostate cancer using biopsies: a diagnostic study. Lancet Oncol. 2020 Feb;21(2):233–241. doi: 10.1016/S1470-2045(19)30739-9. Epub 2020 Jan 8. PMID: 31926805.
16. Catucci I, Osorio A, Arver B, Neidhardt G, Bogliolo M, Zanardi F, Riboni M, Minardi S, Pujol R, Azzollini J, Peissel B, Manoukian S, De Vecchi G, Casola S, Hauke J, Richters L, Rhiem K, Schmutzler RK, Wallander K, Törngren T, Borg Å, Radice P, Surrallés J, Hahnen E, Ehrencrona H, Kvist A, Benitez J, Peterlongo P. Individuals with FANCM biallelic mutations do not develop Fanconi anemia, but show risk for breast cancer, chemotherapy toxicity and may display chromosome fragility. Genet Med. 2018 Apr;20(4):452–457. doi: 10.1038/gim.2017.123. Epub 2017 Aug 24. PMID: 28837162.
17. Ceccaldi R, Sarangi P, D'Andrea AD. The Fanconi anaemia pathway: new players and new functions. Nat Rev Mol Cell Biol. 2016 Jun;17(6):337–49. doi: 10.1038/nrm.2016.48. Epub 2016 May 5. PMID: 27145721.
18. Chiarugi P, Paoli P, Cirri P. Tumor microenvironment and metabolism in prostate cancer. Semin Oncol. 2014 Apr;41(2):267–80. doi: 10.1053/j.seminoncol.2014. 03.004. Epub 2014 Mar 5. PMID: 24787298.
19. Cimadamore A, Lopez-Beltran A, Scarpelli M, Cheng L, Montironi R. Digital pathology and COVID-19 and future crises: pathologists can safely diagnose cases from home using a consumer monitor and a mini PC. J Clin Pathol. 2020 Nov; 73(11):695–696. doi: 10.1136/jclinpath-2020-206943. Epub 2020 Jul 30. PMID: 32732339.
20. Cohen RJ, Shannon BA, Phillips M, Moorin RE, Wheeler TM, Garrett KL. Central zone carcinoma of the prostate gland: a distinct tumor type with poor prognostic features. J Urol. 2008 May;179(5):1762–7; discussion 1767. doi: 10.1016/j.juro. 2008.01.017. Epub 2008 Mar 17. PMID: 18343454.
21. Collin SM, Martin RM, Metcalfe C, Gunnell D, Albertsen PC, Neal D, Hamdy F, Stephens P, Lane JA, Moore R, Donovan J. Prostate-cancer mortality in the USA and UK in 1975–2004: an ecological study. Lancet Oncol. 2008 May;9(5):445–52. doi: 10.1016/S1470-2045(08)70104-9. Epub 2008 Apr 16. PMID: 18424233; PMCID: PMC2760747.
22. Conklin MW, Keely PJ. Why the stroma matters in breast cancer: insights into breast cancer patient outcomes through the examination of stromal biomarkers.

Cell Adh Migr. 2012 May-Jun;6(3):249–60. doi: 10.4161/cam.20567. Epub 2012 May 1. PMID: 22568982; PMCID: PMC3427239.
23. Coulthard R, Deans AJ, Swuec P, Bowles M, Costa A, West SC, McDonald NQ. Architecture and DNA recognition elements of the Fanconi anemia FANCM-FAAP24 complex. Structure. 2013 Sep 3;21(9):1648–58. doi: 10.1016/j.str.2013.07.006. Epub 2013 Aug 8. PMID: 23932590; PMCID: PMC3763369.
24. Cui M, Zhang DY. Artificial intelligence and computational pathology. Lab Invest. 2021 Apr;101(4):412–422. doi: 10.1038/s41374-020-00514-0. Epub 2021 Jan 16. PMID: 33454724; PMCID: PMC7811340.
25. Cunha GR, Hayward SW, Wang YZ, Ricke WA. Role of the stromal microenvironment in carcinogenesis of the prostate. Int J Cancer. 2003 Oct 20;107(1):1–10. doi: 10.1002/ijc.11335. PMID: 12925950.
26. D'Amico AV, Whittington R, Malkowicz SB, Schultz D, Blank K, Broderick GA, Tomaszewski JE, Renshaw AA, Kaplan I, Beard CJ, Wein A. Biochemical outcome after radical prostatectomy, external beam radiation therapy, or interstitial radiation therapy for clinically localized prostate cancer. JAMA. 1998 Sep 16;280(11):969–74. doi: 10.1001/jama.280.11.969. PMID: 9749478.
27. Draisma G, Etzioni R, Tsodikov A, Mariotto A, Wever E, Gulati R, Feuer E, de Koning H. Lead time and overdiagnosis in prostate-specific antigen screening: importance of methods and context. J Natl Cancer Inst. 2009 Mar 18;101(6):374–83. doi: 10.1093/jnci/djp001. Epub 2009 Mar 10. PMID: 19276453; PMCID: PMC2720697.
28. Dzaparidze G, Anion E, Laan M, Minajeva A. The decline of FANCM immunohistochemical expression in prostate cancer stroma correlates with the grade group. Pathol Int. 2020 Aug;70(8):542–550. doi: 10.1111/pin.12953. Epub 2020 May 28. PMID: 32462745.
29. Dzaparidze G, Kazachonok D, Gvozdkov A, Taelma H, Laht K, Minajeva A. Diagnostic significance of stromal changes in biopsies of prostate adenocarcinoma. Pathol Res Pract. 2021 Jun;222:153436. doi: 10.1016/j.prp.2021.153436. Epub 2021 Apr 8. PMID: 33857855.
30. Dzaparidze G, Kazachonok D, Laht K, Taelma H, Minajeva A. Pathadin – The essential set of tools to start with whole slide analysis. Acta Histochem. 2020 Oct;122(7):151619. doi: 10.1016/j.acthis.2020.151619. Epub 2020 Sep 15. PMID: 33066841.
31. Eggener SE, Badani K, Barocas DA, Barrisford GW, Cheng JS, Chin AI, Corcoran A, Epstein JI, George AK, Gupta GN, Hayn MH, Kauffman EC, Lane B, Liss MA, Mirza M, Morgan TM, Moses K, Nepple KG, Preston MA, Rais-Bahrami S, Resnick MJ, Siddiqui MM, Silberstein J, Singer EA, Sonn GA, Sprenkle P, Stratton KL, Taylor J, Tomaszewski J, Tollefson M, Vickers A, White WM, Lowrance WT. Gleason 6 Prostate Cancer: Translating Biology into Population Health. J Urol. 2015 Sep;194(3):626–34. doi: 10.1016/j.juro.2015.01.126. Epub 2015 Apr 4. PMID: 25849602; PMCID: PMC4551510.
32. Eiro N, Fernandez-Gomez J, Sacristán R, Fernandez-Garcia B, Lobo B, Gonzalez-Suarez J, Quintas A, Escaf S, Vizoso FJ. Stromal factors involved in human prostate cancer development, progression and castration resistance. J Cancer Res Clin Oncol. 2017 Feb;143(2):351–359. doi: 10.1007/s00432-016-2284-3. Epub 2016 Oct 27. PMID: 27787597.

33. Enomoto N, Suda T, Kato M, Kaida Y, Nakamura Y, Imokawa S, Ida M, Chida K. Quantitative analysis of fibroblastic foci in usual interstitial pneumonia. Chest. 2006 Jul;130(1):22–9. doi: 10.1378/chest.130.1.22. PMID: 16840378.
34. Epstein JI, Allsbrook WC Jr, Amin MB, Egevad LL; ISUP Grading Committee. The 2005 International Society of Urological Pathology (ISUP) Consensus Conference on Gleason Grading of Prostatic Carcinoma. Am J Surg Pathol. 2005 Sep;29(9):1228–42. doi: 10.1097/01.pas.0000173646.99337.b1. PMID: 16096414.
35. Epstein JI, Feng Z, Trock BJ, Pierorazio PM. Upgrading and downgrading of prostate cancer from biopsy to radical prostatectomy: incidence and predictive factors using the modified Gleason grading system and factoring in tertiary grades. Eur Urol. 2012 May;61(5):1019–24. doi: 10.1016/j.eururo.2012.01.050. Epub 2012 Feb 8. PMID: 22336380; PMCID: PMC4659370.
36. Epstein JI, Zelefsky MJ, Sjoberg DD, Nelson JB, Egevad L, Magi-Galluzzi C, Vickers AJ, Parwani AV, Reuter VE, Fine SW, Eastham JA, Wiklund P, Han M, Reddy CA, Ciezki JP, Nyberg T, Klein EA. A Contemporary Prostate Cancer Grading System: A Validated Alternative to the Gleason Score. Eur Urol. 2016 Mar;69(3):428–35. doi: 10.1016/j.eururo.2015.06.046. Epub 2015 Jul 10. PMID: 26166626; PMCID: PMC5002992.
37. Etzioni R, Tsodikov A, Mariotto A, Szabo A, Falcon S, Wegelin J, DiTommaso D, Karnofski K, Gulati R, Penson DF, Feuer E. Quantifying the role of PSA screening in the US prostate cancer mortality decline. Cancer Causes Control. 2008 Mar;19(2):175–81. doi: 10.1007/s10552-007-9083-8. Epub 2007 Nov 20. PMID: 18027095; PMCID: PMC3064270.
38. Falk T, Mai D, Bensch R, Çiçek Ö, Abdulkadir A, Marrakchi Y, Böhm A, Deubner J, Jäckel Z, Seiwald K, Dovzhenko A, Tietz O, Dal Bosco C, Walsh S, Saltukoglu D, Tay TL, Prinz M, Palme K, Simons M, Diester I, Brox T, Ronneberger O. U-Net: deep learning for cell counting, detection, and morphometry. Nat Methods. 2019 Jan;16(1):67–70. doi: 10.1038/s41592-018-0261-2. Epub 2018 Dec 17. Erratum in: Nat Methods. 2019 Apr;16(4):351. PMID: 30559429.
39. Fine SW. Neuroendocrine tumors of the prostate. Mod Pathol. 2018 Jan; 31(S1):S122–132. doi: 10.1038/modpathol.2017.164. PMID: 29297494.
40. Fiorentino M, Judson G, Penney K, Flavin R, Stark J, Fiore C, Fall K, Martin N, Ma J, Sinnott J, Giovannucci E, Stampfer M, Sesso HD, Kantoff PW, Finn S, Loda M, Mucci L. Immunohistochemical expression of BRCA1 and lethal prostate cancer. Cancer Res. 2010 Apr 15;70(8):3136–9. doi: 10.1158/0008-5472.CAN-09-4100. Epub 2010 Apr 13. PMID: 20388772; PMCID: PMC3049266.
41. Fisher G, Yang ZH, Kudahetti S, Møller H, Scardino P, Cuzick J, Berney DM; Transatlantic Prostate Group. Prognostic value of Ki-67 for prostate cancer death in a conservatively managed cohort. Br J Cancer. 2013 Feb 5;108(2):271–7. doi: 10.1038/bjc.2012.598. Epub 2013 Jan 17. PMID: 23329234; PMCID: PMC3566811.
42. Fukagai T, Namiki T, Namiki H, Carlile RG, Shimada M, Yoshida H. Discrepancies between Gleason scores of needle biopsy and radical prostatectomy specimens. Pathol Int. 2001 May;51(5):364–70. doi: 10.1046/j.1440-1827.2001. 01207. x. PMID: 11422794.
43. García-Rojo M, De Mena D, Muriel-Cueto P, Atienza-Cuevas L, Domínguez-Gómez M, Bueno G. New European Union Regulations Related to Whole Slide Image Scanners and Image Analysis Software. J Pathol Inform. 2019 Jan 24;10:2. doi: 10.4103/jpi.jpi_33_18. PMID: 30783546; PMCID: PMC6369630.

44. Gleason DF. Classification of prostatic carcinomas. Cancer Chemother Rep. 1966 Mar;50(3):125–8. PMID: 5948714.
45. Goel S, Shoag JE, Gross MD, Al Hussein Al Awamlh B, Robinson B, Khani F, Baltich Nelson B, Margolis DJ, Hu JC. Concordance Between Biopsy and Radical Prostatectomy Pathology in the Era of Targeted Biopsy: A Systematic Review and Meta-analysis. Eur Urol Oncol. 2020 Feb;3(1):10–20. doi: 10.1016/j.euo.2019.08.001. Epub 2019 Sep 4. PMID: 31492650.
46. Goode A, Gilbert B, Harkes J, Jukic D, Satyanarayanan M. OpenSlide: A vendor-neutral software foundation for digital pathology. J Pathol Inform. 2013 Sep 27;4:27. doi: 10.4103/2153-3539.119005. PMID: 24244884; PMCID: PMC3815078.
47. Gravina GL, Mancini A, Ranieri G, Di Pasquale B, Marampon F, Di Clemente L, Ricevuto E, Festuccia C. Phenotypic characterization of human prostatic stromal cells in primary cultures derived from human tissue samples. Int J Oncol. 2013 Jun;42(6):2116–22. doi: 10.3892/ijo.2013.1892. Epub 2013 Apr 10. PMID: 23589051.
48. Guo C, Crespo M, Gurel B, Dolling D, Rekowski J, Sharp A, Petremolo A, Sumanasuriya S, Rodrigues DN, Ferreira A, Pereira R, Figueiredo I, Mehra N, Lambros MBK, Neeb A, Gil V, Seed G, Terstappen L, Alimonti A, Drake CG, Yuan W, de Bono JS; International SU2C PCF Prostate Cancer Dream Team. CD38 in Advanced Prostate Cancers. Eur Urol. 2021 Jun;79(6):736–746. doi: 10.1016/j.eururo.2021.01.017. Epub 2021 Mar 5. PMID: 33678520; PMCID: PMC8175332.
49. Halvorsen TB, Seim E. Association between invasiveness, inflammatory reaction, desmoplasia and survival in colorectal cancer. J Clin Pathol. 1989 Feb;42(2):162–6. doi: 10.1136/jcp.42.2.162. PMID: 2921357; PMCID: PMC1141819.
50. Hamilton PW, Bankhead P, Wang Y, Hutchinson R, Kieran D, McArt DG, James J, Salto-Tellez M. Digital pathology and image analysis in tissue biomarker research. Methods. 2014 Nov;70(1):59–73. doi: 10.1016/j.ymeth.2014.06.015. Epub 2014 Jul 15. PMID: 25034370.
51. Hammarsten P, Josefsson A, Thysell E, Lundholm M, Hägglöf C, Iglesias-Gato D, Flores-Morales A, Stattin P, Egevad L, Granfors T, Wikström P, Bergh A. Immunoreactivity for prostate specific antigen and Ki67 differentiates subgroups of prostate cancer related to outcome. Mod Pathol. 2019 Sep;32(9):1310–1319. doi: 10.1038/s41379-019-0260-6. Epub 2019 Apr 12. PMID: 30980038; PMCID: PMC6760646.
52. Henke A, Grace OC, Ashley GR, Stewart GD, Riddick AC, Yeun H, O'Donnell M, Anderson RA, Thomson AA. Stromal expression of decorin, Semaphorin6D, SPARC, Sprouty1 and Tsukushi in developing prostate and decreased levels of decorin in prostate cancer. PLoS One. 2012;7(8):e42516. doi: 10.1371/journal.pone.0042516. Epub 2012 Aug 3. PMID: 22880013; PMCID: PMC3411755.
53. Humphrey P, Amin MB, Berney D, Billis A, et al. Acinar adenocarcinoma. In: Moch H, Humphrey PA, Ulbright T, Reuter VE, eds. Pathology and Genetics: Tumors of the Urinary System and Male Genital Organs. 4th edition. WHO Classification of Tumors. Zurich, Switzerland: WHO Press; 2015:3–28.
54. Hurley PJ, Sundi D, Shinder B, Simons BW, Hughes RM, Miller RM, Benzon B, Faraj SF, Netto GJ, Vergara IA, Erho N, Davicioni E, Karnes RJ, Yan G, Ewing C, Isaacs SD, Berman DM, Rider JR, Jordahl KM, Mucci LA, Huang J, An SS, Park BH, Isaacs WB, Marchionni L, Ross AE, Schaeffer EM. Germline Variants in Asporin Vary by Race, Modulate the Tumor Microenvironment, and Are

Differentially Associated with Metastatic Prostate Cancer. Clin Cancer Res. 2016 Jan 15;22(2):448–58. doi: 10.1158/1078-0432.CCR-15-0256. Epub 2015 Oct 7. PMID: 26446945; PMCID: PMC4715968.
55. Innos K, Baburin A, Kotsar A, Eiche IE, Lang K. Prostate cancer incidence, mortality and survival trends in Estonia, 1995–2014. Scand J Urol. 2017 Dec; 51(6):442–449. doi: 10.1080/21681805.2017.1392600. Epub 2017 Nov 2. PMID: 29092653.
56. Janowczyk A, Zuo R, Gilmore H, Feldman M, Madabhushi A. HistoQC: An Open-Source Quality Control Tool for Digital Pathology Slides. JCO Clin Cancer Inform. 2019 Apr;3:1–7. doi: 10.1200/CCI.18.00157. PMID: 30990737; PMCID: PMC6552675.
57. Kammerer-Jacquet SF, Ahmad A, Møller H, Sandu H, Scardino P, Soosay G, Beltran L, Cuzick J, Berney DM. Ki-67 is an independent predictor of prostate cancer death in routine needle biopsy samples: proving utility for routine assessments. Mod Pathol. 2019 Sep;32(9):1303–1309. doi: 10.1038/s41379-019-0268-y. Epub 2019 Apr 11. PMID: 30976102.
58. Karlou M, Tzelepi V, Efstathiou E. Therapeutic targeting of the prostate cancer microenvironment. Nat Rev Urol. 2010 Sep;7(9):494–509. doi: 10.1038/nrurol. 2010.134. PMID: 20818327.
59. Karram S, Trock BJ, Netto GJ, Epstein JI. Should intervening benign tissue be included in the measurement of discontinuous foci of cancer on prostate needle biopsy? Correlation with radical prostatectomy findings. Am J Surg Pathol. 2011 Sep;35(9):1351–5. doi: 10.1097/PAS.0b013e3182217b79. PMID: 21836493.
60. Kasak L, Punab M, Nagirnaja L, Grigorova M, Minajeva A, Lopes AM, Punab AM, Aston KI, Carvalho F, Laasik E, Smith LB; GEMINI Consortium, Conrad DF, Laan M. Bi-allelic Recessive Loss-of-Function Variants in FANCM Cause Non-obstructive Azoospermia. Am J Hum Genet. 2018 Aug 2;103(2):200–212. doi: 10.1016/j.ajhg.2018.07.005. PMID: 30075111; PMCID: PMC6080835.
61. Kiaris H, Chatzistamou I, Kalofoutis Ch, Koutselini H, Piperi Ch, Kalofoutis A. Tumour-stroma interactions in carcinogenesis: basic aspects and perspectives. Mol Cell Biochem. 2004 Jun;261(1–2):117-22. doi: 10.1023/b:mcbi.0000028746. 54447.6c. PMID: 15362494.
62. Krušlin B, Ulamec M, Tomas D. Prostate cancer stroma: an important factor in cancer growth and progression. Bosn J Basic Med Sci. 2015 May 13;15(2):1–8. doi: 10.17305/bjbms.2015.449. PMID: 26042506; PMCID: PMC4469930.
63. Kweldam CF, van Leenders GJ, van der Kwast T. Grading of prostate cancer: a work in progress. Histopathology. 2019 Jan;74(1):146–160. doi: 10.1111/his. 13767.PMID: 30565302; PMCID: PMC7380027.
64. Lamprecht MR, Sabatini DM, Carpenter AE. CellProfiler: free, versatile software for automated biological image analysis. Biotechniques. 2007 Jan;42(1):71–5. doi: 10.2144/000112257. PMID: 17269487.
65. Langley RR, Fidler IJ. The seed and soil hypothesis revisited--the role of tumor-stroma interactions in metastasis to different organs. Int J Cancer. 2011 Jun 1;128(11):2527–35. doi: 10.1002/ijc.26031. Epub 2011 Mar 25. PMID: 21365651; PMCID: PMC3075088.
66. Lee JJ, Thomas IC, Nolley R, Ferrari M, Brooks JD, Leppert JT. Biologic differences between peripheral and transition zone prostate cancer. Prostate. 2015 Feb;75(2):183–90. doi: 10.1002/pros.22903. Epub 2014 Oct 18. PMID: 25327466; PMCID: PMC4270836.

67. Linkert M, Rueden CT, Allan C, Burel JM, Moore W, Patterson A, Loranger B, Moore J, Neves C, Macdonald D, Tarkowska A, Sticco C, Hill E, Rossner M, Eliceiri KW, Swedlow JR. Metadata matters: access to image data in the real world. J Cell Biol. 2010 May 31;189(5):777–82. doi: 10.1083/jcb.201004104. PMID: 20513764; PMCID: PMC2878938.
68. Lu-Yao GL, Albertsen PC, Moore DF, Shih W, Lin Y, DiPaola RS, Barry MJ, Zietman A, O'Leary M, Walker-Corkery E, Yao SL. Outcomes of localized prostate cancer following conservative management. JAMA. 2009 Sep 16;302(11): 1202–9. doi: 10.1001/jama.2009.1348. PMID: 19755699; PMCID: PMC2822438.
69. Madabhushi A, Lee G. Image analysis and machine learning in digital pathology: Challenges and opportunities. Med Image Anal. 2016 Oct;33:170–175. doi: 10.1016/j.media.2016.06.037. Epub 2016 Jul 4. PMID: 27423409; PMCID: PMC5556681.
70. Mäkelä K, Mäyränpää MI, Sihvo HK, Bergman P, Sutinen E, Ollila H, Kaarteenaho R, Myllärniemi M. Artificial intelligence identifies inflammation and confirms fibroblast foci as prognostic tissue biomarkers in idiopathic pulmonary fibrosis. Hum Pathol. 2021 Jan;107:58–68. doi: 10.1016/j.humpath.2020.10.008. Epub 2020 Nov 5. PMID: 33161029.
71. McNeal JE. Anatomy of the prostate and morphogenesis of BPH. Prog Clin Biol Res. 1984;145:27–53. PMID: 6201879.
72. Miles B, Ittmann M, Wheeler T, Sayeeduddin M, Cubilla A, Rowley D, Bu P, Ding Y, Gao Y, Lee M, Ayala GE. Moving Beyond Gleason Scoring. Arch Pathol Lab Med. 2019 May;143(5):565–570. doi: 10.5858/arpa.2018-0242-RA. Epub 2019 Mar 13. PMID: 30865488.
73. Mottet N, Bellmunt J, Bolla M, Briers E, Cumberbatch MG, De Santis M, Fossati N, Gross T, Henry AM, Joniau S, Lam TB, Mason MD, Matveev VB, Moldovan PC, van den Bergh RCN, Van den Broeck T, van der Poel HG, van der Kwast TH, Rouvière O, Schoots IG, Wiegel T, Cornford P. EAU-ESTRO-SIOG Guidelines on Prostate Cancer. Part 1: Screening, Diagnosis, and Local Treatment with Curative Intent. Eur Urol. 2017 Apr;71(4):618–629. doi: 10.1016/j.eururo.2016.08.003. Epub 2016 Aug 25. PMID: 27568654.
74. Nalisnik M, Amgad M, Lee S, Halani SH, Velazquez Vega JE, Brat DJ, Gutman DA, Cooper LAD. Interactive phenotyping of large-scale histology imaging data with HistomicsML. Sci Rep. 2017 Nov 6;7(1):14588. doi: 10.1038/s41598-017-15092-3. PMID: 29109450; PMCID: PMC5674015.
75. Nguyen-Dumont T, Myszka A, Karpinski P, Sasiadek MM, Akopyan H, Hammet F, Tsimiklis H, Park DJ, Pope BJ, Slezak R, Kitsera N, Siekierzynska A, Southey MC. FANCM and RECQL genetic variants and breast cancer susceptibility: relevance to South Poland and West Ukraine. BMC Med Genet. 2018 Jan 19;19(1):12. doi: 10.1186/s12881-018-0524-x. PMID: 29351780; PMCID: PMC5775547.
76. Nikolaidi A, Konstantopoulou I, Pistalmantzian N, Fostira F, Yannoukakos D, Athanasiadis I. A Patient Affected with Serous Ovarian/Peritoneal Carcinoma Carrying the *FANCM* Mutation. Case Rep Oncol Med. 2019 May 16;2019:9357924. doi: 10.1155/2019/9357924. PMID: 31223512; PMCID: PMC6541994.
77. O'Rourke JJ, Bythell-Douglas R, Dunn EA, Deans AJ. ALT control, delete: FANCM as an anti-cancer target in Alternative Lengthening of Telomeres. Nucleus. 2019 Dec;10(1):221-230. doi: 10.1080/19491034.2019.1685246. PMID: 31663812; PMCID: PMC6949022.

78. Olumi AF, Grossfeld GD, Hayward SW, Carroll PR, Tlsty TD, Cunha GR. Carcinoma-associated fibroblasts direct tumor progression of initiated human prostatic epithelium. Cancer Res. 1999 Oct 1;59(19):5002–11. doi: 10.1186/bcr138. PMID: 10519415; PMCID: PMC3300837.
79. Osorio CFEM, Costa WS, Gallo CBM, Sampaio FJB. Expression of stromal elements of prostatic adenocarcinoma in different gleason scores. Acta Cir Bras. 2019 Dec 13;34(10):e201901005. doi: 10.1590/s0102-865020190100000005. PMID: 31851213; PMCID: PMC6912842.
80. Ozok HU, Sagnak L, Tuygun C, Oktay M, Karakoyunlu N, Ersoy H, Alper M. Will the modification of the Gleason grading system affect the urology practice? Int J Surg Pathol. 2010 Aug;18(4):248–54. doi: 10.1177/1066896909346272. Epub 2009 Sep 30. PMID: 19793829.
81. Pan X, Ahmed N, Kong J, Zhang D. Breaking the end: Target the replication stress response at the ALT telomeres for cancer therapy. Mol Cell Oncol. 2017 Sep 22;4(6):e1360978. doi: 10.1080/23723556.2017.1360978. PMID: 29209649; PMCID: PMC5706943.
82. Pantanowitz L, Sharma A, Carter AB, Kurc T, Sussman A, Saltz J. Twenty Years of Digital Pathology: An Overview of the Road Travelled, What is on the Horizon, and the Emergence of Vendor-Neutral Archives. J Pathol Inform. 2018 Nov 21;9:40. doi: 10.4103/jpi.jpi_69_18. PMID: 30607307; PMCID: PMC6289005.
83. Patasius A, Innos K, Barchuk A, Ryzhov A, Leja M, Misins J, Yaumenenka A, Smailyte G. Prostate cancer incidence and mortality in the Baltic states, Belarus, the Russian Federation and Ukraine. BMJ Open. 2019 Oct 9;9(10):e031856. doi: 10.1136/bmjopen-2019-031856. PMID: 31601600; PMCID: PMC6797259.
84. Planche A, Bacac M, Provero P, Fusco C, Delorenzi M, Stehle JC, Stamenkovic I. Identification of prognostic molecular features in the reactive stroma of human breast and prostate cancer. PLoS One. 2011;6(5):e18640. doi: 10.1371/journal.pone.0018640. Epub 2011 May 18. PMID: 21611158; PMCID: PMC3097176.
85. Quinn M, Babb P. Patterns and trends in prostate cancer incidence, survival, prevalence and mortality. Part I: international comparisons. BJU Int. 2002 Jul;90(2):162–73. doi: 10.1046/j.1464-410x.2002.2822.x. PMID: 12081758.
86. Rawla P. Epidemiology of Prostate Cancer. World J Oncol. 2019 Apr;10(2):63-89. doi: 10.14740/wjon1191. Epub 2019 Apr 20. PMID: 31068988; PMCID: PMC6497009.
87. Reissigl A, Pointner J, Strasser H, Ennemoser O, Klocker H, Bartsch G. Frequency and clinical significance of transition zone cancer in prostate cancer screening. Prostate. 1997 Feb 1;30(2):130–5. doi: 10.1002/(sici)1097-0045(19970201)30:2<130::aid-pros8>3.0.co;2-s. PMID: 9051151.
88. Riaz N, Blecua P, Lim RS, Shen R, Higginson DS, Weinhold N, Norton L, Weigelt B, Powell SN, Reis-Filho JS. Pan-cancer analysis of bi-allelic alterations in homologous recombination DNA repair genes. Nat Commun. 2017 Oct 11;8(1):857. doi: 10.1038/s41467-017-00921-w. PMID: 29021619; PMCID: PMC5636842.
89. Richardsen E, Andersen S, Al-Saad S, Rakaee M, Nordby Y, Pedersen MI, Ness N, Grindstad T, Movik I, Dønnem T, Bremnes R, Busund LT. Evaluation of the proliferation marker Ki-67 in a large prostatectomy cohort. PLoS One. 2017 Nov 15;12(11):e0186852. doi: 10.1371/journal.pone.0186852. PMID: 29141018; PMCID: PMC5687762.

90. Rochette A, Boufaied N, Scarlata E, Hamel L, Brimo F, Whitaker HC, Ramos-Montoya A, Neal DE, Dragomir A, Aprikian A, Chevalier S, Thomson AA. Asporin is a stromally expressed marker associated with prostate cancer progression. Br J Cancer. 2017 Mar 14;116(6):775–784. doi: 10.1038/bjc.2017.15. Epub 2017 Feb 2. PMID: 28152543; PMCID: PMC5355923.
91. Ross J, Li G, Yang XJ. Application and Pitfalls of Immunohistochemistry in Diagnosis of Challenging Genitourinary Cases. Arch Pathol Lab Med. 2020 Mar; 144(3):290–304. doi: 10.5858/arpa.2019-0550-RA. PMID: 32101059.
92. Saha M, Chakraborty C, Arun I, Ahmed R, Chatterjee S. An Advanced Deep Learning Approach for Ki-67 Stained Hotspot Detection and Proliferation Rate Scoring for Prognostic Evaluation of Breast Cancer. Sci Rep. 2017 Jun 12;7(1):3213. doi: 10.1038/s41598-017-03405-5. PMID: 28607456; PMCID: PMC5468356.
93. Schneider CA, Rasband WS, Eliceiri KW. NIH Image to ImageJ: 25 years of image analysis. Nat Methods. 2012 Jul;9(7):671–5. doi: 10.1038/nmeth.2089. PMID: 22930834; PMCID: PMC5554542.
94. Schayek H, Haugk K, Sun S, True LD, Plymate SR, Werner H. Tumor suppressor BRCA1 is expressed in prostate cancer and controls insulin-like growth factor I receptor (IGF-IR) gene transcription in an androgen receptor-dependent manner. Clin Cancer Res. 2009 Mar 1;15(5):1558–65. doi: 10.1158/1078-0432.CCR-08-1440. Epub 2009 Feb 17. PMID: 19223505; PMCID: PMC2935172.
95. Schmitt M, Maron RC, Hekler A, Stenzinger A, Hauschild A, Weichenthal M, Tiemann M, Krahl D, Kutzner H, Utikal JS, Haferkamp S, Kather JN, Klauschen F, Krieghoff-Henning E, Fröhling S, von Kalle C, Brinker TJ. Hidden Variables in Deep Learning Digital Pathology and Their Potential to Cause Batch Effects: Prediction Model Study. J Med Internet Res. 2021 Feb 2;23(2):e23436. doi: 10.2196/23436. PMID: 33528370; PMCID: PMC7886613.
96. Scholzen T, Gerdes J. The Ki-67 protein: from the known and the unknown. J Cell Physiol. 2000 Mar;182(3):311–22. doi: 10.1002/(SICI)1097-4652(200003)182:3<311::AID-JCP1>3.0.CO;2-9. PMID: 10653597.
97. Seisen T, Roudot-Thoraval F, Bosset PO, Beaugerie A, Allory Y, Vordos D, Abbou CC, De La Taille A, Salomon L. Predicting the risk of harboring high-grade disease for patients diagnosed with prostate cancer scored as Gleason ≤ 6 on biopsy cores. World J Urol. 2015 Jun;33(6):787–92. doi: 10.1007/s00345-014-1348-8. Epub 2014 Jul 2. PMID: 24985552.
98. Sfoungaristos S, Katafigiotis I, Perimenis P. The role of PSA density to predict a pathological tumour upgrade between needle biopsy and radical prostatectomy for low risk clinical prostate cancer in the modified Gleason system era. Can Urol Assoc J. 2013 Nov-Dec;7(11–12):E722–7. doi: 10.5489/cuaj.374. PMID: 24282465; PMCID: PMC3840515.
99. Sfoungaristos S, Perimenis P. Clinical and pathological variables that predict changes in tumour grade after radical prostatectomy in patients with prostate cancer. Can Urol Assoc J. 2013 Jan-Feb;7(1–2):E93–7. doi: 10.5489/cuaj.270. PMID: 23671515; PMCID: PMC3650813.
100. Shah, R. B., Zhou, M. Histologic Variants of Acinar Adenocarcinoma, Ductal Adenocarcinoma, Neuroendocrine Tumors, and Other Carcinomas. in Prostate Biopsy Interpretation: An Illustrated Guide 69–95 (Springer International Publishing, 2019). doi:10.1007/978-3-030-13601-7_6.

101. Sis B, Sarioglu S, Sokmen S, Sakar M, Kupelioglu A, Fuzun M. Desmoplasia measured by computer assisted image analysis: an independent prognostic marker in colorectal carcinoma. J Clin Pathol. 2005 Jan;58(1):32–8. doi: 10.1136/jcp.2004.018705. PMID: 15623479; PMCID: PMC1770537.
102. Silva MM Jr, Matheus WE, Garcia PV, Stopiglia RM, Billis A, Ferreira U, Fávaro WJ. Characterization of reactive stroma in prostate cancer: involvement of growth factors, metalloproteinase matrix, sexual hormones receptors and prostatic stem cells. Int Braz J Urol. 2015 Sep–Oct;41(5):849–58. doi: 10.1590/S1677-5538.IBJU.2014.0355. PMID: 26689510; PMCID: PMC4756961.
103. Suhovskih AV, Mostovich LA, Kunin IS, Boboev MM, Nepomnyashchikh GI, Aidagulova SV, Grigorieva EV. Proteoglycan expression in normal human prostate tissue and prostate cancer. ISRN Oncol. 2013 Apr 18;2013:680136. doi: 10.1155/2013/680136. PMID: 23691363; PMCID: PMC3654277.
104. Taitt HE. Global Trends and Prostate Cancer: A Review of Incidence, Detection, and Mortality as Influenced by Race, Ethnicity, and Geographic Location. Am J Mens Health. 2018 Nov;12(6):1807–1823. doi: 10.1177/1557988318798279. Epub 2018 Sep 11. PMID: 30203706; PMCID: PMC6199451.
105. Thorgeirsson T, Jordahl KM, Flavin R, Epstein MM, Fiorentino M, Andersson SO, Andren O, Rider JR, Mosquera JM, Ingoldsby H, Fall K, Tryggvadottir L, Mucci LA; Transdisciplinary Prostate Cancer Partnership (ToPCaP). Intracellular location of BRCA2 protein expression and prostate cancer progression in the Swedish Watchful Waiting Cohort. Carcinogenesis. 2016 Mar;37(3):262–8. doi: 10.1093/carcin/bgw001. Epub 2016 Jan 16. PMID: 26775038; PMCID: PMC6233023.
106. Tretiakova MS, Wei W, Boyer HD, Newcomb LF, Hawley S, Auman H, Vakar-Lopez F, McKenney JK, Fazli L, Simko J, Troyer DA, Hurtado-Coll A, Thompson IM Jr, Carroll PR, Ellis WJ, Gleave ME, Nelson PS, Lin DW, True LD, Feng Z, Brooks JD. Prognostic value of Ki67 in localized prostate carcinoma: a multi-institutional study of >1000 prostatectomies. Prostate Cancer Prostatic Dis. 2016 Sep;19(3):264–70. doi: 10.1038/pcan.2016.12. Epub 2016 May 3. PMID: 27136741; PMCID: PMC5536893.
107. Tretiakova MS, Wei W, Boyer HD, Newcomb LF, Hawley S, Auman H, Vakar-Lopez F, McKenney JK, Fazli L, Simko J, Troyer DA, Hurtado-Coll A, Thompson IM Jr, Carroll PR, Ellis WJ, Gleave ME, Nelson PS, Lin DW, True LD, Feng Z, Brooks JD. Prognostic value of Ki67 in localized prostate carcinoma: a multi-institutional study of >1000 prostatectomies. Prostate Cancer Prostatic Dis. 2016 Sep;19(3):264–70. doi: 10.1038/pcan.2016.12. Epub 2016 May 3. PMID: 27136741; PMCID: PMC5536893.
108. Truong M, Slezak JA, Lin CP, Iremashvili V, Sado M, Razmaria AA, Leverson G, Soloway MS, Eggener SE, Abel EJ, Downs TM, Jarrard DF. Development and multi-institutional validation of an upgrading risk tool for Gleason 6 prostate cancer. Cancer. 2013 Nov 15;119(22):3992–4002. doi: 10.1002/cncr.28303. Epub 2013 Sep 4. PMID: 24006289; PMCID: PMC4880351.
109. Tsui V, Crismani W. The Fanconi Anemia Pathway and Fertility. Trends Genet. 2019 Mar;35(3):199–214. doi: 10.1016/j.tig.2018.12.007. Epub 2019 Jan 22. PMID: 30683429.
110. Tuxhorn JA, Ayala GE, Smith MJ, Smith VC, Dang TD, Rowley DR. Reactive stroma in human prostate cancer: induction of myofibroblast phenotype and extracellular matrix remodeling. Clin Cancer Res. 2002 Sep;8(9):2912–23. PMID: 12231536.

111. Valkenburg KC, de Groot AE, Pienta KJ. Targeting the tumour stroma to improve cancer therapy. Nat Rev Clin Oncol. 2018 Jun;15(6):366–381. doi: 10.1038/s41571-018-0007-1. PMID: 29651130; PMCID: PMC5960434.
112. Van Praet C, Libbrecht L, D'Hondt F, Decaestecker K, Fonteyne V, Verschuere S, Rottey S, Praet M, De Visschere P, Lumen N; Uro-Oncology Group Ghent. Agreement of Gleason score on prostate biopsy and radical prostatectomy specimen: is there improvement with increased number of biopsy cylinders and the 2005 revised Gleason scoring? Clin Genitourin Cancer. 2014 Jun;12(3):160–6. doi: 10.1016/j.clgc.2013.11.008. Epub 2013 Nov 12. PMID: 24361055.
113. Van Leenders GJLH, van der Kwast TH, Grignon DJ, Evans AJ, Kristiansen G, Kweldam CF, Litjens G, McKenney JK, Melamed J, Mottet N, Paner GP, Samaratunga H, Schoots IG, Simko JP, Tsuzuki T, Varma M, Warren AY, Wheeler TM, Williamson SR, Iczkowski KA; ISUP Grading Workshop Panel Members. The 2019 International Society of Urological Pathology (ISUP) Consensus Conference on Grading of Prostatic Carcinoma. Am J Surg Pathol. 2020 Aug;44(8):e87–e99. doi: 10.1097/PAS.0000000000001497. PMID: 32459716; PMCID: PMC7382533.
114. Vellekoop A, Loeb S, Folkvaljon Y, Stattin P. Population based study of predictors of adverse pathology among candidates for active surveillance with Gleason 6 prostate cancer. J Urol. 2014 Feb;191(2):350–7. doi: 10.1016/j.juro.2013.09.034. Epub 2013 Sep 23. PMID: 24071481.
115. Verma R, Gupta V, Singh J, Verma M, Gupta G, Gupta S, Sen R, Ralli M. Significance of p53 and ki-67 expression in prostate cancer. Urol Ann. 2015 Oct-Dec;7(4):488–93. doi: 10.4103/0974-7796.158507. PMID: 26692671; PMCID: PMC4660702.
116. Xie T, Dong B, Yan Y, Hu G, Xu Y. Association between MMP-2 expression and prostate cancer: A meta-analysis. Biomed Rep. 2016 Feb;4(2):241–245. doi: 10.3892/br.2015.553. Epub 2015 Dec 8. PMID: 26893846; PMCID: PMC4734094.
117. Xue X, Sung P, Zhao X. Functions and regulation of the multitasking FANCM family of DNA motor proteins. Genes Dev. 2015 Sep 1;29(17):1777–88. doi: 10.1101/gad.266593.115. PMID: 26341555; PMCID: PMC4573851.
118. Yan Z, Delannoy M, Ling C, Daee D, Osman F, Muniandy PA, Shen X, Oostra AB, Du H, Steltenpool J, Lin T, Schuster B, Décaillet C, Stasiak A, Stasiak AZ, Stone S, Hoatlin ME, Schindler D, Woodcock CL, Joenje H, Sen R, de Winter JP, Li L, Seidman MM, Whitby MC, Myung K, Constantinou A, Wang W. A histone-fold complex and FANCM form a conserved DNA-remodeling complex to maintain genome stability. Mol Cell. 2010 Mar 26;37(6):865–78. doi: 10.1016/j.molcel.2010.01.039. PMID: 20347428; PMCID: PMC2847587.
119. Yang Z, Peng YC, Gopalan A, Gao D, Chen Y, Joyner AL. Stromal hedgehog signaling maintains smooth muscle and hampers micro-invasive prostate cancer. Dis Model Mech. 2017 Jan 1;10(1):39–52. doi: 10.1242/dmm.027417. Epub 2016 Nov 30. PMID: 27935821; PMCID: PMC5278527.

PUBLICATIONS

CURRICULUM VITAE

Name: Georgi Dzaparidze
Date of birth: July 20, 1990, Tartu
Citizenship: Estonian
Phone: +372 566 49 315
E-mail: geodza@gmail.com

Education:

2021–…	the University of Tartu, Faculty of Medicine, Obstetrics and Gynecology residency
2017–2021	the University of Tartu, Faculty of Medicine, Doctoral studies
2016–2020	the University of Tartu, Faculty of Medicine, Pathology residency
2010–2016	the University of Tartu, Faculty of Medicine
2009–2010	Chemistry and biotechnology, TalTech
2001–2009	Tallinn Tynismay School of Sciences
01.09.1997–01.06.2001	Tallinn Russian Lyceum

Language skills: English, Russian, Georgian

Professional employment:

2020–…	East Tallinn Central Hospital Pathologist

ELULOOKIRJELDUS

Nimi: Georgi Dzaparidze
Sünniaeg: 20. juuli 1990, Tartu
Kodakonsus: Eesti
Telefon: +372 566 49 315
E-mail: geodza@gmail.com

Haridus:

2021–…	Sünnitusabi ja günekoloogia residentuur
2017– 2021	Tartu ülikool, Meditsiiniteaduste valdkond, bio- ja siirde-meditsiini instituut, doktorant
2016–2020	Residentuur kliinilise patoloogia erialal
2010–2016	Arstiteadus, Tartu Ülikool
2009–2010	Rakenduskeemia ja biotehnoloogia, Tallinna Tehnikaülikool.
2001–2009	Tallinna Tõnismäe Reaalkool.
01.09.1997–01.06.2001	Tallinna Linnamäe Vene Lütseum

Keelteoskus: inglise, vene, gruusia

Teenistuskäik:

2020–…	Ida-Tallinna Keskhaiglas, patoloog

DISSERTATIONES MEDICINAE UNIVERSITATIS TARTUENSIS

1. **Heidi-Ingrid Maaroos**. The natural course of gastric ulcer in connection with chronic gastritis and *Helicobacter pylori*. Tartu, 1991.
2. **Mihkel Zilmer**. Na-pump in normal and tumorous brain tissues: Structural, functional and tumorigenesis aspects. Tartu, 1991.
3. **Eero Vasar**. Role of cholecystokinin receptors in the regulation of behaviour and in the action of haloperidol and diazepam. Tartu, 1992.
4. **Tiina Talvik**. Hypoxic-ischaemic brain damage in neonates (clinical, biochemical and brain computed tomographical investigation). Tartu, 1992.
5. **Ants Peetsalu**. Vagotomy in duodenal ulcer disease: A study of gastric acidity, serum pepsinogen I, gastric mucosal histology and *Helicobacter pylori*. Tartu, 1992.
6. **Marika Mikelsaar**. Evaluation of the gastrointestinal microbial ecosystem in health and disease. Tartu, 1992.
7. **Hele Everaus**. Immuno-hormonal interactions in chronic lymphocytic leukaemia and multiple myeloma. Tartu, 1993.
8. **Ruth Mikelsaar**. Etiological factors of diseases in genetically consulted children and newborn screening: dissertation for the commencement of the degree of doctor of medical sciences. Tartu, 1993.
9. **Agu Tamm**. On metabolic action of intestinal microflora: clinical aspects. Tartu, 1993.
10. **Katrin Gross**. Multiple sclerosis in South-Estonia (epidemiological and computed tomographical investigations). Tartu, 1993.
11. **Oivi Uibo**. Childhood coeliac disease in Estonia: occurrence, screening, diagnosis and clinical characterization. Tartu, 1994.
12. **Viiu Tuulik**. The functional disorders of central nervous system of chemistry workers. Tartu, 1994.
13. **Margus Viigimaa**. Primary haemostasis, antiaggregative and anticoagulant treatment of acute myocardial infarction. Tartu, 1994.
14. **Rein Kolk**. Atrial versus ventricular pacing in patients with sick sinus syndrome. Tartu, 1994.
15. **Toomas Podar**. Incidence of childhood onset type 1 diabetes mellitus in Estonia. Tartu, 1994.
16. **Kiira Subi**. The laboratory surveillance of the acute respiratory viral infections in Estonia. Tartu, 1995.
17. **Irja Lutsar**. Infections of the central nervous system in children (epidemiologic, diagnostic and therapeutic aspects, long term outcome). Tartu, 1995.
18. **Aavo Lang**. The role of dopamine, 5-hydroxytryptamine, sigma and NMDA receptors in the action of antipsychotic drugs. Tartu, 1995.
19. **Andrus Arak**. Factors influencing the survival of patients after radical surgery for gastric cancer. Tartu, 1996.

20. **Tõnis Karki**. Quantitative composition of the human lactoflora and method for its examination. Tartu, 1996.
21. **Reet Mändar**. Vaginal microflora during pregnancy and its transmission to newborn. Tartu, 1996.
22. **Triin Remmel**. Primary biliary cirrhosis in Estonia: epidemiology, clinical characterization and prognostication of the course of the disease. Tartu, 1996.
23. **Toomas Kivastik**. Mechanisms of drug addiction: focus on positive reinforcing properties of morphine. Tartu, 1996.
24. **Paavo Pokk**. Stress due to sleep deprivation: focus on $GABA_A$ receptor-chloride ionophore complex. Tartu, 1996.
25. **Kristina Allikmets**. Renin system activity in essential hypertension. Associations with atherothrombogenic cardiovascular risk factors and with the efficacy of calcium antagonist treatment. Tartu, 1996.
26. **Triin Parik**. Oxidative stress in essential hypertension: Associations with metabolic disturbances and the effects of calcium antagonist treatment. Tartu, 1996.
27. **Svetlana Päi**. Factors promoting heterogeneity of the course of rheumatoid arthritis. Tartu, 1997.
28. **Maarike Sallo**. Studies on habitual physical activity and aerobic fitness in 4 to 10 years old children. Tartu, 1997.
29. **Paul Naaber**. *Clostridium difficile* infection and intestinal microbial ecology. Tartu, 1997.
30. **Rein Pähkla**. Studies in pinoline pharmacology. Tartu, 1997.
31. **Andrus Juhan Voitk**. Outpatient laparoscopic cholecystectomy. Tartu, 1997.
32. **Joel Starkopf**. Oxidative stress and ischaemia-reperfusion of the heart. Tartu, 1997.
33. **Janika Kõrv**. Incidence, case-fatality and outcome of stroke. Tartu, 1998.
34. **Ülla Linnamägi**. Changes in local cerebral blood flow and lipid peroxidation following lead exposure in experiment. Tartu, 1998.
35. **Ave Minajeva**. Sarcoplasmic reticulum function: comparison of atrial and ventricular myocardium. Tartu, 1998.
36. **Oleg Milenin**. Reconstruction of cervical part of esophagus by revascularised ileal autografts in dogs. A new complex multistage method. Tartu, 1998.
37. **Sergei Pakriev**. Prevalence of depression, harmful use of alcohol and alcohol dependence among rural population in Udmurtia. Tartu, 1998.
38. **Allen Kaasik**. Thyroid hormone control over β-adrenergic signalling system in rat atria. Tartu, 1998.
39. **Vallo Matto**. Pharmacological studies on anxiogenic and antiaggressive properties of antidepressants. Tartu, 1998.
40. **Maire Vasar**. Allergic diseases and bronchial hyperreactivity in Estonian children in relation to environmental influences. Tartu, 1998.
41. **Kaja Julge**. Humoral immune responses to allergens in early childhood. Tartu, 1998.

42. **Heli Grünberg**. The cardiovascular risk of Estonian schoolchildren. A cross-sectional study of 9-, 12- and 15-year-old children. Tartu, 1998.
43. **Epp Sepp**. Formation of intestinal microbial ecosystem in children. Tartu, 1998.
44. **Mai Ots**. Characteristics of the progression of human and experimental glomerulopathies. Tartu, 1998.
45. **Tiina Ristimäe**. Heart rate variability in patients with coronary artery disease. Tartu, 1998.
46. **Leho Kõiv**. Reaction of the sympatho-adrenal and hypothalamo-pituitary-adrenocortical system in the acute stage of head injury. Tartu, 1998.
47. **Bela Adojaan**. Immune and genetic factors of childhood onset IDDM in Estonia. An epidemiological study. Tartu, 1999.
48. **Jakov Shlik**. Psychophysiological effects of cholecystokinin in humans. Tartu, 1999.
49. **Kai Kisand**. Autoantibodies against dehydrogenases of α-ketoacids. Tartu, 1999.
50. **Toomas Marandi**. Drug treatment of depression in Estonia. Tartu, 1999.
51. **Ants Kask**. Behavioural studies on neuropeptide Y. Tartu, 1999.
52. **Ello-Rahel Karelson**. Modulation of adenylate cyclase activity in the rat hippocampus by neuropeptide galanin and its chimeric analogs. Tartu, 1999.
53. **Tanel Laisaar**. Treatment of pleural empyema — special reference to intrapleural therapy with streptokinase and surgical treatment modalities. Tartu, 1999.
54. **Eve Pihl**. Cardiovascular risk factors in middle-aged former athletes. Tartu, 1999.
55. **Katrin Õunap**. Phenylketonuria in Estonia: incidence, newborn screening, diagnosis, clinical characterization and genotype/phenotype correlation. Tartu, 1999.
56. **Siiri Kõljalg**. *Acinetobacter* – an important nosocomial pathogen. Tartu, 1999.
57. **Helle Karro**. Reproductive health and pregnancy outcome in Estonia: association with different factors. Tartu, 1999.
58. **Heili Varendi**. Behavioral effects observed in human newborns during exposure to naturally occurring odors. Tartu, 1999.
59. **Anneli Beilmann**. Epidemiology of epilepsy in children and adolescents in Estonia. Prevalence, incidence, and clinical characteristics. Tartu, 1999.
60. **Vallo Volke**. Pharmacological and biochemical studies on nitric oxide in the regulation of behaviour. Tartu, 1999.
61. **Pilvi Ilves**. Hypoxic-ischaemic encephalopathy in asphyxiated term infants. A prospective clinical, biochemical, ultrasonographical study. Tartu, 1999.
62. **Anti Kalda**. Oxygen-glucose deprivation-induced neuronal death and its pharmacological prevention in cerebellar granule cells. Tartu, 1999.
63. **Eve-Irene Lepist**. Oral peptide prodrugs – studies on stability and absorption. Tartu, 2000.

64. **Jana Kivastik**. Lung function in Estonian schoolchildren: relationship with anthropometric indices and respiratory symptomas, reference values for dynamic spirometry. Tartu, 2000.
65. **Karin Kull**. Inflammatory bowel disease: an immunogenetic study. Tartu, 2000.
66. **Kaire Innos**. Epidemiological resources in Estonia: data sources, their quality and feasibility of cohort studies. Tartu, 2000.
67. **Tamara Vorobjova**. Immune response to *Helicobacter pylori* and its association with dynamics of chronic gastritis and epithelial cell turnover in antrum and corpus. Tartu, 2001.
68. **Ruth Kalda**. Structure and outcome of family practice quality in the changing health care system of Estonia. Tartu, 2001.
69. **Annika Krüüner**. *Mycobacterium tuberculosis* – spread and drug resistance in Estonia. Tartu, 2001.
70. **Marlit Veldi**. Obstructive Sleep Apnoea: Computerized Endopharyngeal Myotonometry of the Soft Palate and Lingual Musculature. Tartu, 2001.
71. **Anneli Uusküla**. Epidemiology of sexually transmitted diseases in Estonia in 1990–2000. Tartu, 2001.
72. **Ade Kallas**. Characterization of antibodies to coagulation factor VIII. Tartu, 2002.
73. **Heidi Annuk**. Selection of medicinal plants and intestinal lactobacilli as antimicrobil components for functional foods. Tartu, 2002.
74. **Aet Lukmann**. Early rehabilitation of patients with ischaemic heart disease after surgical revascularization of the myocardium: assessment of health-related quality of life, cardiopulmonary reserve and oxidative stress. A clinical study. Tartu, 2002.
75. **Maigi Eisen**. Pathogenesis of Contact Dermatitis: participation of Oxidative Stress. A clinical – biochemical study. Tartu, 2002.
76. **Piret Hussar**. Histology of the post-traumatic bone repair in rats. Elaboration and use of a new standardized experimental model – bicortical perforation of tibia compared to internal fracture and resection osteotomy. Tartu, 2002.
77. **Tõnu Rätsep**. Aneurysmal subarachnoid haemorrhage: Noninvasive monitoring of cerebral haemodynamics. Tartu, 2002.
78. **Marju Herodes**. Quality of life of people with epilepsy in Estonia. Tartu, 2003.
79. **Katre Maasalu**. Changes in bone quality due to age and genetic disorders and their clinical expressions in Estonia. Tartu, 2003.
80. **Toomas Sillakivi**. Perforated peptic ulcer in Estonia: epidemiology, risk factors and relations with *Helicobacter pylori*. Tartu, 2003.
81. **Leena Puksa**. Late responses in motor nerve conduction studies. F and A waves in normal subjects and patients with neuropathies. Tartu, 2003.
82. **Krista Lõivukene**. *Helicobacter pylori* in gastric microbial ecology and its antimicrobial susceptibility pattern. Tartu, 2003.

83. **Helgi Kolk**. Dyspepsia and *Helicobacter pylori* infection: the diagnostic value of symptoms, treatment and follow-up of patients referred for upper gastrointestinal endoscopy by family physicians. Tartu, 2003.
84. **Helena Soomer**. Validation of identification and age estimation methods in forensic odontology. Tartu, 2003.
85. **Kersti Oselin**. Studies on the human MDR1, MRP1, and MRP2 ABC transporters: functional relevance of the genetic polymorphisms in the *MDR1* and *MRP1* gene. Tartu, 2003.
86. **Jaan Soplepmann**. Peptic ulcer haemorrhage in Estonia: epidemiology, prognostic factors, treatment and outcome. Tartu, 2003.
87. **Margot Peetsalu**. Long-term follow-up after vagotomy in duodenal ulcer disease: recurrent ulcer, changes in the function, morphology and *Helicobacter pylori* colonisation of the gastric mucosa. Tartu, 2003.
88. **Kersti Klaamas**. Humoral immune response to *Helicobacter pylori* a study of host-dependent and microbial factors. Tartu, 2003.
89. **Pille Taba**. Epidemiology of Parkinson's disease in Tartu, Estonia. Prevalence, incidence, clinical characteristics, and pharmacoepidemiology. Tartu, 2003.
90. **Alar Veraksitš**. Characterization of behavioural and biochemical phenotype of cholecystokinin-2 receptor deficient mice: changes in the function of the dopamine and endopioidergic system. Tartu, 2003.
91. **Ingrid Kalev**. CC-chemokine receptor 5 (CCR5) gene polymorphism in Estonians and in patients with Type I and Type II diabetes mellitus. Tartu, 2003.
92. **Lumme Kadaja**. Molecular approach to the regulation of mitochondrial function in oxidative muscle cells. Tartu, 2003.
93. **Aive Liigant**. Epidemiology of primary central nervous system tumours in Estonia from 1986 to 1996. Clinical characteristics, incidence, survival and prognostic factors. Tartu, 2004.
94. **Andres, Kulla**. Molecular characteristics of mesenchymal stroma in human astrocytic gliomas. Tartu, 2004.
95. **Mari Järvelaid**. Health damaging risk behaviours in adolescence. Tartu, 2004.
96. **Ülle Pechter**. Progression prevention strategies in chronic renal failure and hypertension. An experimental and clinical study. Tartu, 2004.
97. **Gunnar Tasa**. Polymorphic glutathione S-transferases – biology and role in modifying genetic susceptibility to senile cataract and primary open angle glaucoma. Tartu, 2004.
98. **Tuuli Käämbre**. Intracellular energetic unit: structural and functional aspects. Tartu, 2004.
99. **Vitali Vassiljev**. Influence of nitric oxide syntase inhibitors on the effects of ethanol after acute and chronic ethanol administration and withdrawal. Tartu, 2004.

100. **Aune Rehema**. Assessment of nonhaem ferrous iron and glutathione redox ratio as markers of pathogeneticity of oxidative stress in different clinical groups. Tartu, 2004.
101. **Evelin Seppet**. Interaction of mitochondria and ATPases in oxidative muscle cells in normal and pathological conditions. Tartu, 2004.
102. **Eduard Maron**. Serotonin function in panic disorder: from clinical experiments to brain imaging and genetics. Tartu, 2004.
103. **Marje Oona**. *Helicobacter pylori* infection in children: epidemiological and therapeutic aspects. Tartu, 2004.
104. **Kersti Kokk**. Regulation of active and passive molecular transport in the testis. Tartu, 2005.
105. **Vladimir Järv**. Cross-sectional imaging for pretreatment evaluation and follow-up of pelvic malignant tumours. Tartu, 2005.
106. **Andre Õun**. Epidemiology of adult epilepsy in Tartu, Estonia. Incidence, prevalence and medical treatment. Tartu, 2005.
107. **Piibe Muda**. Homocysteine and hypertension: associations between homocysteine and essential hypertension in treated and untreated hypertensive patients with and without coronary artery disease. Tartu, 2005.
108. **Külli Kingo**. The interleukin-10 family cytokines gene polymorphisms in plaque psoriasis. Tartu, 2005.
109. **Mati Merila**. Anatomy and clinical relevance of the glenohumeral joint capsule and ligaments. Tartu, 2005.
110. **Epp Songisepp**. Evaluation of technological and functional properties of the new probiotic *Lactobacillus fermentum* ME-3. Tartu, 2005.
111. **Tiia Ainla**. Acute myocardial infarction in Estonia: clinical characteristics, management and outcome. Tartu, 2005.
112. **Andres Sell**. Determining the minimum local anaesthetic requirements for hip replacement surgery under spinal anaesthesia – a study employing a spinal catheter. Tartu, 2005.
113. **Tiia Tamme**. Epidemiology of odontogenic tumours in Estonia. Pathogenesis and clinical behaviour of ameloblastoma. Tartu, 2005.
114. **Triine Annus**. Allergy in Estonian schoolchildren: time trends and characteristics. Tartu, 2005.
115. **Tiia Voor**. Microorganisms in infancy and development of allergy: comparison of Estonian and Swedish children. Tartu, 2005.
116. **Priit Kasenõmm**. Indicators for tonsillectomy in adults with recurrent tonsillitis – clinical, microbiological and pathomorphological investigations. Tartu, 2005.
117. **Eva Zusinaite**. Hepatitis C virus: genotype identification and interactions between viral proteases. Tartu, 2005.
118. **Piret Kõll**. Oral lactoflora in chronic periodontitis and periodontal health. Tartu, 2006.
119. **Tiina Stelmach**. Epidemiology of cerebral palsy and unfavourable neurodevelopmental outcome in child population of Tartu city and county, Estonia Prevalence, clinical features and risk factors. Tartu, 2006.

120. **Katrin Pudersell**. Tropane alkaloid production and riboflavine excretion in the field and tissue cultures of henbane (*Hyoscyamus niger* L.). Tartu, 2006.
121. **Külli Jaako**. Studies on the role of neurogenesis in brain plasticity. Tartu, 2006.
122. **Aare Märtson**. Lower limb lengthening: experimental studies of bone regeneration and long-term clinical results. Tartu, 2006.
123. **Heli Tähepõld**. Patient consultation in family medicine. Tartu, 2006.
124. **Stanislav Liskmann**. Peri-implant disease: pathogenesis, diagnosis and treatment in view of both inflammation and oxidative stress profiling. Tartu, 2006.
125. **Ruth Rudissaar**. Neuropharmacology of atypical antipsychotics and an animal model of psychosis. Tartu, 2006.
126. **Helena Andreson**. Diversity of *Helicobacter pylori* genotypes in Estonian patients with chronic inflammatory gastric diseases. Tartu, 2006.
127. **Katrin Pruus**. Mechanism of action of antidepressants: aspects of serotoninergic system and its interaction with glutamate. Tartu, 2006.
128. **Priit Põder**. Clinical and experimental investigation: relationship of ischaemia/reperfusion injury with oxidative stress in abdominal aortic aneurysm repair and in extracranial brain artery endarterectomy and possibilities of protection against ischaemia using a glutathione analogue in a rat model of global brain ischaemia. Tartu, 2006.
129. **Marika Tammaru**. Patient-reported outcome measurement in rheumatoid arthritis. Tartu, 2006.
130. **Tiia Reimand**. Down syndrome in Estonia. Tartu, 2006.
131. **Diva Eensoo**. Risk-taking in traffic and Markers of Risk-Taking Behaviour in Schoolchildren and Car Drivers. Tartu, 2007.
132. **Riina Vibo**. The third stroke registry in Tartu, Estonia from 2001 to 2003: incidence, case-fatality, risk factors and long-term outcome. Tartu, 2007.
133. **Chris Pruunsild**. Juvenile idiopathic arthritis in children in Estonia. Tartu, 2007.
134. **Eve Õiglane-Šlik**. Angelman and Prader-Willi syndromes in Estonia. Tartu, 2007.
135. **Kadri Haller**. Antibodies to follicle stimulating hormone. Significance in female infertility. Tartu, 2007.
136. **Pille Ööpik**. Management of depression in family medicine. Tartu, 2007.
137. **Jaak Kals**. Endothelial function and arterial stiffness in patients with atherosclerosis and in healthy subjects. Tartu, 2007.
138. **Priit Kampus**. Impact of inflammation, oxidative stress and age on arterial stiffness and carotid artery intima-media thickness. Tartu, 2007.
139. **Margus Punab**. Male fertility and its risk factors in Estonia. Tartu, 2007.
140. **Alar Toom**. Heterotopic ossification after total hip arthroplasty: clinical and pathogenetic investigation. Tartu, 2007.

141. **Lea Pehme**. Epidemiology of tuberculosis in Estonia 1991–2003 with special regard to extrapulmonary tuberculosis and delay in diagnosis of pulmonary tuberculosis. Tartu, 2007.
142. **Juri Karjagin**. The pharmacokinetics of metronidazole and meropenem in septic shock. Tartu, 2007.
143. **Inga Talvik**. Inflicted traumatic brain injury shaken baby syndrome in Estonia – epidemiology and outcome. Tartu, 2007.
144. **Tarvo Rajasalu**. Autoimmune diabetes: an immunological study of type 1 diabetes in humans and in a model of experimental diabetes (in RIP-B7.1 mice). Tartu, 2007.
145. **Inga Karu**. Ischaemia-reperfusion injury of the heart during coronary surgery: a clinical study investigating the effect of hyperoxia. Tartu, 2007.
146. **Peeter Padrik**. Renal cell carcinoma: Changes in natural history and treatment of metastatic disease. Tartu, 2007.
147. **Neve Vendt**. Iron deficiency and iron deficiency anaemia in infants aged 9 to 12 months in Estonia. Tartu, 2008.
148. **Lenne-Triin Heidmets**. The effects of neurotoxins on brain plasticity: focus on neural Cell Adhesion Molecule. Tartu, 2008.
149. **Paul Korrovits**. Asymptomatic inflammatory prostatitis: prevalence, etiological factors, diagnostic tools. Tartu, 2008.
150. **Annika Reintam**. Gastrointestinal failure in intensive care patients. Tartu, 2008.
151. **Kristiina Roots**. Cationic regulation of Na-pump in the normal, Alzheimer's and CCK_2 receptor-deficient brain. Tartu, 2008.
152. **Helen Puusepp**. The genetic causes of mental retardation in Estonia: fragile X syndrome and creatine transporter defect. Tartu, 2009.
153. **Kristiina Rull**. Human chorionic gonadotropin beta genes and recurrent miscarriage: expression and variation study. Tartu, 2009.
154. **Margus Eimre**. Organization of energy transfer and feedback regulation in oxidative muscle cells. Tartu, 2009.
155. **Maire Link**. Transcription factors FoxP3 and AIRE: autoantibody associations. Tartu, 2009.
156. **Kai Haldre**. Sexual health and behaviour of young women in Estonia. Tartu, 2009.
157. **Kaur Liivak**. Classical form of congenital adrenal hyperplasia due to 21-hydroxylase deficiency in Estonia: incidence, genotype and phenotype with special attention to short-term growth and 24-hour blood pressure. Tartu, 2009.
158. **Kersti Ehrlich**. Antioxidative glutathione analogues (UPF peptides) – molecular design, structure-activity relationships and testing the protective properties. Tartu, 2009.
159. **Anneli Rätsep**. Type 2 diabetes care in family medicine. Tartu, 2009.
160. **Silver Türk**. Etiopathogenetic aspects of chronic prostatitis: role of mycoplasmas, coryneform bacteria and oxidative stress. Tartu, 2009.

161. **Kaire Heilman**. Risk markers for cardiovascular disease and low bone mineral density in children with type 1 diabetes. Tartu, 2009.
162. **Kristi Rüütel**. HIV-epidemic in Estonia: injecting drug use and quality of life of people living with HIV. Tartu, 2009.
163. **Triin Eller**. Immune markers in major depression and in antidepressive treatment. Tartu, 2009.
164. **Siim Suutre**. The role of TGF-β isoforms and osteoprogenitor cells in the pathogenesis of heterotopic ossification. An experimental and clinical study of hip arthroplasty. Tartu, 2010.
165. **Kai Kliiman**. Highly drug-resistant tuberculosis in Estonia: Risk factors and predictors of poor treatment outcome. Tartu, 2010.
166. **Inga Villa**. Cardiovascular health-related nutrition, physical activity and fitness in Estonia. Tartu, 2010.
167. **Tõnis Org**. Molecular function of the first PHD finger domain of Autoimmune Regulator protein. Tartu, 2010.
168. **Tuuli Metsvaht**. Optimal antibacterial therapy of neonates at risk of early onset sepsis. Tartu, 2010.
169. **Jaanus Kahu**. Kidney transplantation: Studies on donor risk factors and mycophenolate mofetil. Tartu, 2010.
170. **Koit Reimand**. Autoimmunity in reproductive failure: A study on associated autoantibodies and autoantigens. Tartu, 2010.
171. **Mart Kull**. Impact of vitamin D and hypolactasia on bone mineral density: a population based study in Estonia. Tartu, 2010.
172. **Rael Laugesaar**. Stroke in children – epidemiology and risk factors. Tartu, 2010.
173. **Mark Braschinsky**. Epidemiology and quality of life issues of hereditary spastic paraplegia in Estonia and implemention of genetic analysis in everyday neurologic practice. Tartu, 2010.
174. **Kadri Suija**. Major depression in family medicine: associated factors, recurrence and possible intervention. Tartu, 2010.
175. **Jarno Habicht**. Health care utilisation in Estonia: socioeconomic determinants and financial burden of out-of-pocket payments. Tartu, 2010.
176. **Kristi Abram**. The prevalence and risk factors of rosacea. Subjective disease perception of rosacea patients. Tartu, 2010.
177. **Malle Kuum**. Mitochondrial and endoplasmic reticulum cation fluxes: Novel roles in cellular physiology. Tartu, 2010.
178. **Rita Teek**. The genetic causes of early onset hearing loss in Estonian children. Tartu, 2010.
179. **Daisy Volmer**. The development of community pharmacy services in Estonia – public and professional perceptions 1993–2006. Tartu, 2010.
180. **Jelena Lissitsina**. Cytogenetic causes in male infertility. Tartu, 2011.
181. **Delia Lepik**. Comparison of gunshot injuries caused from Tokarev, Makarov and Glock 19 pistols at different firing distances. Tartu, 2011.
182. **Ene-Renate Pähkla**. Factors related to the efficiency of treatment of advanced periodontitis. Tartu, 2011.

183. **Maarja Krass**. L-Arginine pathways and antidepressant action. Tartu, 2011.
184. **Taavi Lai**. Population health measures to support evidence-based health policy in Estonia. Tartu, 2011.
185. **Tiit Salum**. Similarity and difference of temperature-dependence of the brain sodium pump in normal, different neuropathological, and aberrant conditions and its possible reasons. Tartu, 2011.
186. **Tõnu Vooder**. Molecular differences and similarities between histological subtypes of non-small cell lung cancer. Tartu, 2011.
187. **Jelena Štšepetova**. The characterisation of intestinal lactic acid bacteria using bacteriological, biochemical and molecular approaches. Tartu, 2011.
188. **Radko Avi**. Natural polymorphisms and transmitted drug resistance in Estonian HIV-1 CRF06_cpx and its recombinant viruses. Tartu, 2011, 116 p.
189. **Edward Laane**. Multiparameter flow cytometry in haematological malignancies. Tartu, 2011, 152 p.
190. **Triin Jagomägi**. A study of the genetic etiology of nonsyndromic cleft lip and palate. Tartu, 2011, 158 p.
191. **Ivo Laidmäe**. Fibrin glue of fish (*Salmo salar*) origin: immunological study and development of new pharmaceutical preparation. Tartu, 2012, 150 p.
192. **Ülle Parm**. Early mucosal colonisation and its role in prediction of invasive infection in neonates at risk of early onset sepsis. Tartu, 2012, 168 p.
193. **Kaupo Teesalu**. Autoantibodies against desmin and transglutaminase 2 in celiac disease: diagnostic and functional significance. Tartu, 2012, 142 p.
194. **Maksim Zagura**. Biochemical, functional and structural profiling of arterial damage in atherosclerosis. Tartu, 2012, 162 p.
195. **Vivian Kont**. Autoimmune regulator: characterization of thymic gene regulation and promoter methylation. Tartu, 2012, 134 p.
196. **Pirje Hütt**. Functional properties, persistence, safety and efficacy of potential probiotic lactobacilli. Tartu, 2012, 246 p.
197. **Innar Tõru**. Serotonergic modulation of CCK-4- induced panic. Tartu, 2012, 132 p.
198. **Sigrid Vorobjov**. Drug use, related risk behaviour and harm reduction interventions utilization among injecting drug users in Estonia: implications for drug policy. Tartu, 2012, 120 p.
199. **Martin Serg**. Therapeutic aspects of central haemodynamics, arterial stiffness and oxidative stress in hypertension. Tartu, 2012, 156 p.
200. **Jaanika Kumm**. Molecular markers of articular tissues in early knee osteoarthritis: a population-based longitudinal study in middle-aged subjects. Tartu, 2012, 159 p.
201. **Kertu Rünkorg**. Functional changes of dopamine, endopioid and endocannabinoid systems in CCK2 receptor deficient mice. Tartu, 2012, 125 p.
202. **Mai Blöndal**. Changes in the baseline characteristics, management and outcomes of acute myocardial infarction in Estonia. Tartu, 2012, 127 p.

203. **Jana Lass**. Epidemiological and clinical aspects of medicines use in children in Estonia. Tartu, 2012, 170 p.
204. **Kai Truusalu**. Probiotic lactobacilli in experimental persistent *Salmonella* infection. Tartu, 2013, 139 p.
205. **Oksana Jagur**. Temporomandibular joint diagnostic imaging in relation to pain and bone characteristics. Long-term results of arthroscopic treatment. Tartu, 2013, 126 p.
206. **Katrin Sikk**. Manganese-ephedrone intoxication – pathogenesis of neurological damage and clinical symptomatology. Tartu, 2013, 125 p.
207. **Kai Blöndal**. Tuberculosis in Estonia with special emphasis on drug-resistant tuberculosis: Notification rate, disease recurrence and mortality. Tartu, 2013, 151 p.
208. **Marju Puurand**. Oxidative phosphorylation in different diseases of gastric mucosa. Tartu, 2013, 123 p.
209. **Aili Tagoma**. Immune activation in female infertility: Significance of autoantibodies and inflammatory mediators. Tartu, 2013, 135 p.
210. **Liis Sabre**. Epidemiology of traumatic spinal cord injury in Estonia. Brain activation in the acute phase of traumatic spinal cord injury. Tartu, 2013, 135 p.
211. **Merit Lamp**. Genetic susceptibility factors in endometriosis. Tartu, 2013, 125 p.
212. **Erik Salum**. Beneficial effects of vitamin D and angiotensin II receptor blocker on arterial damage. Tartu, 2013, 167 p.
213. **Maire Karelson**. Vitiligo: clinical aspects, quality of life and the role of melanocortin system in pathogenesis. Tartu, 2013, 153 p.
214. **Kuldar Kaljurand**. Prevalence of exfoliation syndrome in Estonia and its clinical significance. Tartu, 2013, 113 p.
215. **Raido Paasma**. Clinical study of methanol poisoning: handling large outbreaks, treatment with antidotes, and long-term outcomes. Tartu, 2013, 96 p.
216. **Anne Kleinberg**. Major depression in Estonia: prevalence, associated factors, and use of health services. Tartu, 2013, 129 p.
217. **Triin Eglit**. Obesity, impaired glucose regulation, metabolic syndrome and their associations with high-molecular-weight adiponectin levels. Tartu, 2014, 115 p.
218. **Kristo Ausmees**. Reproductive function in middle-aged males: Associations with prostate, lifestyle and couple infertility status. Tartu, 2014, 125 p.
219. **Kristi Huik**. The influence of host genetic factors on the susceptibility to HIV and HCV infections among intravenous drug users. Tartu, 2014, 144 p.
220. **Liina Tserel**. Epigenetic profiles of monocytes, monocyte-derived macrophages and dendritic cells. Tartu, 2014, 143 p.
221. **Irina Kerna**. The contribution of *ADAM12* and *CILP* genes to the development of knee osteoarthritis. Tartu, 2014, 152 p.

222. **Ingrid Liiv**. Autoimmune regulator protein interaction with DNA-dependent protein kinase and its role in apoptosis. Tartu, 2014, 143 p.
223. **Liivi Maddison**. Tissue perfusion and metabolism during intra-abdominal hypertension. Tartu, 2014, 103 p.
224. **Krista Ress**. Childhood coeliac disease in Estonia, prevalence in atopic dermatitis and immunological characterisation of coexistence. Tartu, 2014, 124 p.
225. **Kai Muru**. Prenatal screening strategies, long-term outcome of children with marked changes in maternal screening tests and the most common syndromic heart anomalies in Estonia. Tartu, 2014, 189 p.
226. **Kaja Rahu**. Morbidity and mortality among Baltic Chernobyl cleanup workers: a register-based cohort study. Tartu, 2014, 155 p.
227. **Klari Noormets**. The development of diabetes mellitus, fertility and energy metabolism disturbances in a Wfs1-deficient mouse model of Wolfram syndrome. Tartu, 2014, 132 p.
228. **Liis Toome**. Very low gestational age infants in Estonia. Tartu, 2014, 183 p.
229. **Ceith Nikkolo**. Impact of different mesh parameters on chronic pain and foreign body feeling after open inguinal hernia repair. Tartu, 2014, 132 p.
230. **Vadim Brjalin**. Chronic hepatitis C: predictors of treatment response in Estonian patients. Tartu, 2014, 122 p.
231. **Vahur Metsna**. Anterior knee pain in patients following total knee arthroplasty: the prevalence, correlation with patellar cartilage impairment and aspects of patellofemoral congruence. Tartu, 2014, 130 p.
232. **Marju Kase**. Glioblastoma multiforme: possibilities to improve treatment efficacy. Tartu, 2015, 137 p.
233. **Riina Runnel**. Oral health among elementary school children and the effects of polyol candies on the prevention of dental caries. Tartu, 2015, 112 p.
234. **Made Laanpere**. Factors influencing women's sexual health and reproductive choices in Estonia. Tartu, 2015, 176 p.
235. **Andres Lust**. Water mediated solid state transformations of a polymorphic drug – effect on pharmaceutical product performance. Tartu, 2015, 134 p.
236. **Anna Klugman**. Functionality related characterization of pretreated wood lignin, cellulose and polyvinylpyrrolidone for pharmaceutical applications. Tartu, 2015, 156 p.
237. **Triin Laisk-Podar**. Genetic variation as a modulator of susceptibility to female infertility and a source for potential biomarkers. Tartu, 2015, 155 p.
238. **Mailis Tõnisson**. Clinical picture and biochemical changes in blood in children with acute alcohol intoxication. Tartu, 2015, 100 p.
239. **Kadri Tamme**. High volume haemodiafiltration in treatment of severe sepsis – impact on pharmacokinetics of antibiotics and inflammatory response. Tartu, 2015, 133 p.

240. **Kai Part**. Sexual health of young people in Estonia in a social context: the role of school-based sexuality education and youth-friendly counseling services. Tartu, 2015, 203 p.
241. **Urve Paaver**. New perspectives for the amorphization and physical stabilization of poorly water-soluble drugs and understanding their dissolution behavior. Tartu, 2015, 139 p.
242. **Aleksandr Peet**. Intrauterine and postnatal growth in children with HLA-conferred susceptibility to type 1 diabetes. Tartu. 2015, 146 p.
243. **Piret Mitt**. Healthcare-associated infections in Estonia – epidemiology and surveillance of bloodstream and surgical site infections. Tartu, 2015, 145 p.
244. **Merli Saare**. Molecular Profiling of Endometriotic Lesions and Endometria of Endometriosis Patients. Tartu, 2016, 129 p.
245. **Kaja-Triin Laisaar**. People living with HIV in Estonia: Engagement in medical care and methods of increasing adherence to antiretroviral therapy and safe sexual behavior. Tartu, 2016, 132 p.
246. **Eero Merilind**. Primary health care performance: impact of payment and practice-based characteristics. Tartu, 2016, 120 p.
247. **Jaanika Kärner**. Cytokine-specific autoantibodies in AIRE deficiency. Tartu, 2016, 182 p.
248. **Kaido Paapstel**. Metabolomic profile of arterial stiffness and early biomarkers of renal damage in atherosclerosis. Tartu, 2016, 173 p.
249. **Liidia Kiisk**. Long-term nutritional study: anthropometrical and clinico-laboratory assessments in renal replacement therapy patients after intensive nutritional counselling. Tartu, 2016, 207 p.
250. **Georgi Nellis**. The use of excipients in medicines administered to neonates in Europe. Tartu, 2017, 159 p.
251. **Aleksei Rakitin**. Metabolic effects of acute and chronic treatment with valproic acid in people with epilepsy. Tartu, 2017, 125 p.
252. **Eveli Kallas**. The influence of immunological markers to susceptibility to HIV, HBV, and HCV infections among persons who inject drugs. Tartu, 2017, 138 p.
253. **Tiina Freimann**. Musculoskeletal pain among nurses: prevalence, risk factors, and intervention. Tartu, 2017, 125 p.
254. **Evelyn Aaviksoo**. Sickness absence in Estonia: determinants and influence of the sick-pay cut reform. Tartu, 2017, 121 p.
255. **Kalev Nõupuu**. Autosomal-recessive Stargardt disease: phenotypic heterogeneity and genotype-phenotype associations. Tartu, 2017, 131 p.
256. **Ho Duy Binh**. Osteogenesis imperfecta in Vietnam. Tartu, 2017, 125 p.
257. **Uku Haljasorg**. Transcriptional mechanisms in thymic central tolerance. Tartu, 2017, 147 p.
258. **Živile Riispere**. IgA Nephropathy study according to the Oxford Classification: IgA Nephropathy clinical-morphological correlations, disease progression and the effect of renoprotective therapy. Tartu, 2017, 129 p.

259. **Hiie Soeorg**. Coagulase-negative staphylococci in gut of preterm neonates and in breast milk of their mothers. Tartu, 2017, 216 p.
260. **Anne-Mari Anton Willmore**. Silver nanoparticles for cancer research. Tartu, 2017, 132 p.
261. **Ott Laius**. Utilization of osteoporosis medicines, medication adherence and the trend in osteoporosis related hip fractures in Estonia. Tartu, 2017, 134 p.
262. **Alar Aab**. Insights into molecular mechanisms of asthma and atopic dermatitis. Tartu, 2017, 164 p.
263. **Sander Pajusalu**. Genome-wide diagnostics of Mendelian disorders: from chromosomal microarrays to next-generation sequencing. Tartu, 2017, 146 p.
264. **Mikk Jürisson**. Health and economic impact of hip fracture in Estonia. Tartu, 2017, 164 p.
265. **Kaspar Tootsi**. Cardiovascular and metabolomic profiling of osteoarthritis. Tartu, 2017, 150 p.
266. **Mario Saare**. The influence of AIRE on gene expression – studies of transcriptional regulatory mechanisms in cell culture systems. Tartu, 2017, 172 p.
267. **Piia Jõgi**. Epidemiological and clinical characteristics of pertussis in Estonia. Tartu, 2018, 168 p.
268. **Elle Põldoja**. Structure and blood supply of the superior part of the shoulder joint capsule. Tartu, 2018, 116 p.
269. **Minh Son Nguyen**. Oral health status and prevalence of temporomandibular disorders in 65–74-year-olds in Vietnam. Tartu, 2018, 182 p.
270. **Kristian Semjonov**. Development of pharmaceutical quench-cooled molten and melt-electrospun solid dispersions for poorly water-soluble indomethacin. Tartu, 2018, 125 p.
271. **Janne Tiigimäe-Saar**. Botulinum neurotoxin type A treatment for sialorrhea in central nervous system diseases. Tartu, 2018, 109 p.
272. **Veiko Vengerfeldt**. Apical periodontitis: prevalence and etiopathogenetic aspects. Tartu, 2018, 150 p.
273. **Rudolf Bichele**. TNF superfamily and AIRE at the crossroads of thymic differentiation and host protection against *Candida albicans* infection. Tartu, 2018, 153 p.
274. **Olga Tšuiko**. Unravelling Chromosomal Instability in Mammalian Preimplantation Embryos Using Single-Cell Genomics. Tartu, 2018, 169 p.
275. **Kärt Kriisa**. Profile of acylcarnitines, inflammation and oxidative stress in first-episode psychosis before and after antipsychotic treatment. Tartu, 2018, 145 p.
276. **Xuan Dung Ho**. Characterization of the genomic profile of osteosarcoma. Tartu, 2018, 144 p.
277. **Karit Reinson**. New Diagnostic Methods for Early Detection of Inborn Errors of Metabolism in Estonia. Tartu, 2018, 201 p.

278. **Mari-Anne Vals**. Congenital N-glycosylation Disorders in Estonia. Tartu, 2019, 148 p.
279. **Liis Kadastik-Eerme**. Parkinson's disease in Estonia: epidemiology, quality of life, clinical characteristics and pharmacotherapy. Tartu, 2019, 202 p.
280. **Hedi Hunt**. Precision targeting of intraperitoneal tumors with peptide-guided nanocarriers. Tartu, 2019, 179 p.
281. **Rando Porosk**. The role of oxidative stress in Wolfram syndrome 1 and hypothermia. Tartu, 2019, 123 p.
282. **Ene-Ly Jõgeda**. The influence of coinfections and host genetic factor on the susceptibility to HIV infection among people who inject drugs. Tartu, 2019, 126 p.
283. **Kristel Ehala-Aleksejev**. The associations between body composition, obesity and obesity-related health and lifestyle conditions with male reproductive function. Tartu, 2019, 138 p.
284. **Aigar Ottas**. The metabolomic profiling of psoriasis, atopic dermatitis and atherosclerosis. Tartu, 2019, 136 p.
285. **Elmira Gurbanova**. Specific characteristics of tuberculosis in low default, but high multidrug–resistance prison setting. Tartu, 2019, 129 p.
286. **Van Thai Nguyeni**. The first study of the treatment outcomes of patients with cleft lip and palate in Central Vietnam. Tartu, 2019, 144 p.
287. **Maria Yakoreva**. Imprinting Disorders in Estonia. Tartu, 2019, 187 p.
288. **Kadri Rekker**. The putative role of microRNAs in endometriosis pathogenesis and potential in diagnostics. Tartu, 2019, 140 p.
289. **Ülle Võhma**. Association between personality traits, clinical characteristics and pharmacological treatment response in panic disorder. Tartu, 2019, 121 p.
290. **Aet Saar**. Acute myocardial infarction in Estonia 2001–2014: towards risk-based prevention and management. Tartu, 2019, 124 p.
291. **Toomas Toomsoo**. Transcranial brain sonography in the Estonian cohort of Parkinson's disease. Tartu, 2019, 114 p.
292. **Lidiia Zhytnik**. Inter- and intrafamilial diversity based on genotype and phenotype correlations of Osteogenesis Imperfecta. Tartu, 2019, 224 p.
293. **Pilleriin Soodla**. Newly HIV-infected people in Estonia: estimation of incidence and transmitted drug resistance. Tartu, 2019, 194 p.
294. **Kristiina Ojamaa**. Epidemiology of gynecological cancer in Estonia. Tartu, 2020, 133 p.
295. **Marianne Saard**. Modern Cognitive and Social Intervention Techniques in Paediatric Neurorehabilitation for Children with Acquired Brain Injury. Tartu, 2020, 168 p.
296. **Julia Maslovskaja**. The importance of DNA binding and DNA breaks for AIRE-mediated transcriptional activation. Tartu, 2020, 162 p.
297. **Natalia Lobanovskaya**. The role of PSA-NCAM in the survival of retinal ganglion cells. Tartu, 2020, 105 p.

298. **Madis Rahu**. Structure and blood supply of the postero-superior part of the shoulder joint capsule with implementation of surgical treatment after anterior traumatic dislocation. Tartu, 2020, 104 p.
299. **Helen Zirnask**. Luteinizing hormone (LH) receptor expression in the penis and its possible role in pathogenesis of erectile disturbances. Tartu, 2020, 87 p.
300. **Kadri Toome**. Homing peptides for targeting of brain diseases. Tartu, 2020, 152 p.
301. **Maarja Hallik**. Pharmacokinetics and pharmacodynamics of inotropic drugs in neonates. Tartu, 2020, 172 p.
302. **Raili Müller**. Cardiometabolic risk profile and body composition in early rheumatoid arthritis. Tartu, 2020, 133 p.
303. **Sergo Kasvandik**. The role of proteomic changes in endometrial cells – from the perspective of fertility and endometriosis. Tartu, 2020, 191 p.
304. **Epp Kaleviste**. Genetic variants revealing the role of STAT1/STAT3 signaling cytokines in immune protection and pathology. Tartu, 2020, 189 p.
305. **Sten Saar**. Epidemiology of severe injuries in Estonia. Tartu, 2020, 104 p.
306. **Kati Braschinsky**. Epidemiology of primary headaches in Estonia and applicability of web-based solutions in headache epidemiology research. Tartu, 2020, 129 p.
307. **Helen Vaher**. MicroRNAs in the regulation of keratinocyte responses in *psoriasis vulgaris* and atopic dermatitis. Tartu, 2020, 242 p.
308. **Liisi Raam**. Molecular Alterations in the Pathogenesis of Two Chronic Dermatoses – Vitiligo and Psoriasis. Tartu, 2020, 164 p.
309. **Artur Vetkas**. Long-term quality of life, emotional health, and associated factors in patients after aneurysmal subarachnoid haemorrhage. Tartu, 2020, 127 p.
310. **Teele Kasepalu**. Effects of remote ischaemic preconditioning on organ damage and acylcarnitines' metabolism in vascular surgery. Tartu, 2020, 130 p.
311. **Prakash Lingasamy**. Development of multitargeted tumor penetrating peptides. Tartu, 2020, 246 p.
312. **Lille Kurvits.** Parkinson's disease as a multisystem disorder: whole transcriptome study in Parkinson's disease patients' skin and blood. Tartu, 2021, 142 p.
313. **Mariliis Põld.** Smoking, attitudes towards smoking behaviour, and nicotine dependence among physicians in Estonia: cross-sectional surveys 1982–2014. Tartu, 2021, 172 p.
314. **Triin Kikas**. Single nucleotide variants affecting placental gene expression and pregnancy outcome. Tartu, 2021, 160 p.
315. **Hedda Lippus-Metsaots**. Interpersonal violence in Estonia: prevalence, impact on health and health behaviour. Tartu, 2021, 172 p.